ABSTRACT

Title of dissertation: NUMERICAL SIMULATION OF LOW-PRESSURE EXPLOSIVE COMBUSTION IN COMPARTMENT FIRES

Hu Zhixin
Doctor of Philosophy, 2008

Dissertation directed by: Professor Arnaud Trouvé
Department of Mechanical Engineering

A filtered progress variable approach is adopted for large eddy simulations (LES) of turbulent deflagrations. The deflagration model is coupled with a non-premixed combustion model, either an equilibrium-chemistry, mixture-fraction based model, or an eddy dissipation model. The coupling interface uses a LES-resolved flame index formulation and provides partially-premixed combustion (PPC) modeling capability. The PPC sub-model is implemented into the Fire Dynamic Simulator (FDS) developed by the National Institute of Standards and Technology, which is then applied to the study of explosive combustion in confined fuel vapor clouds. Current limitations of the PPC model are identified first in two separate series of simulations: 1) a series of simulation corresponding to laminar flame propagation across homogeneous mixtures in open or closed tunnel-like configurations; and 2) a grid refinement study corresponding to laminar flame propagation across a vertically-stratified layer.

An experimental database previously developed by FM Global Research, featuring controlled ignition followed by explosive combustion in an enclosure filled with vertically-stratified mixtures of propane in air, is used as a test configuration for model validation. Sealed and vented configurations are both considered, with and without obstacles in the chamber. These pressurized combustion cases present a particular challenge to the bulk pressure algorithm in FDS, which has robustness, accuracy and stability issues, in particular in vented configurations. Two modified bulk pressure models are proposed and evaluated by comparison between measured and simulated pressure data in the Factory Mutual Global (FMG) test configuration. The first model is based on a modified bulk pressure algorithm and uses a simplified expression for pressure valid in a vented compartment under quasi-steady conditions. The second model is based on solving an ordinary differential equation for bulk pressure (including a relaxation term proposed to stabilize possible Helmholtz oscillations) and modified vent flow velocity boundary conditions that are made bulk-pressure-sensitive. Comparisons with experiments are encouraging and demonstrate the potential of the new modeling capability for simulations of low pressure explosions in stratified fuel vapor clouds.

NUMERICAL SIMULATION OF LOW-PRESSURE EXPLOSIVE COMBUSTION IN COMPARTMENT FIRES

by

Hu Zhixin

Dissertation submitted to the Faculty of the Graduate School of the
University of Maryland, College Park in partial fulfillment
of the requirements for the degree of
Doctor of Philosophy
2008

Advisory Committee:
Professor Arnaud Trouvé, Chair/Advisor
Professor James G. Quintiere
Professor Gregory Jackson
Professor Andre Marshall
Professor Peter B. Sunderland

Dedication

To my family - mom, dad and zhijun.

Acknowledgements

I would like to gratefully acknowledge the consistent and motivating supervision of Dr. Arnaud Trouvé, at all times. His guidance not only helps me finish the work that will be presented in this document, but more importantly, it will keep reminding me of the responsibility for the pursuit of high quality work in the future.

I also thank Professor Quintiere for the numerous discussions and general advice on the project. Thanks goes to other committee members as well: Professor Sunderland, Professor Jackson and Professor Marshall for their inspiring questions upon the completion of the project. I am also grateful to National Institute of Standards and Technology (NIST) for their sponsorship.

I owe my sincere thanks to all other professors that I take classes with, their name cannot be counted here, but the education they passed to me is extremely invaluable. I would also like to thank my colleague graduate students, especially in the Fire Protection Engineering department office, I enjoyed every minute of us being together.

Finally, I am indebted to the endless and unconditional love from my family members, that I would never be able to pay back. So this thesis is devoted to my father, my mother and my brother.

Table of Contents

List of Figures

Nomenclature

A_v	vent area
c	reaction progress variable
C_d	transport coefficient
c_p	specific heat
f_{ign}	ad-hoc ignition factor
g	gravity force
k	helmholtz frequency
L	effective length of vent
L_z	height of flammable gas range
p	pressure
$\bar{P}$	bulk pressure
$\tilde{p}$	pressure perturbation
q	heat release rate
q_c	heat source
$q_{R,j}$	radiation heat loss at x-j direction
r_s	stoichiometric oxygen-to-fuel ratio
Sc_t	turbulent Schimdt number
s_L	laminar flame speed
T_1	temperature in the fuel stream
T_2	temperature in the oxygen stream
T_c	critical temperature
u_i	x_i-component of flow velocity
u, v, w	velocity in x,y,z direction
V	volume of compartment
W_k	molecular weight of species k
$Y_{F,1}$	mass fraction of fuel in the fuel stream
Y_k	mass fraction of species k
$Y_{O_2,2}$	mass fraction of oxygen in the oxidizer stream
$Y_{O_2,c}$	lower oxygen index
Z	mixture fraction
Z_1	mixture fraction represents the reaction from fuel to CO
Z_2	mixture fraction represents the reaction from CO to CO2
Z_{st}	stoichiometric mixture fraction

Greek Symbols

ν_k	mole number of species k in a reaction
Δ	grid size
Δ_c	LES filter size
ΔH_F	heat of combustion for the fuel
ϵ	outflow/inflow indicator
ν_t	turbulent viscosity
γ	ratio of specific heats
ρ	mass density

ϕ	global/local equivalence ratio
ω	mass reaction rate
τ	characteristic time scale
χ	scalar dissipation rate
Σ	LES-filtered flame surface-to-volume ratio
Ξ	subgrid-scale flame wrinkling factor

Superscripts

$\tilde{}$	Favre-average
$'''$	volume differential
-	space average
b	burnt
u	unburnt

Subscripts

F	fuel
LFL	Lower Flammability Limit
UFL	Upper Flammability Limit
c	reaction progress variable
d	diffusion
eq	equilibrium
ex	extinction
st	stoichiometric
ign	ignitor
L	laminar
p	premix
L	left of imaginary tube in chapter 6
R	right of imaginary tube in chapter 6
ref	reference value
v	vent
0	ambient value
∞	ambient value

Operators

∇	gradient operator
δ	Dirac function
H	Heaviside function

Abbreviations

CFL	CourantFriedrichsLewy condition
CV	Control Volume

CS	Control Surface
FDS	Fire Dynamic Simulator
FEF	Flame Extinction Factor
FI	Flame Index
FMG	Factory Mutual Global
fpv	flame propagation velocity
LES	Large Eddy Simulation
LHS	Left-Hand-Side
LNG	Liquefied Natural Gas
LPG	Liquefied Petroleum Gas
RHS	Right-Hand-Side
NFPA	National Fire Protection Association
PPC	Partially-Premixed Combustion
S1,2,3	Scheme 1,2,3
VPC	Velocity-Pressure Coupling

Chapter 1

Introduction

1.1 Overview

Confined or partially confined gas explosions are one of the major accidents that occur in spilling/leaking fuel tank, fuel pipe scenarios, mining accidents, or backdraft scenarios in buildings [1, 80, 95]. Compared to stabilised flames, which feature moderate burning intensities, large scale explosions present more hazards, resulting from the flame acceleration caused by a wrinkled premixed flame surface, whose dynamics have been reviewed previously [7] (including the developing hydrodynamic instabilities and cellular structure). Depending on the combustion intensity, the explosion could remain a deflagration (subsonic combustion) or lead to a detonation (supersonic combustion). In a detonation, the shock wave compresses the material so to increase the temperature to the point of ignition [90], the ignited material burns behind the shock and releases energy that supports the shock propagation. This self-sustained shock wave generates high pressures and presents more destructive hazards than a deflagration, which has neither shock nor significant pressure changes. In the current study, the explosive combustion corresponds to deflagration in low-pressure environment.

Because of the unrealistic cost to study these real-world large-scale explosion,

small-scale experiments [81, 82] and numerical tools [46, 47, 48, 49, 50, 51] are usually adopted to help understand the physics and characteristics of confined or partially confined gas explosions.

One crucial problem in the study of explosions is the combustion pattern during and after the explosion, where both premixed and non-premixed combustion are involved. Previous CFD modeling studies typically can handle only one of these two categories of combustion: studies in which flammable conditions are assumed across the bulk of the fuel vapor cloud, and combustion is described as premixed [10, 46, 59, 60, 61, 66]; and studies in which ultra-rich conditions are assumed and combustion is described as non-premixed [47, 48, 49, 50, 51, 73]. Here a more general formulation in which combustion can be described as both, simultaneously or sequentially, premixed and non-premixed is required for the purpose of modeling confined and vented gas explosions. The present study considers such a formulation and focuses on specific issues resulting from the coupling of premixed and non-premixed turbulent flame models. This coupling has received growing interest in recent years, primarily driven by the need to adapt combustion formulations for a CFD treatment of lifted turbulent diffusion flames [18, 69, 85]. The burning regime in the stabilization region of lifted diffusion flames is usually referred to as partially-premixed combustion (PPC), so that the combustion model used in the present work will be referred to as a PPC model.

Another key challenge in modeling gas explosions is the hazard presented by

pressure. Venting is known to be an effective way to relieve the pressure, so as to prevent the facilities from being destroyed by internal explosions. A number of empirical and semi-empirical methods are available that can be used for determining the size of explosion venting [70, 76]. Bradley studied the venting of gaseous explosions in spherical vessels [8, 9], in which he also reviewed the model by Fairweather [20] that the vented gas velocity is correlated with the ratio of internal pressure divided by ambient pressure, so that the overpressure generated in totally confined and/or vented explosions can be predicted.

Experimental work on vented explosions also includes McCann's gas dynamics study [52], in which he concluded that "when venting occurs through large and intermediate vent areas, Helmholtz oscillations are generated within the vessel, and the resulting flame accelerations give rise to Taylor instabilities of the flame front. For smaller vent areas the fundamental acoustic mode of the vessel is excited, which, at higher breaking pressures, is usually coupled with a second pressure peak". When Cooper and Fairweather [15] were studying the mechanisms of pressure generation in vented explosions, they also observed the pressure oscillation, although they did not identify them as Helmholtz oscillation. They proposed that for ignition at the center of a vessel the combustion process gives rise to four major pressure peaks: 1) one peak depends on the failure strength of the explosion relief installed; 2)one peak due to either the reactivity of the fuel or induced turbulence; 3) one peak comes from a maximum in the rate of production of burned product; 4) one peak identified as acoustical pressure peak. It was also confirmed in their work that in

vessels containing obstacles, the generation of turbulence during phase of the combustion process can lead to a larger third peak, while eliminating the fourth peak, because the generation of acoustically enhanced pressure depends on the coupling between acoustic waves and combustion dynamics, any situation in which this process is hindered is likely to produce much smaller fourth pressure peaks. Yu et al [94] studied low-frequency combustion instabilities, which also included pressure and velocity oscillations. The same feature of Helmholtz oscillations presented in the vented explosion pressure is also predicted in DeHaan's numerical work [17], which will therefore be explored in the present study on the simulation of vented explosions. McCann also measured the maximum exit velocity in vented explosions [53], and it turns out to be lower than the one predicted by theory, i.e., the model by Fairweather [20].

There are also some CFD efforts on the modeling of vented explosions. Ferrara et al [22] used a two-dimensional axi-symmetric computational fluid dynamic model based on the unsteady Reynolds Averaged Navier Stokes (RANS) approach to model gas explosions vented through relief pipes. Work by Molkov et al. [59, 60, 61, 62, 63, 64, 65, 66] recently focuses on the Large Eddy Simulation (LES) modeling of large-scale hydrocarbon-air or hydrogen-air deflagration, with two combustion submodels, one based on the renormalization group (RNG) theory and another on the fractal theory by Bradley [7]. These studies consider the acceleration of combustion due to the displacement and compression of unburned gases ahead of the flame, by taking into account that the laminar burning velocity depends on pressure and

temperature [40, 96], but there is no specific treatment for Helmholtz oscillations, which is essential for the correct vent explosion behavior.

Motivated by previous work on premixed/non-premixed combustion and venting pressure, the interest here is first to examine the vented explosion starting from the accidental release and possible subsequent ignition of vaporized fuel in ambient air, which usually occurs in backdraft explosion or fuel vapor cloud accidents. For the rest of the chapter, the mechanism of fuel vapor cloud formation is examined. Then relevant studies of backdraft phenomena and fuel vapor cloud combustion will be reviewed, followed by a presentation of the objectives of the present thesis.

1.2 Fuel vapor cloud formation and ignition

When fuel is released into ambient air and forms a fuel vapor cloud, depending on the velocity of the fuel-air mixing process, the composition of the bulk of the fuel vapor could be ultra-lean (*i.e.*, below the lower flammability limit) in the case of fast mixing, ultra-rich (*i.e.*, above the upper flammability limit) in the case of slow mixing (Fig 1.1)), or flammable (*i.e.*, within the flammability limits) in the intermediate case (Fig 1.2). The fast mixing case corresponds to a desirable safe dispersion scenario in which there is no fire or explosion hazard, so the slow mixing and intermediate cases that correspond to a hazard will be the focus here (Figs 1.1a-1.2a). It is assumed that ignition takes place somewhere at a flammable location

in the fuel vapor cloud (Figs 1.1b-1.2b). Following ignition, the combustion will proceed initially as a thin deflagration or detonation wave that propagates across the flammable portions of the fuel vapor cloud.

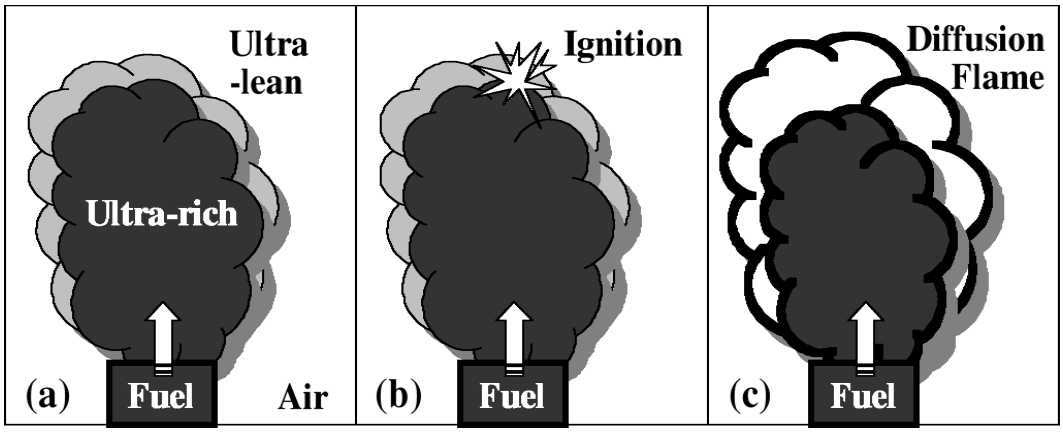

Figure 1.1: Illustration of (a) the formation of a large ultra-rich fuel vapor cloud, followed by (b) ignition and (c) diffusion burning.

The deflagration scenario will be focused on in the following, in which the premixed flame propagates at subsonic speeds and pressure remains quasi-uniform across the combustion zone (pressure may change with time but not with spatial location). Even with this limited scope, the combustion dynamics remain quite complex since they depend strongly on the state of the fuel-air mixing field found at ignition time. In the case of an ultra-rich fuel vapor cloud, combustion corresponds predominantly to a diffusion burning mode (Fig 1.1c); in the case of a flammable fuel vapor cloud, combustion corresponds predominantly to a premixed burning mode (Fig 1.2c). In cases dominated by premixed burning, one may also differentiate

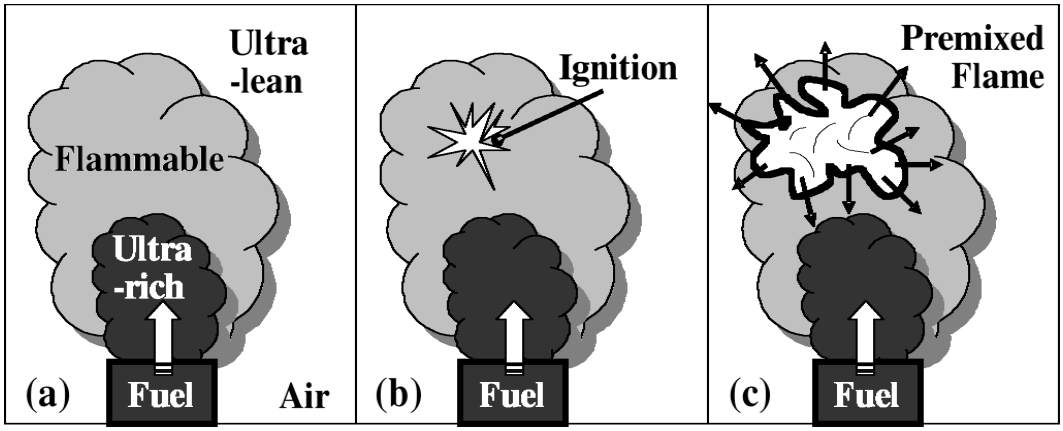

Figure 1.2: Illustration of (a) the formation of a large flammable fuel vapor cloud, followed by (b) ignition and (c) deflagration.

between pure premixed burning modes and partially premixed burning modes. Pure premixed burning modes are observed when the bulk of the fuel vapor cloud is flammable and/or fuel-lean, while partially-premixed burning modes are observed when some portions of the fuel vapor cloud are flammable and/or fuel-rich: in that case, the combustion starts as a fuel-rich deflagration wave that propagates across the flammable region and leaves excess fuel in the post-deflagration gases; the residual fuel may then subsequently mix with ambient air and burn in a diffusion flame mode.

1.3 Backdraft

According to NFPA's definition, backdraft is "the explosive or rapid burning of heated gases that occurs when oxygen is introduced into a building that has not been properly ventilated and has a depleted supply of oxygen due to fire". The de-

velopment of a backdraft incident in a building compartment generally goes through a succession of stages, from under-ventilated, quasi-extinguished fire conditions, to sudden reignition triggered by an accidental or intentional change in the fire room ventilation capacity, followed in turn by a violent deflagration and possibly fireball formation [23, 25].

An important ingredient in backdraft scenarios is the presence of gravity-driven flows, which are results of fuel-air mixing and determine whether a deflagration may occur as well as its intensity. The gravity-driven flow is the flow of one fluid into another caused by a difference in mass density. In backdraft scenarios, when a vent is opened, due to the temperature difference between inside and outside of the fire room, dense ambient air flows into the lighter, fuel rich, compartment gas. So the oxygen layer will go underneath the fuel layer, and if the zone where the two layer mix happens to meet some hot spot, it maybe ignited as a premixed flame and propagates through the compartment to form a large and intense flame. Fleischmann used salt water to study gravity-driven flow and to determine the flow speed and the extent of the mixing region [24], using non-dimensionalization and scaling parameters. Also with McGrattan, they used a buoyancy-driven flow model to study the gravity-driven flow numerically [55] (a detailed description of this buoyancy-driven flow model can be found in [56]).

Small scale experiments on backdraft include elaborate work from Fleischmann [25, 26], in which a methane burner is ignited in a closed compartment of 1.2 m by

1.2 m by 2.4 m, and burns until the initial oxygen is consumed. The gas burner is kept on for a certain duration to form a fuel-rich mixture. Then, following the opening of the hatch, an air gravity-driven flow comes in and travels across the compartment, mixes with the unburned fuel, and is ignited by a spark near the end wall of the compartment. Once the mixture ignites, a backdraft is observed to occur as a deflagration propagates through the compartment culminating in a large external fireball. Data are recorded, in particular the fuel flow rates, upper layer temperatures, lower layer temperatures, and upper layer species concentrations for O_2, CO_2, CO, HC, to quantify the backdraft in terms of opening gas flow velocities and compartment pressures. This work indicates that the unburned fuel mass fractions should be larger than 10% for a backdraft to occur.

Gottuk's experimental study of backdraft explosions [28, 29] reveals that the critical fuel mass fraction required for the development of diesel fuel backdrafts is $Y_f = 0.16$ for fully vitiated conditions (to be compared to $Y_f = 0.10$ reported by Fleischmann for methane backdraft). This higher value of the critical fuel mass fraction is attributed primarily to the oxygen concentrations within the compartments. The average compartment oxygen concentration in Gottuk's experiment is 1 % by volume while in Fleischmann's tests it takes values between 10% to 12%, and this difference in oxygen concentration can result in a factor of 1.5 to 2 difference in the critical fuel mass fraction (Gottuk shows that the standard flammability diagram can be used to predict bounding limits and trends on critical fuel mass fractions with respect to oxygen concentrations). Gottuk's research also reveals that the injection

of water spray is an effective mitigating tactic to completely prevent backdrafts, mainly by means of diluting the atmosphere and reducing the fuel mass fraction, rather than by a thermal mechanism of cooling. In Gottuk's experiment, at the time the door was opened to induce the gravity current for the backdraft to happen, the average compartment temperatures are 340 to 400 ℃; when injecting water, the temperature were typically between 310 to 360 ℃, which is still greater than the auto-ignition temperature of diesel. Since the compartment temperatures are high enough to evaporate all injected water, water injection will dilute the fuel mass fraction, and when dilution levels are high enough no explosion or even external flaming is observed.

Snegrirev studied the flame projection through openings under limited ventilation conditions both experimentally and numerically [79], which should not be confused with the deflagration in the backdraft cases. They studied the critical flow rate of the fuel sufficient for flame projection as well as the delay between fuel ignition and flame projection with subsequent establishment of external combustion. The flame projection observed is when there is a lack of oxygen, the flame moves from burning inside to outside, and there is no smoldering process and no reignition of a partially premixed gas, so the flame projection speed is much less than the deflagration speed in backdraft.

Ferraris and Wen adopted a subgrid-scale (SGS) model for partially premixed combustion to simulate backdraft [23]. The model is based on the linear coupling of

two independent approaches for premixed and non-premixed combustion through the 'flame index' concept, which is similar to the modeling framework adopted in the present work. A Large Eddy Laminar Flamelet Model (LELFM) is used for non-premixed combustion and a flame surface density approach is adopted for premixed combustion. While their results are mostly analyzed qualitatively, the simulation gives the insight that the development of backdraft can be divided into five phases, i.e., initial condition, free "spherical propagation", "plane" front propagation, stretching of the flame front through the opening and fireball outside the container. Their quantitative comparison finds that the experimentally measured and numerically predicted lapse of time between the maximum over- and under-pressure at the opening of the container are in good agreement.

CFD work on backdraft also includes Horvat and Sinai's preliminary work on simulations of compartment backdraft phenomena [34], in which a Detached Eddy Simulation (DES) turbulence model and an Eddy Dissipation Model (EDM) combustion model are used to model fire spread through the mixture of methane, air and combustion products. The DES model uses a RANS formulation near solid walls and the Large Eddy Simulation (LES) model in the bulk of the flow to avoid computationally expensive grid resolution that is necessary for realistic LES predictions in wall layers. By validating against Gottuk's experiment [28, 29], it is found that the predicted ignition time agrees qualitatively with the experimental data, while the differences between the simulations and the experiment are greater for pressure and temperature, which are projected in their paper to be due to possible

shortcomings in their ignition and combustion models, as well as inaccuracies in the gravity current predictions.

1.4 Fuel spill and deflagration

Concerns on Liquefied Natural Gas (LNG) tank releases motivate research on fuel spill, pool vaporization, turbulent dispersion and fuel-vapor mixing. Fay has produced analytical and computer models that predict the behavior of spills of LNG and oil from the holds of tankers [21]. Conrado and Vesovic devised a numerical model estimating the vaporization rate of LNG and liquefied petroleum gas (LPG) on unconfined water surfaces [14]. A turbulent dispersion model called DEGADIS model is used to study the dispersion of denser-than-air gases [30]. SLAB, developed by Lawrence Livermore National Laboratory, the USAF Engineering and Services Center, and the American Petroleum Institute, also models the dispersion of denser-than-air gases [19]. McGill [54] used FDS coupled with a deflagration model to simulate the vaporization, dispersion and deflagration of liquid methane pools boiling on water while subjected to airflow around a prismatic body. The research in his study is sharing the same framework of the deflagration model as the one adopted in the present study, which will be presented in detail in Chapter 2.

Molkov and his co-workers developed a model to simulate large-scale confined and unconfined gaseous deflagrations [59, 60, 61, 62], which adopts the reaction progress variable (c) to simulate the propagation of turbulent premixed flame fronts

and the gradient method to provide the mass burning rate, in which the local mass burning rate is assumed to be proportional to the magnitude of the gradient of c ($|\nabla \tilde{c}|$). Flame front wrinkling is partially resolved by LES, while the unresolved sub-grid-scale (SGS) increase in flame front area is modeled by a deflagration-outflow interaction (DOI) number. The LES model in their work is validated against vented explosion experiments in two vessels of 0.95 m^3 and 6.37 m^3 volume, with different vent diameters and vent relief pressures, and hydrogen-air mixtures of different concentrations.

Makhviladze and colleagues studied non-premixed combustion in fuel vapor clouds corresponding to fuel rich conditions across the bulk of the flammable cloud [47, 48, 49, 50]. The model solves the incompressible Navier-Stokes equations with species equations for fuel, O_2, N_2, H_2O and CO_2. An eddy-break-up (EBU) model is used for the reaction rate, while the reaction zone is viewed as a collection of fresh and burned gas pockets. The model is used to study the structure of the fireball resulting from the ignition of the vertical release of fuel from an axially-symmetric jet, which is then compared to the predictions from empirical relationships for fireballs and shows reasonable results. A correlation for the fireball lifetime as a function of Froude number is presented. The model is then extended to a treatment of two-phase fuel releases. Finally, the model was applied to simulate the development and combustion of a fuel vapor cloud formed from an instantaneous fuel release, instead of finite-time releases.

1.5 Objective

The objective of this study is to explore the feasibility of a Large Eddy Simulation (LES) approach combined with a partially-premixed combustion (PPC) model in addressing the hazards associated with the transient combustion of fuel vapor clouds, with a particular emphasis on the flame propagation speed, burning intensity and the time evolution of pressure. The developments and tests are made in the context of a CFD solver called the Fire Dynamics Simulator (FDS) [57].

FDS is developed by the National Institute of Standards and Technology (NIST), and is oriented toward fire applications; it uses a Large Eddy Simulation (LES) approach for turbulence (based on the classical Smagorinsky model) and a fast chemistry model for non-premixed combustion (based on the Eddy Dissipation Concept) [56, 57, 58].

A premixed combustion modeling capability has been recently incorporated into FDS to give an enhanced PPC modeling capability [87, 88, 89, 92, 93]. An extension to FDS Version 5 (earlier developments had been made in the context of FDS Version 4) has also been made during the present work. The preliminary work in Refs. [92, 93] is focused on integrating a turbulent deflagration model into FDS and performing verification tests in configurations in which the fuel-air mixture is uniform. In the work of Refs. [87, 88, 89], a detailed discussion of the grid resolution requirement of the PPC model formulation when used in non-homogeneous

configurations is presented, and it is found that the model is limited by the demand that the LES premixed flame remains thin in mixture fraction space. Thus the LES filter-to-grid length ratio is proposed to be $\Delta_c/\Delta \geq 4$. Also a modified PPC formulation is proposed based on a two-speed treatment of flame speed (s_L^*, s_L^{**}) [89]. This scheme has been shown to successfully eliminate spurious premixed burning near the edges of the flammable cloud and provides a clean description of the burn out phase after premixed burning is completed. These recent developments are also adopted in the PPC model and used here as a starting point. The PPC model will be described in Chapter 2 along with its incorporation into FDS.

In the present study, a series of verification tests are performed corresponding to uniform mixture premixed flames propagating horizontally in tunnel configurations, for further evaluating the flame speed algorithm, then a grid study in a similar configuration, but with a vertically-stratified fuel-air mixture, is conducted since fuel spills or flammable gas releases often form stratified fuel/air mixtures that present explosion hazards. In the end of Chapter 3 the computational grid requirement of the PPC model is characterized.

In Chapter 4, the bulk pressure algorithm in FDS is first reviewed and found to be incapable of correct pressure solution in compartment with open vents, which is a key issue in vented explosions. A modified pressure algorithm is proposed, based on the quasi-steady Bernoulli theory, and tested in a simple compartment configuration for verification purposes. The comparison between the performance of the

original FDS pressure algorithm and modified algorithm will also be shown.

In Chapter 5 a validation study is performed, aiming to examine the capability of the PPC model and the modified pressure algorithm in simulating a real-scale confined and vented gas explosion. The experimental database has been previously developed by Factory Mutual (FM) Global Research [81], corresponding to a scenario of controlled ignition followed by explosive combustion in an enclosure filled with vertically-stratified mixtures of propane in air, both with and without venting, and with and without obstacles. This database corresponds to low-pressure explosions in confined fuel vapor clouds and is well-suited for a validation study of the PPC model.

Another concern when examining the FDS performance in vented explosion in previous chapters is that the mass outflow prediction upon vent opening is incorrect. In Chapter 6 a study of the vent flow velocity boundary condition in FDS is conducted, followed by a proposed modified treatment that is sensitive to the pressure difference on both sides of the vent. It is found that the new formulation helps capture the Helmholtz oscillation phenomena, which are observed in experiments by [15, 17, 52]. The new velocity boundary condition scheme is coupled with the FDS pressure algorithm, and is referred to as velocity-pressure coupling (VPC) scheme. It will be discussed in detail in Chapter 6.

Finally in Chapter 7 the VPC scheme is adopted along with the PPC model to

simulate the FMG test configuration, mainly two cases characterized by the presence of a vent and featuring low vent opening pressure. The simulated pressure will be compared with the experimental data, and the ability of the FDS-based model to simulate large scale vented explosions will also be discussed.

Chapter 2

Partially-Premixed Combustion (PPC) Model in Fire Dynamic Simulator (FDS)

The combustion modeling capability of FDS, including Version 4 and Version 5 (released in 2007) [57] is presented in this chapter. FDS is widely used in the fire protection engineering field, and it features a Large Eddy Simulation (LES) approach for turbulence modeling and either an equilibrium-chemistry, mixture-fraction-based model (FDS version 4) or an Eddy Dissipation Concept model (FDS version 5), for non-premixed combustion. FDS uses an incompressible flow solver, solving low-Mach number forms of the Navier-Stokes equations, so the domain of application of FDS is limited to scenarios that are quasi-incompressible and with no blast wave. First the non-premixed combustion models available in the NIST official releases of FDS versions 4 and 5 will be reviewed in the following, followed by a presentation of the developments made at the University of Maryland over the past few years, including a deflagration model, and a coupling interface that couples the non-premixed and premixed combustion models.

2.1 Diffusion flame modeling with flame extinction

In FDS4, the combustion model is based on the classical Burke-Schumann theory of diffusion flames in which fast chemistry is assumed and the flame structure

is described in terms of a conserved mixture fraction $\tilde{Z}$. Consider the following reaction:

$$C_nH_m + \nu_{O_2}O_2 \longrightarrow (n - \nu_{CO} - \nu_{soot})CO_2 + \frac{m}{2}H_2O + \nu_{CO}CO + \nu_{soot}C \quad (R1) \quad (2.1)$$

where ν_{co} and ν_{soot} are the number of moles of carbon monoxide and carbon atoms in soot produced per unit mole of fuel consumed, and ν_{O_2} is the corresponding number of moles of oxygen consumed. In FDS 4, ν_{co} and ν_{soot} are prescribed by users from empirical or experimental data, instead of being solved. More advanced models for CO and soot formulation are presented in [35, 36]. However, in FDS 5, a different framework of the combustion model is adopted which provides enhanced descriptions of CO and soot. But first the combustion model in FDS4 will be reviewed, which adopts mixture fraction as the main variable. The mixture fraction is defined as the mass fraction of carbon mass:

$$Z = Y_{C_nH_m} + (\frac{W_{C_nH_m}}{nW_{CO_2}})Y_{CO_2} + (\frac{W_{C_nH_m}}{nW_{CO}})Y_{CO} + (\frac{W_{C_nH_m}}{nW_{soot}})Y_{soot} \quad (2.2)$$

where Y_k and W_k are the mass fraction and molecular weight of species k. Mixture fraction is a conserved scalar representing the fraction of material at a given point that originated as fuel. All species mass fraction in the system can be derived from the mixture fraction Z using the so-called "state relations", as shown in Fig 2.1.

Mixture fraction satisfies the following turbulent mixing equation:

$$\frac{\partial}{\partial t}(\bar{\rho}\tilde{Z}) + \frac{\partial}{\partial x_i}(\bar{\rho}\tilde{u}_i\tilde{Z}) = \frac{\partial}{\partial x_i}(\bar{\rho}\frac{\nu_t}{Sc_t}\frac{\partial \tilde{Z}}{\partial x_i}) \quad (2.3)$$

where ν_t is the turbulent viscosity, Sc_t the turbulent Schimdt number. In FDS4,

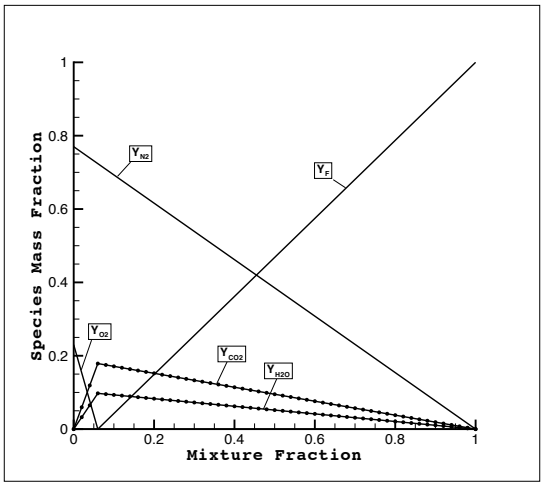

Figure 2.1: State relations (with propane as fuel)

the heat release rate is calculated from a classical flamelet expression:

$$\bar{\dot{\omega}}_F = -(\frac{Y_F^{\infty}}{1 - Z_{st}})(\frac{1}{2}\bar{\rho}\tilde{\chi}_{st})\tilde{p}(Z_{st}) \times \Delta H_F \tag{2.4}$$

where Y_F^{∞} is the fuel mass fraction in the fuel supply stream, Z_{st} is the stoichiometric value of mixture fraction, $\tilde{\chi}_{st}$ is the LES-filtered scalar dissipation rate (Favre-averaged along the subgrid-scale flame surface contour $Z = Z_{st}$), $\bar{\rho}$ is the LES-filtered mass density, ΔH_F is the heat of combustion per unit mass of fuel, and $\tilde{p}(Z_{st})$ is the stoichiometric value of the probability density function for subgrid-scale fluctuations in mixture fraction Z.

Here additional information is needed to describe $\tilde{\chi}_{st}$ and $\tilde{p}(Z_{st})$. First it can be assumed that $\tilde{\chi}_{st}$ is approximated by the unconditional scalar dissipation rate $\tilde{\chi}$. $\tilde{\chi}_{st}$ gives a measure of the turbulent rate of fuel-air mixing and a simple closure

model for this quantity is [71]:

$$\tilde{\chi}_{st} = 2(\frac{\nu_t}{Sc_t})|\nabla \tilde{Z}|^2 \tag{2.5}$$

$\tilde{p}(Z_{st})$ is a measure of the local probability of presence of the flame. A β-pdf model of $\tilde{p}(Z_{st})$ is explored in Ref. [37] to model non-premixed combustion in FDS4. Here a simple δ-Pdf model is adopted:

$$\tilde{p}(Z_{st}) = \delta(\tilde{Z} - Z_{st}) \tag{2.6}$$

in which the subgrid-scale variations in mixture fraction are neglected. So finally the LES-filtered heat release rate per unit volume can be expressed as:

$$\overline{\dot{q}_d'''} = (\frac{Y_F^\infty}{1 - Z_{st}})(\bar{\rho}\frac{\nu_t}{Sc_t}|\nabla \tilde{Z}|^2)\delta(\tilde{Z} - Z_{st}) \times \Delta H_F \tag{2.7}$$

In FDS5, the framework of the combustion model is changed to a two-variable formulation. The mixture fraction is then decomposed into two components from the global reaction R1 (see Eq.(2.1)):

$$\begin{aligned} Z_1 &= Y_{C_nH_m} \\ Z_2 &= (\frac{W_{C_nH_m}}{nW_{CO_2}})Y_{CO_2} + (\frac{W_{C_nH_m}}{nW_{CO}})Y_{CO} + (\frac{W_{C_nH_m}}{nW_{soot}})Y_{soot} \\ Z &= Z_1 + Z_2 \end{aligned} \tag{2.8}$$

where Z_1 represents the carbon mass fraction contained in the fuel, Z_2 represents the carbon mass fraction contained in CO_2, CO and soot. Again the entire mixture composition can be derived from the knowledge of Z_1 and Z_2 via state relationships.

The governing equations for Z_1 and Z_2 are:

$$\begin{aligned}
\frac{\partial}{\partial t}(\bar{\rho}\tilde{Z}_1) + \frac{\partial}{\partial x_i}(\bar{\rho}\tilde{u}_i\tilde{Z}_1) &= \frac{\partial}{\partial x_i}(\bar{\rho}\frac{\nu_t}{Sc_t}\frac{\partial \tilde{Z}_1}{\partial x_i}) - \overline{\dot{\omega}'''_{R1}} \\
\frac{\partial}{\partial t}(\bar{\rho}\tilde{Z}_2) + \frac{\partial}{\partial x_i}(\bar{\rho}\tilde{u}_i\tilde{Z}_2) &= \frac{\partial}{\partial x_i}(\bar{\rho}\frac{\nu_t}{Sc_t}\frac{\partial \tilde{Z}_2}{\partial x_i}) + \overline{\dot{\omega}'''_{R1}}
\end{aligned} \tag{2.9}$$

where $\overline{\dot{\omega}'''_{R1}}$ is the mass reaction rate of the global combustion reaction ($R1$). In FDS5, combustion is treated using a closure expression known as the Eddy Dissipation Concept model [45]:

$$\begin{aligned}
\overline{\dot{\omega}'''_{R1}} &= \bar{\rho} \times \frac{min(\tilde{Y}_F; \tilde{Y}_{O_2}/r_s)}{\tau} \\
\overline{\dot{q}'''_d} &= \overline{\dot{\omega}'''_{R1}} \times \Delta H_F
\end{aligned} \tag{2.10}$$

where r_s is the stoichiometric oxygen-to-fuel mass ratio, τ is a characteristic combustion time scale. In recent update of FDS version 5, τ is set to be $\frac{\Delta^2}{\nu_t}$, Δ is FDS computational grid size, ν_t is turbulent viscosity. This expression assumes that combustion is fast, so the burning rate depends on the mixing rate. Species mass fractions are calculated directly from the solution of Z_1, Z_2:

$$\begin{aligned}
Y_F &= Z_1 \\
Y_{N_2} &= (1 - Z_1 - Z_2)Y^{\infty}_{N_2} \\
Y_{O_2} &= (1 - Z_1 - Z_2)Y^{\infty}_{O_2} - \frac{\nu_{O_2}W_{O_2}}{W_{C_nH_m}}Z_2 \\
Y_{CO_2} &= \frac{\nu_{CO_2}W_{CO_2}}{W_{C_nH_m}}Z_2 \\
Y_{H_2O} &= \frac{\nu_{H_2O}W_{H_2O}}{W_{C_nH_m}}Z_2 \\
Y_{CO} &= \frac{\nu_{CO}W_{CO}}{W_{C_nH_m}}Z_2 \\
Y_{soot} &= \frac{\nu_{soot}W_{soot}}{W_{C_nH_m}}Z_2
\end{aligned} \tag{2.11}$$

An optional diffusion flame extinction model is also available in FDS4/FDS5 to account for quenching by oxygen starvation in under-ventilated fires. The diffusion flame extinction model starts from recognizing the importance of air vitiation effects in smoke-filling enclosure fires. The reduction in flame strength resulting from smoke-air mixing is incorporated into the model via the introduction of a flame extinction factor FEF, so that the above expressions for the heat release rate are modified as:

$$\overline{\dot{q}'''_{d,ex}} = \overline{\dot{q}'''_{d}} \times (1 - FEF) \tag{2.12}$$

where FEF is the locally-defined probability of finding active flame elements in a given LES computational grid cell: $FEF = 0$ corresponds to a fully burning flame, while $FEF = 1$ corresponds to a fully extinguished flame.

The model formulation for FEF starts from a classical Burke-Schumann flamelet temperature model assuming a constant c_p:

$$T_{st} = T_1 \frac{Y_{O_2,2}}{r_s Y_{F,1} + Y_{O_2,2}} + T_2 \frac{r_s Y_{F,1}}{r_s Y_{F,1} + Y_{O_2,2}} + \frac{\Delta H_F}{c_p} \frac{Y_{F,1} Y_{O_2,2}}{r_s Y_{F,1} + Y_{O_2,2}} \tag{2.13}$$

where T_1 and T_2 are the temperatures in the fuel and oxidizer streams feeding the flame, $Y_{F,1}$ and $Y_{O_2,2}$ the mass fractions of fuel and oxygen in those feeding streams, r_s the stoichiometric oxygen-to-fuel mass ratio, and c_p the specific heat of the reactive mixture at constant pressure. The first two terms on the right-hand-side (RHS) of Eq.(2.13) accounts for mixing, while the last term accounts for combustion. Assuming that the fuel stream temperature T_1 and fuel mass fraction $Y_{F,1}$ are constant, the flame temperature reduces to a function of the oxidizer stream properties $Y_{O_2,2}$

and T_2.

Next, the concept of a critical flame temperature T_c and that of a lower oxygen limit $Y_{O_2,c}$ are introduced. T_c is the minimum temperature that can sustain a flame, here $T_c \approx 1,700K$ is used from [3] as the critical stoichiometric flame temperature in Eq.(2.13). The lower oxygen limit $Y_{O_2,c}$ is defined as the limiting value of the oxygen mass fraction that corresponds to burning in normal temperature ($T_2 = T_\infty$) diluted air. It is shown in Refs. [67, 68] that $Y_{O_2,c} \approx 0.17$. The condition that relates the critical flame temperature and lower oxygen limit can be expressed:

$$T_c = T_\infty \frac{Y_{O_2,c}}{r_s Y_{F,1} + Y_{O_2,c}} + T_\infty \frac{r_s Y_{F,1}}{r_s Y_{F,1} + Y_{O_2,c}} + \frac{\Delta H_F}{c_p} \frac{Y_{F,1} Y_{O_2,c}}{r_s Y_{F,1} + Y_{O_2,c}} \tag{2.14}$$

where assuming $T_1 = T_\infty$. Eq.(2.14) yields:

$$\frac{\Delta H_F}{c_p} = \frac{r_s Y_{F,1} + Y_{O_2,c}}{Y_{F,1} Y_{O_2,c}} (T_c - T_\infty) \tag{2.15}$$

Combining Eqs.(2.15) and (2.13), that gives the alternative expression of the stoichiometric flame temperature with the combustion term expressed in terms of T_c and $Y_{O_2,c}$:

$$T_{st} = T_\infty \frac{Y_{O_2,2}}{r_s Y_{F,1} + Y_{O_2,2}} + T_2 \frac{r_s Y_{F,1}}{r_s Y_{F,1} + Y_{O_2,2}} + \frac{r_s Y_{F,1} + Y_{O_2,c}}{Y_{F,1} Y_{O_2,c}} (T_c - T_\infty) \frac{Y_{F,1} Y_{O_2,2}}{r_s Y_{F,1} + Y_{O_2,2}} \tag{2.16}$$

After some algebraic manipulation, Eq.(2.16) can be simplified to:

$$T_{st} = T_c + (T_c - T_\infty) \frac{r_s Y_{F,1}}{r_s Y_{F,1} + Y_{O_2,2}} \left(\frac{Y_{O_2,2}}{Y_{O_2,c}} - \frac{(T_c - T_2)}{(T_c - T_\infty)} \right) \tag{2.17}$$

This expression can be used to construct a flammability diagram in terms of the vitiated air variables $Y_{O_2,2}$ and T_2 as shown in Fig 2.2. In this diagram, non-flammable (flammable) conditions correspond to sub-critical (super-critical) flame temperatures, *i.e.* flame temperatures such that $T_{st} \leq T_c$ ($T_{st} \geq T_c$), or

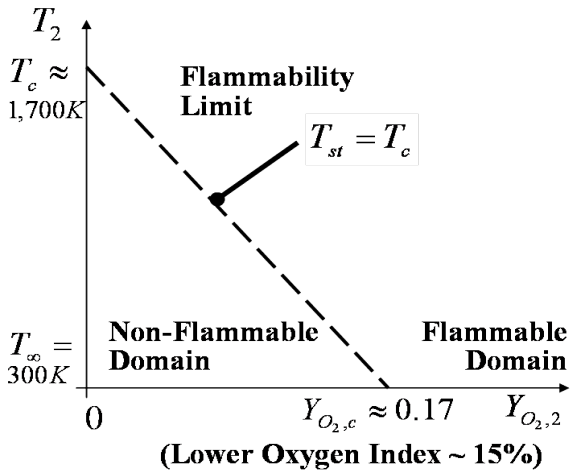

Figure 2.2: Flammability diagram in terms of the vitiated air properties $Y_{O_2,2}$ and T_2

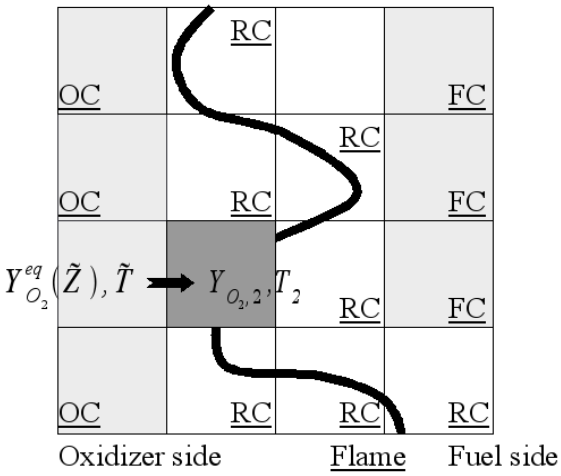

Figure 2.3: Numerical search algorithm for vitiated air conditions

$$\frac{(T_c - T_2)}{(T_c - T_\infty)} - \frac{Y_{O_2,2}}{Y_{O_2,c}} \geq 0 \qquad (\leq 0) \tag{2.18}$$

So the following definition of the flame extinction factor FEF is proposed:

$$FEF = H(\frac{(T_c - T_2)}{(T_c - T_\infty)} - \frac{Y_{O_2,2}}{Y_{O_2,c}}) \tag{2.19}$$

where H is the Heaviside function,

$$H(x) = 1 \quad if \quad x \geq 0$$

$$H(x) = 0 \quad if \quad x \leq 0$$

(2.20)

Eq.(2.19) is a closure model for FEF, provided that the variables $Y_{O_2,2}$ and T_2 are known. In FDS, these two variables are determined based on a search algorithm applied to any computational grid cell where heat release is taking place, as can be seen in Fig 2.3. The search algorithm interrogates neighboring cells and identifies among them the cells that are both non-reacting ($\bar{\dot{q}}_d''' = 0$) and located on the lean side of the flame ($\tilde{Z} \leq Z_{st}$); the LES grid-resolved oxygen mass fraction and temperature in those oxidizer cells are then used to estimate the vitiated air conditions at the LES flame location. Thus,

$$\overline{\dot{q}_{d,ex}'''} = \overline{\dot{q}_d'''} \times (1 - FEF) \tag{2.21}$$

provides an extended HRR model for cases with flame extinction. This flame extinction model along with FDS4 are used to model under-ventilated compartment fires in Refs. [35, 39], and the two-variable combustion model proposed in FDS5 along with this extinction model are adopted in Ref. [36] to study CO/soot emissions in under-ventilated compartment fires.

2.2 Deflagration modeling for premixed combustion

A classical model for premixed combustion is based on the concept of a reaction progress variable c: $c = 0$ in the fresh reactants (upstream of the flame), $c = 1$ in the burnt products (downstream of the flame), and the flame is the region where c goes

from 0 to 1 [72, 86, 91]. The c variable can be defined starting from the following reaction:

$$C_nH_mO_p + (n + \frac{m}{4} - \frac{p}{2})O_2 \longrightarrow nCO_2 + \frac{m}{2}H_2O \tag{2.22}$$

where $C_nH_mO_p$ represents the gaseous fuel (also noted F). Assuming equal molecular diffusion coefficients, the reaction progress variable is:

$$c = \frac{(Y_F^u - Y_F)}{(Y_F^u - Y_F^b)} = \frac{(Y_{O_2}^u - Y_{O_2})}{(Y_{O_2}^u - Y_{O_2}^b)} = \frac{Y_{CO_2}}{Y_{CO_2}^b} = \frac{Y_{H_2O}}{Y_{H_2O}^b} \tag{2.23}$$

where Y_k is the mass fraction of species k, Y_k^u the value of Y_k in the unburnt gas, and Y_k^b the value of Y_k in the burnt gas. Y_k^u is an input quantity to the combustion problem that characterizes the initial state of the reactive mixture (prior to combustion); Y_k^b is a quantity that characterizes the final mixture composition and that may be obtained from equilibrium thermodynamics.

The reaction progress variable framework is general and flexible, and it has been adapted to a LES treatment of propagating turbulent flames [4, 5, 6, 11, 31, 32, 43, 44, 83]. The treatment is based on a transport equation for the LES-filtered reaction progress variable $\tilde{c}$, and flame propagation is described via the LES-resolved $\tilde{c}$-field variations. Starting from the classical balance equation for c [72, 86, 91]:

$$\frac{\partial}{\partial t}(\rho c) + \frac{\partial}{\partial x_i}(\rho u_i c) = \frac{\partial}{\partial x_i}(\rho D \frac{\partial c}{\partial x_i}) + \dot{\omega}_c \tag{2.24}$$

where ρ is the mass density, u_i the x_i-component of the flow velocity vector, D the mass molecular diffusion coefficient, and $\dot{\omega}_c$ the reaction rate (the mass of product formed by combustion, per unit time and per unit volume). Applying a LES filter

treatment to Eq.(2.24) gives:

$$\frac{\partial}{\partial t}(\bar{\rho}\tilde{c}) + \frac{\partial}{\partial x_i}(\bar{\rho}\tilde{u}_i\tilde{c}) = -\frac{\partial}{\partial x_i}(\overline{\rho u_i c} - \bar{\rho}\tilde{u}_i\tilde{c}) + \frac{\partial}{\partial x_i}(\overline{\rho D\frac{\partial c}{\partial x_i}}) + \bar{\dot{\omega}}_c \tag{2.25}$$

where the over-bar symbol denotes straight LES-filtered quantities, and the tilde symbol denotes Favre-weighted LES-filtered quantities. The first term on the RHS of Eq.(2.25) represents convective transport of c due to subgrid-scale turbulent fluctuations; the second term represents transport of c due to molecular diffusion; and the last term represents production of c due to chemical reaction. These three terms require three closure models, which are proposed in Refs. [5, 6] and will be reviewed herein. The convective transport terms can be described using the turbulent eddy viscosity concept and assuming gradient-transport:

$$(\overline{\rho u_i c} - \bar{\rho}\tilde{u}_i\tilde{c}) = -\bar{\rho}\frac{\nu_t}{Sc_t}\frac{\partial \tilde{c}}{\partial x_i} \tag{2.26}$$

While the contribution of molecular diffusion is expected to be small in flame regions where the turbulence intensity is high, this contribution will be significant, and possibly dominant, in regions where the turbulence intensity is low. The closure model for the molecular transport of c is proposed as [5, 6]:

$$\overline{\rho D\frac{\partial c}{\partial x_i}} = \frac{\rho_u s_L \Delta_c}{16\sqrt{6/\pi}}\frac{\partial \tilde{c}}{\partial x_i} \tag{2.27}$$

where Δ_c is the LES filter size, s_L the laminar flame speed. This model meets the realizability requirement that under laminar flow conditions ($\nu_t = 0$ and $\Xi = 1$ which will be described below), the flame propagates at the laminar flame speed s_L.

A classical flamelet viewpoint is also adopted in which the chemical reaction term is written as the product of a laminar-like reaction rate per unit flame surface area times a flame surface density:

$$\bar{\dot{\omega}}_c = (\rho_u s_L) \times \Sigma \tag{2.28}$$

where ρ_u is the unburnt gas mass density, s_L the laminar flame speed, and Σ the LES-filtered flame surface-to-volume ratio (in units of $1/m$). In previous work [4, 5, 6, 11, 31, 32, 43], it is proposed to write Σ as:

$$\Sigma = \Xi \times \sqrt{\frac{6}{\pi}} \frac{\tilde{c}(1-\tilde{c})}{\Delta_c} \tag{2.29}$$

where Ξ is the subgrid-scale flame wrinkling factor ($\Xi \geq 1$). While elaborate closure model expressions have been proposed in previous work [12, 13], in current work Ξ will be chosen as a model constant.

Adopting the previous 3 closure models, the balance equation for c features a classical convection-diffusion-reaction structure and reduces to:

$$\frac{\partial}{\partial t}(\bar{\rho}\tilde{c}) + \frac{\partial}{\partial x_i}(\bar{\rho}\tilde{u}_i\tilde{c}) = \frac{\partial}{\partial x_i}((\bar{\rho}\frac{\nu_t}{Sc_t} + \frac{\rho_u s_L \Delta_c}{16\sqrt{6/\pi}})\frac{\partial \tilde{c}}{\partial x_i}) + (\rho_u s_L)\Xi \times 4\sqrt{\frac{6}{\pi}}\frac{\tilde{c}(1-\tilde{c})}{\Delta_c} + \bar{\dot{\omega}}_{ign} \tag{2.30}$$

where $\bar{\dot{\omega}}_{ign}$ is a spatially- and temporally-localized extra source term that will be used to describe ignition. The corresponding expression for the LES-filtered fuel mass reaction rate is:

$$\overline{\dot{\omega}_p'''} = (4\rho_u s_L \Xi \sqrt{\frac{6}{\pi}}\frac{\tilde{c}(1-\tilde{c})}{\Delta_c} + \bar{\dot{\omega}}_{ign}) \times (Y_F^u - Y_F^b) \tag{2.31}$$

where Y_F^u is the value of the fuel mass fraction in the unburnt gas, and Y_F^b its value in the burnt gas. Y_F^u is an input quantity to the combustion problem that characterizes the pre-combustion state of the reactive mixture; Y_F^b is a quantity that characterizes the post-premixed-flame state. Upstream of the deflagration front, $\tilde{c} = 0$ and the mixture composition corresponds to the pure mixing solution, $Y_F = Y_F^u(\tilde{Z})$, with $\tilde{Z}$ the mixture fraction, whereas downstream of the deflagration front, $\tilde{c} = 1$ and the mixture composition may be approximated by the classical Burke-Schumann equilibrium solution, $Y_F = Y_F^b(\tilde{Z})$. Assuming that the fuel mass fraction is equal to 1 in the fuel supply stream, we can write:

$$\begin{aligned} (Y_F^u - Y_F^b) &= \tilde{Z} \quad if \quad \tilde{Z} \leq Z_{st} \\ (Y_F^u - Y_F^b) &= (1 - \tilde{Z}) \times \frac{Z_{st}}{1 - Z_{st}} \quad if \quad \tilde{Z} \geq Z_{st} \end{aligned} \tag{2.32}$$

For FDS 5, in the case of a pure premixed combustion regime, the premixed combustion source term given by Eq.(2.31) is simply added to the Z_1 and Z_2 conservation equations in Eq.(2.9); in the case of a partially-premixed combustion regime, the formulation requires additional considerations as will be described in the next section.

2.3 Partially premixed combustion

This section describes the coupling of the above premixed and non-premixed combustion models so that scenarios that feature both combustion modes can be treated. For instance, if mixing is fast and/or the duration of mixing is long enough,

the size of the flammable cloud in the fire room will be large, and premixed combustion will be the dominant mode of combustion. In contrast, if mixing is slow and/or the duration of mixing is short, the size of the flammable cloud will remain small, the fire room will essentially be filled with an ultra-rich fuel-air mixture; while premixed combustion will start as the dominant mode of combustion during the deflagration stage, a transition to non-premixed combustion will be observed soon after. The goal here is to extend the FDS modeling capability to a treatment of the simultaneous or sequential occurrence of both premixed and non-premixed combustion.

First of all, an extension of the filtered-c model to the case of non-homogeneous fuel-air mixtures is required to describe the variations of the laminar flame speed s_L with fuel-air ratio, and provide a corresponding description of the fuel-air mixture flammability limits. The variation of s_L with $\tilde{Z}$ may be obtained from experimental measurements, or from numerical calculations of the inner structure of laminar premixed flames, using detailed description of chemical kinetics and molecular transport [85, 86, 91]. Here a convenient alternative is proposed using an *ad-hoc* analytical expression parametrized in terms of four input variables, Z_{LFL}, Z_{UFL}, Z_{st} and $s_{L,st}$. Z_{LFL} and Z_{UFL} are the values of Z at the lower and upper flammability limits; Z_{st} and $s_{L,st}$ are the stoichiometric values of Z and s_L. A piecewise second-order polynomial function is presented in Fig 2.4, with the constraints that s_L vanishes at Z_{LFL}, Z_{UFL}, is maximum at Z_{st} and features a peak value equal to $s_{L,st}$. It is

formulated as:

$$s_L = s_{L,st} \times (1 - (\frac{(Z_{st} - Z)}{(Z_{st} - Z_{LFL})})^2) \quad if \quad Z_{LFL} \leq Z \leq Z_{st}$$
$$s_L = s_{L,st} \times (1 - (\frac{(Z - Z_{st})}{(Z_{UFL} - Z_{st})})^2) \quad if \quad Z_{st} \leq Z \leq Z_{UFL}$$

(2.33)

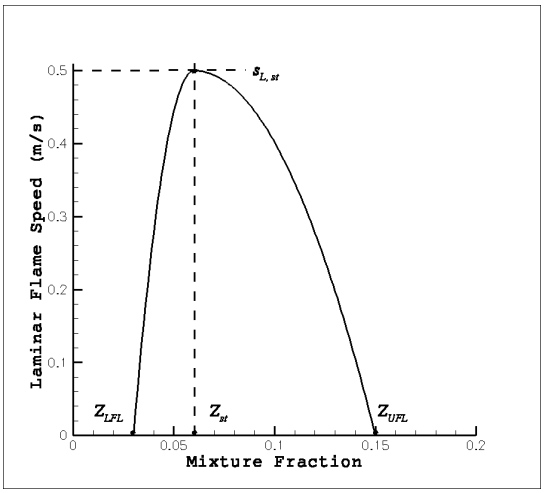

Figure 2.4: Variations of laminar flame speed with mixture fraction (methane as the fuel)

This is an ad-hoc treatment based on experimental study by Zhu et al [96]. Furthermore, the s_L algorithm can be extended by making s_L a function of the unburnt gas temperature T_u as well as bulk pressure $\bar{p}$, as described in [84].

$$\begin{aligned} s_L &= s_{L,ref}(\frac{T_u}{T_{u,ref}})^{\gamma}(\frac{\bar{p}}{\bar{p}_{ref}})^{\beta} \\ \gamma &= 2.18 - 0.8(\phi - 1) \end{aligned}$$

$$\begin{aligned} \beta &= -0.16 + 0.22(\phi - 1) \\ \phi &= \frac{1 - Z_{st}}{Z_{st}} \times \frac{\tilde{Z}}{1 - \tilde{Z}} \end{aligned} \tag{2.34}$$

where $T_{u,ref} = 298$ K, $\bar{p}_{ref} = 101325$ Pa, $s_{L,ref}$ is the value of s_L that is obtained at normal temperature and pressure conditions, and is a function of Z as shown in Fig 2.4. γ and β are model coefficients that are functions of the local equivalence ratio ϕ, and ϕ can be derived from the local mixture fraction Z as given in Eq.(2.34). This expression of s_L is adopted in the simulation of explosive combustion in Chapters 5 and 7. A test of this modification will be shown in the 2-D tunnel flame propagation in Appendix B.

The filtered-c model equations are now simply modified as follows:

$$\frac{\partial}{\partial t}(\bar{\rho}\tilde{c}) + \frac{\partial}{\partial x_i}(\bar{\rho}\tilde{u}_i\tilde{c}) = \frac{\partial}{\partial x_i}\left((\bar{\rho}\frac{\nu_t}{Sc_t} + \frac{\rho_u s_L(\tilde{Z}, T_u, \bar{p})\Delta_c}{16\sqrt{6/\pi}})\frac{\partial \tilde{c}}{\partial x_i}\right) + (\rho_u s_L(\tilde{Z}, T_u, \bar{p}))\Xi \times 4\sqrt{\frac{6}{\pi}}\frac{\tilde{c}(1-\tilde{c})}{\Delta_c} + \bar{\dot{\omega}}_{ign} \tag{2.35}$$

$$\overline{\dot{q}'''_p} = (\Xi \times 4\rho_u s_L(\tilde{Z}, T_u, \bar{p})\sqrt{\frac{6}{\pi}}\frac{\tilde{c}(1-\tilde{c})}{\Delta_c} + \bar{\dot{\omega}}_{ign}) \times (Y_F^u - Y_F^b) \times \Delta H_F \tag{2.36}$$

where the variations of s_L, Y_F^m and Y_F^{eq} with fuel-air mixture composition are accounted for. Note that this extended model has the capability to differentiate between cases of successful ignition and misfires. For instance, if the numerical ignitor is located outside of the flammable region, $0 \leq \tilde{Z}_{ign} \leq Z_{LFL}$ or $Z_{UFL} \leq \tilde{Z}_{ign} \leq 1$ ($\tilde{Z}_{ign}$ is the value of mixture fraction at the ignitor location), the ignition source term $\bar{\dot{\omega}}_{ign}$ will succeed in establishing an ignition kernel but will fail in initiating a propagating flame, $s_L(\tilde{Z}_{ign}) = 0$. Under such conditions, after $\bar{\dot{\omega}}_{ign}$ is turned off, combustion will cease and the ignition kernel will simply mix and dissipate.

The non-premixed combustion models in FDS4 and FDS 5 are:

$$\overline{\dot{q}_d'''} = (\frac{Y_F^\infty}{1-Z_{st}})(\bar{\rho}\frac{\nu_t}{Sc_t}|\nabla\tilde{Z}|^2)\delta(\tilde{Z}-Z_{st})\times\Delta H_F\times(1-FEF) \quad (2.37)$$

$$\overline{\dot{q}_d'''} = \bar{\rho}\times\frac{min(\tilde{Y}_F;\tilde{Y}_{O_2}/r_s)}{\tau}\times\Delta H_F\times(1-FEF) \quad (2.38)$$

The premixed and non-premixed contributions to combustion will be coupled using the concept of a flame index [18]:

$$FI = \frac{1}{2}(\frac{\nabla\tilde{Y}_F\cdot\nabla\tilde{Y}_{O2}}{|\nabla\tilde{Y}_F|\times|\nabla\tilde{Y}_{O2}|}+1) \quad (2.39)$$

where $\tilde{Y}_F$ and $\tilde{Y}_{O2}$ are the LES grid-resolved fuel and oxygen mass fractions, which are obtained from Fig 2.1 in FDS 4 or Eq.(2.11) in FDS 5. FI is a non-dimensional field quantity that varies between 0 and 1; inert mixing between cross-diffusing fuel and air corresponds to $FI = 0$; a diffusion flame configuration in which fuel and air enter the chemical reaction zone from opposite directions also corresponds to $FI = 0$; in contrast, a premixed flame configuration in which fuel and air enter the chemical reaction zone from the same directions corresponds to $FI = 1$.

Using FI as a weight coefficient, a simple partially-premixed combustion model can now be proposed that describes the heat release rate as a weighted average between the premixed and non-premixed contributions [18]:

$$\overline{\dot{q}'''} = FI\times\overline{\dot{q}_p'''} + (1-FI)\times f_{ign}\times\overline{\dot{q}_d'''} \quad (2.40)$$

where f_{ign} is an *ad hoc* ignition factor. f_{ign} is introduced in Eq. (2.40) so that the

diffusion flame model remains inactive when inert mixing is taking place ($f_{ign} = 0$ when $\tilde{c} = 0$), and is only activated as a post-premixed flame event ($f_{ign} = 1$ when $\tilde{c} = 1$). As a first step, it is proposed that:

$$f_{ign} = \frac{1}{2} + \frac{1}{2} tanh(\frac{\tilde{c} - 0.6}{0.05}) \tag{2.41}$$

The above two equations correctly describe the two limiting cases that correspond to pure premixed or non-premixed combustion: premixed flames corresponds to $FI = 1$ and $\overline{\dot{q}'''} = \overline{\dot{q}'''_p}$, while non-premixed flames correspond to $FI = 0$, $f_{ign} = 1$ and $\overline{\dot{q}'''} = \overline{\dot{q}'''_d}$.

In FDS 5, the fuel mass reaction rate used in the Z_1 and Z_2 equations (Eq.(2.9)) is given by the expressions above and $\overline{\dot{\omega}'''_{R1}} = \overline{\dot{q}'''}/\Delta H_F$. Again, Z_1 and Z_2 solved in Eq.(2.9) will be used to calculate all species mass fraction as in Eq.(2.11).

Chapter 3

Flame Propagation Velocity in Tunnel Configurations with Closed or Open Boundaries

This chapter will discuss the performance as well as some limitations of the deflagration model in treating different scenarios corresponding to laminar flame propagation across a homogeneous fuel-air mixtures in 2D tunnels. Two cases are considered: a case in which the flame propagates from an open end toward a wall, and a case in which the flame propagates from a wall towards an open end. In the first case, the flame should propagate with an apparent velocity equal to the laminar flame speed s_L, whereas in the second case, the flame should propagate with a much larger apparent velocity equal to the product of s_L times a density ratio, as will be explained in detail in this chapter. In addition, extensions of the first case will also be investigated while the flame propagates towards opposing flow instead of a wall. In the last section the same configuration will both ends open will be used to evaluate the grid size requirement of the PPC model by conducting simulations of horizontal laminar flame propagation through vertically stratified flammable mixture, so as to provide insight into the grid requirement of the PPC model.

3.1 Overview

A series of simple tests are conducted here in configurations corresponding to 1-dimensional, plane, laminar, premixed flames that propagate along the x-direction, through a uniform methane-air stoichiometric mixture. The 2-D tunnel is 5 m $\times$ 1 m. In case 1 and case 2, the numerical boundary condition at $x = 0$ is a wall and it is open at $x = 5$, while in case 3 and 4 the boundary at $x = 0$ and $x = 5$ are both open. Case 1 corresponds to a scenario in which the flame propagates into quiescent gas towards a wall (Fig 3.1); case 2 corresponds to a scenario in which the flame propagates from a wall (Fig 3.2). In case 3, air is blown at $x = 0$ into the tunnel at the laminar flame speed $s_{L,st}$ to push against the incoming flame (Fig 3.3), while in case 4, the air flow is half of the laminar flame speed $s_{L,st}/2$. The air flow in case 3 and 4 is only blown after $t = 2$ s, and the first 2 seconds of the simulations are similar to case 1.

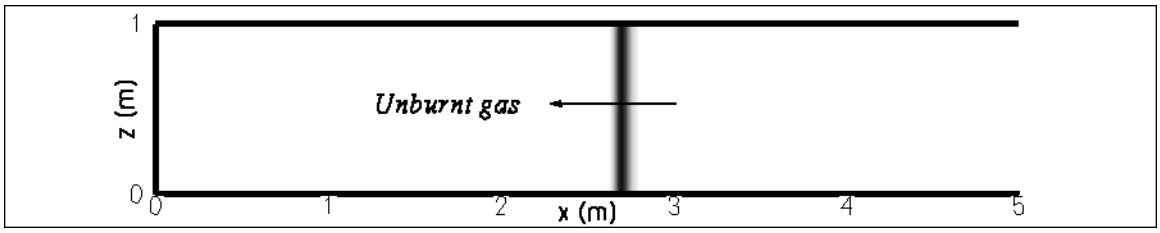

Figure 3.1: Tunnel configuration in case 1

The computational domain is the size of the tunnel (5 $\times$ 1)m^2, while the computational grid corresponds to a uniform rectangular mesh of (250 $\times$ 50) grids, with a grid cell size $\Delta = 0.02$ m. At initial time, the methane-air mixture is at its

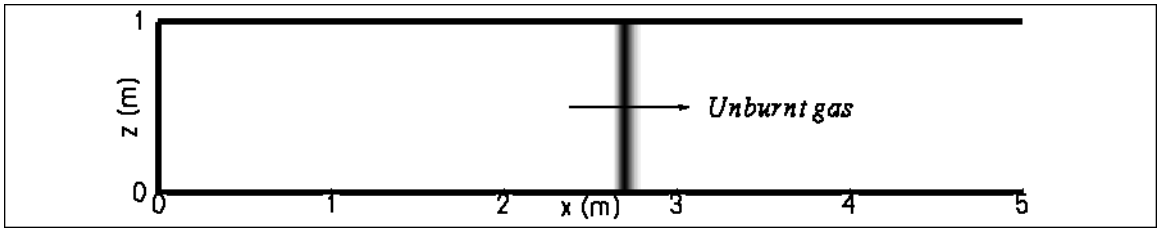

Figure 3.2: Tunnel configuration in case 2

stoichiometric ratio, assumed to be at rest and in a chemically frozen state ($\tilde{c} = 0$). Flame initiation is triggered by a numerical ignitor located at $x = 0$ m (case 2) or $x = 5$ m (case 1,3,4); this numerical ignitor is modeled as a spatially- and temporally-localized extra source term introduced into Eq.(2.30). The laminar flame speed is set to $s_L = s_{L,st} = 0.4$ m/s.

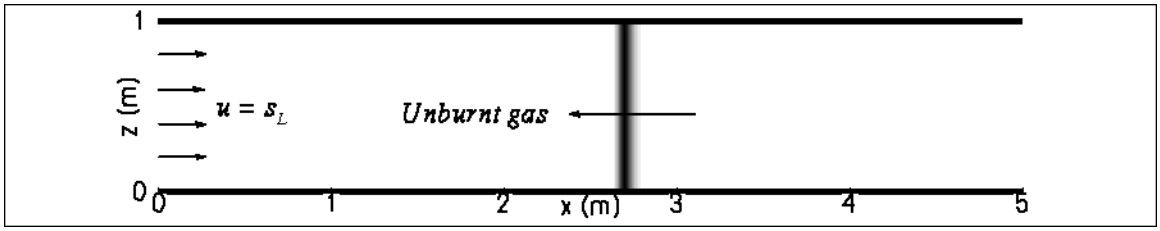

Figure 3.3: Tunnel configuration in case 3

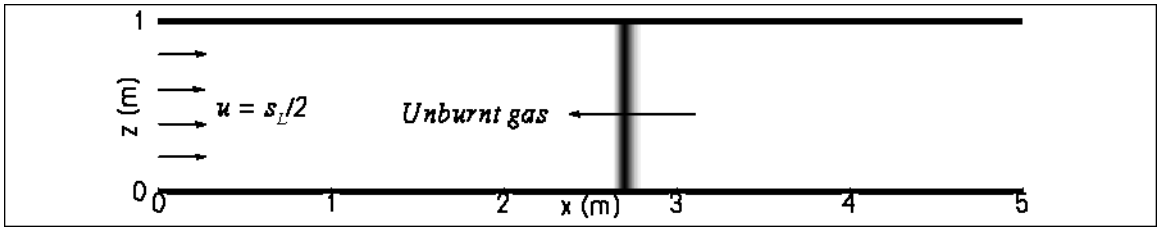

Figure 3.4: Tunnel configuration in case 4

3.2 Theoretical analysis

The diagnostic that will be used to interpret the numerical results is the apparent flame velocity fpv, defined as the velocity at which the flame propagates relative to the wall. In case 1 (Fig 3.5), u_u is the gas velocity in the unburnt stream, u_b the gas velocity in the burnt gas field, ρ_u is the density of cold unburnt gas, ρ_b is the density of hot burnt gas. fpv can be expressed as:

$$fpv = u_u - s_L \tag{3.1}$$

Also from mass conservation:

$$\rho_u s_L = \rho_b(u_b - fpv) \tag{3.2}$$

Recognize that here $u_u = 0$ because of wall, $s_L = -fpv$ applies considering that fpv points to negative direction, while s_L is the given laminar flame speed in terms of positive constant. u_b is in the positive direction as in Fig 3.5, so that Eq.(3.2) gives:

$$u_b = s_L(\frac{\rho_u}{\rho_b} - 1) \tag{3.3}$$

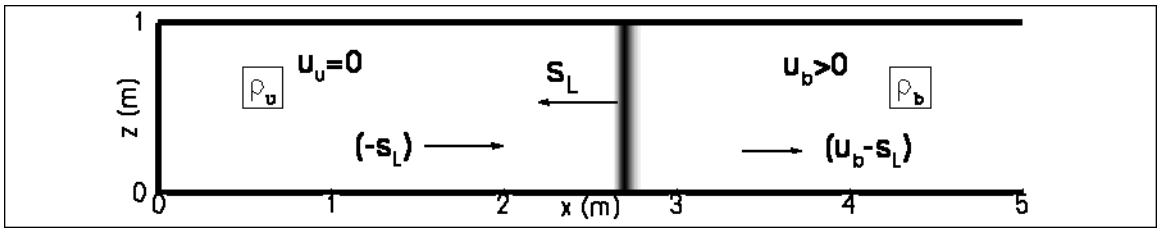

Figure 3.5: Illustration of theoretical velocity distribution in case 1

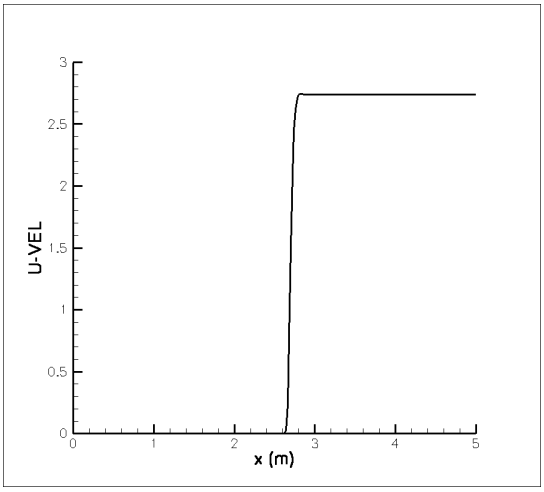

Figure 3.6: Flow velocity distribution in simulation of case 1

From the ideal gas law:

$$\frac{\rho_u}{\rho_b} = \frac{T_b}{T_u} \tag{3.4}$$

in which T_b is the post-flame temperature, which for methane is 2232 K, T_u is the fresh gas temperature, equals to 300 K

$$u_b = (\frac{T_b}{T_u} - 1)s_L \tag{3.5}$$

for methane, the laminar flame speed $s_L = 0.4$ m/s. So u_b is calculated to be about 2.576 m/s, which agrees with what the value of the flow velocity in the post-flame gas as seen in Fig 3.6 (2.7 m/s), with a 10% discrepancy, which is attributed to numerical errors accumulated during the flame propagation.

In case 2 (Fig 3.7), the relationship between the apparent flame velocity and laminar flame speed is

$$fpv = s_L + u_u \tag{3.6}$$

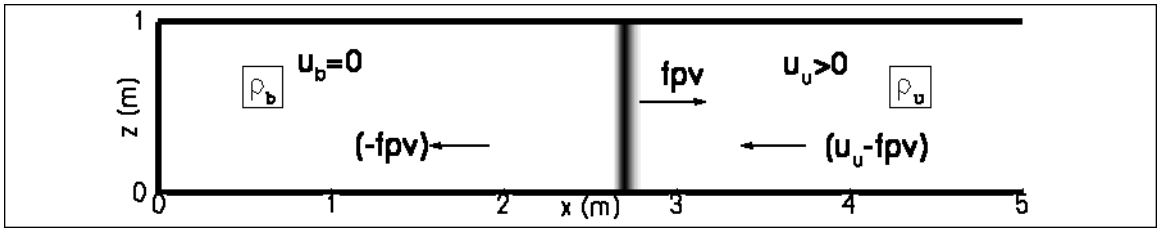

Figure 3.7: Illustration of theoretical velocity distribution in case 2

From the mass conservation upstream and downstream of flame:

$$\rho_u s_L = \rho_b f pv \tag{3.7}$$

which gives the apparent flame velocity

$$fpv = \frac{\rho_u}{\rho_b} s_L = \frac{T_b}{T_u} s_L \tag{3.8}$$

Eq.(3.8) predicts the apparent flame velocity to be around 2.976 m/s.

3.3 Numerical results

In the calculation, the apparent flame velocity is extracted from the simulation by recording the time variations of the total burned gas volume V_b:

$$V_b(t) = \iiint_V \tilde{c}(x, y, z, t) dx dy dz \tag{3.9}$$

where spatial integration is performed over the whole computational volume V. For case 1 in Fig 3.5, from mass conservation, one can write:

$$\rho_b \frac{dV_b}{dt} = \rho_u s_L S - \rho_b u_b S \tag{3.10}$$

where S is the cross section area of the tunnel. Consider Eq.(3.2), the above equation can be expressed as:

$$\frac{dV_b}{dt} = S \times (-fpv) \tag{3.11}$$

Note that fpv is negative in this case, as from Eq.(3.1). In case 2 when the flame is propagating away from the wall (Fig 3.7), the mass conservation can be written:

$$\rho_b \frac{dV_b}{dt} = \rho_b \times fpv \times S \tag{3.12}$$

which also gives Eq.(3.11). This suggests that the apparent flame propagation velocity fpv can be calculated from the time derivative of the volume of burnt gas:

$$fpv = \frac{1}{S}\frac{dV_b}{dt} \tag{3.13}$$

In case 1 the apparent flame propagation velocity should be equal to the laminar flame speed, and here it is found that $fpv = 0.44$ m/s (Fig 3.8), which corresponds to a 10% over-estimate, which may due to numerical errors which tend to accelerate the flame. Fig 3.8 also shows that fpv remains constant after the initial transient time, indicating that the flame is moving steadily. In contrast, for case 2, while the apparent flame propagation velocity is calculated theoretically to be 2.9 m/s, Fig 3.9 shows that although the flame starts propagating at around 2 m/s, it is accelerating and by the time that the flame goes out of the tunnel, it still has not reach the steady state. Here the flame goes out of the tunnel in less than 3 s. This result suggest a weakness in the model formulation that will need to be revised in future work.

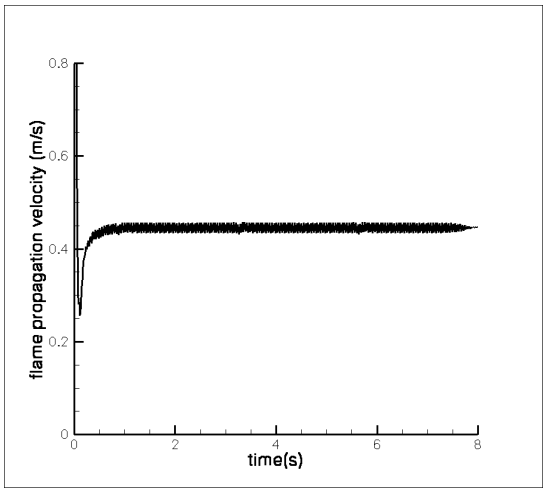

Figure 3.8: Time variations of the apparent flame propagation velocity fpv in case 1

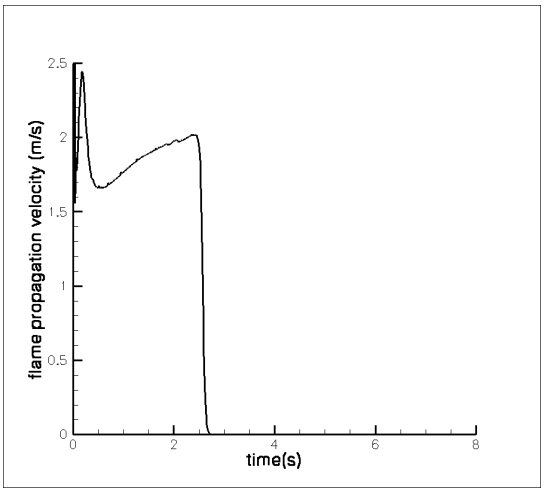

Figure 3.9: Time variations of the apparent flame propagation velocity fpv in case 2

In case 3 (Fig 3.10), the apparent flame propagation velocity jumps from $fpv \approx s_L$ at initial times to $fpv \approx 0$ after an opposing air flow has been activated. The peak in Fig 3.10 maybe explained by the noise generated when the entire flame is put to frozen (the delay of peak from flame propagation velocity dropped to zero is due to the certain thickness of flame). In case 4 (Fig 3.11), because the air flow velocity is half the laminar flame speed after 2 s, the flame is slowing down, and fpv drops to about 0.2 m/s, as expected.

3.4 Numerical requirement of grid size in PPC model

It has been determined in preliminary studies [87, 88, 89] that the thickness of the LES premixed flame needs to be resolved on the grid for a correct description of

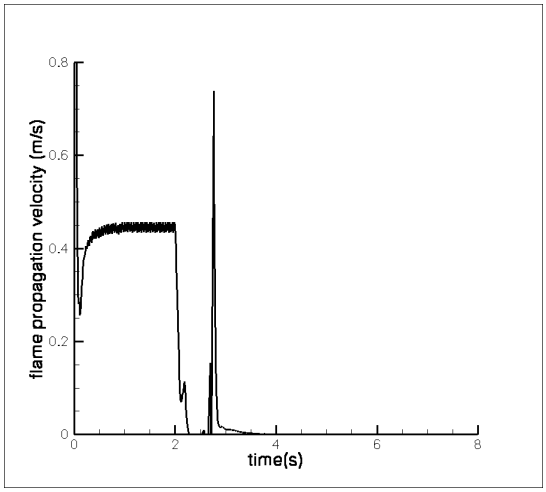

Figure 3.10: Time variations of the apparent flame propagation velocity fpv in case 3

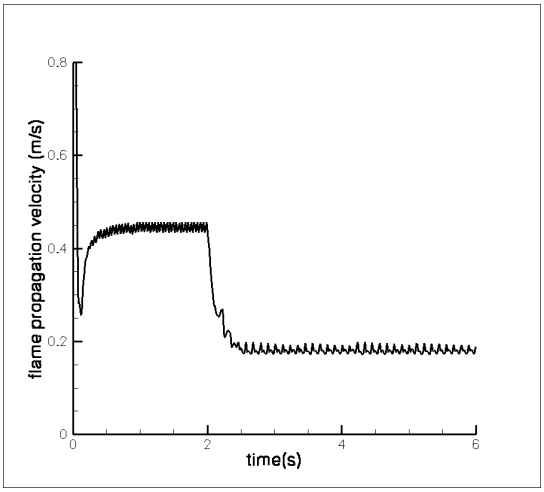

Figure 3.11: Time variations of the apparent flame propagation velocity fpv in case 4

deflagrations, and the requirement $\Delta_c/\Delta \geq 4$ has been established. Here grid resolution requirements are further studied in a two-dimensional configuration where the flame propagates perpendicular to a frozen vertical mixture fraction gradient. Here both ends of the tunnel are open, and the premixed flame propagates from one end to the other.

The initial mixture fraction distribution of methane and air is illustrated in Fig 3.12, from below the lower flammability limit of methane to above its upper flammability limit, and is prescribed as a simple function of elevation, as in Fig 3.13. The faint vertical white lines in Fig 3.12 are due to plots constructed from multi-processor data.

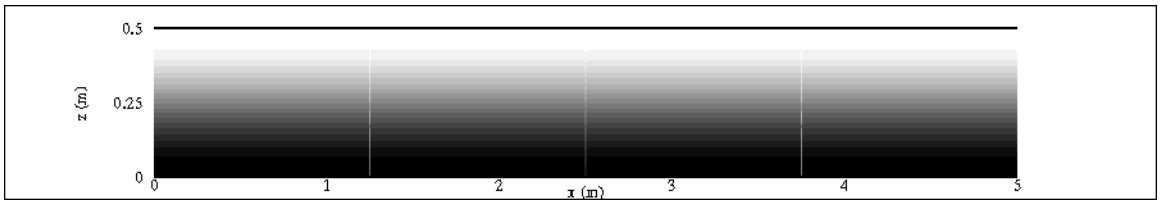

Figure 3.12: Vertically stratified mixture of methane and air in the tunnel

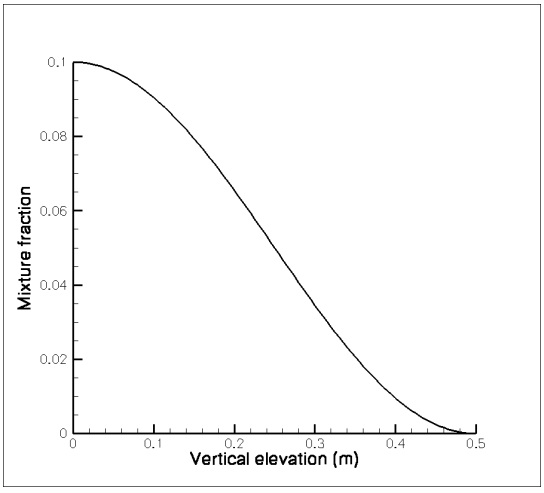

Figure 3.13: Prescribed mixture fraction distribution in the tunnel

A dimensionless number L_z/Δ_c is identified as the main parameters for the grid study here, L_z is the vertical thickness of the flammable gas layer, Δ_c is the LES filter size, $\Delta_c/\Delta = 5$. Five simulations are conducted with different values of the L_z/Δ_c parameter. The steady state values of the premixed combustion heat release rate are plotted in Fig 3.14 as a function of L_z/Δ_c.

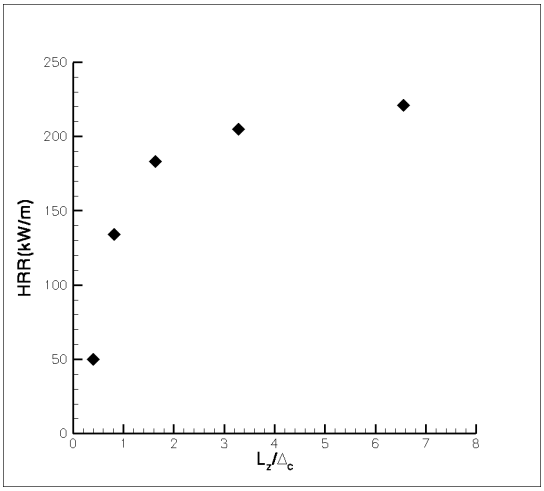

Figure 3.14: Grid requirement of PPC model in solving width/height of premixed flame

It is concluded from Fig 3.14 that the dimensionless number L_z/Δ_c needs to be at least 2 to achieve values of the burning intensity that are approximately grid-independent. This requirement is considered in Chapters 5 and 7 for the validation study of the PPC model. Fig 3.15 describes the flame shape and its propagation through the stratified mixture layer, this calculation corresponds to $L_z/\Delta_c = 3.6$. Since the gas now in the tunnel has mixture fraction ranging from below the lower flammability limit to above the upper flammability limit, and laminar flame speed

depends on mixture fraction in the deflagration model, the flame shape corresponds to a classical edge flame structure. 5 successive snapshots of the flame are shown from $t = 1$ to 9 seconds. By measuring the flame location as a function of time, the apparent flame is found to propagate steadily at 0.4 m/s.

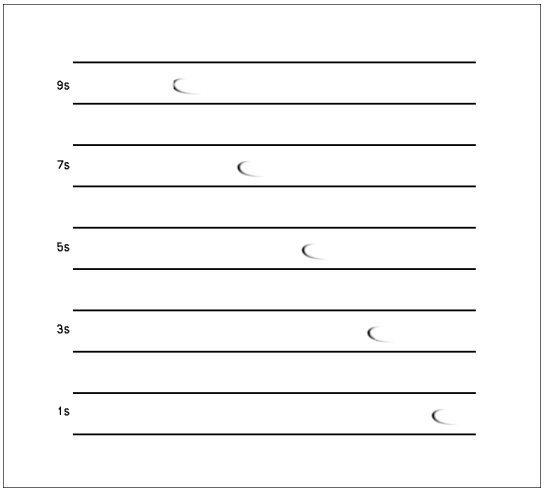

Figure 3.15: Instantaneous snapshots of the flame as it propagates from right to left through the stratified mixture - $L_z/\Delta_c = 3.6$

Chapter 4

Bulk Pressure Modeling

This chapter describes verification tests of the pressure algorithm available in FDS to calculate the averaged pressure in sealed or vented compartment fire configurations. It is found that an improved bulk pressure model is desired in vented compartment fire cases for the correct treatment. The bulk pressure model available in FDS currently (as derived in Appendix A1) has shown success in solving problems in sealed compartments. However, for compartments with open vents, or scenarios in which vents change from closed to open, this model is not correct. The calculation of the compartment bulk pressure is challenging because of numerical stiffness issues. A modified bulk pressure model is introduced in this chapter to help simulate compartments with open vents, that are initially open or are open at a prescribed time. A series of verification tests are performed to assess the original bulk pressure model in FDS and the modified model.

4.1 Model description

Start from the bulk pressure equation [57]:

$$\frac{d\bar{P}}{dt} = \frac{-\oint\!\!\!\!\!\!\diagup_{CS} \tilde{u}_j n_j dS + \iiint_{CV} \frac{\gamma-1}{\gamma\bar{p}}\left(\frac{\partial}{\partial x_i}\left(\bar{\rho}\frac{\nu_t}{Sc_t}c_p\frac{\partial\tilde{T}}{\partial x_i}\right) - \frac{\partial\overline{\dot{q}''_{R,j}}}{\partial x_i} + \overline{\dot{q}'''_c}\right)dV}{\iiint_{CV}\frac{dV}{\gamma\overline{P}}} \tag{4.1}$$

which is equivalent to the equation in Appendix A1. Here c_p is the specific heat (at constant pressure), γ the ratio of specific heats, $\tilde{T}$ the temperature, $\overline{\dot{q}''_{R,j}}$ the x_j-

component of the radiation heat flux vector (in units of W/m^2), $\overline{\dot{q}_c'''}$ the combustion heat release rate (W/m^3). The integral terms are calculated as volume integrals over the arbitrary control volume (CV, here the fire compartment), or surface integrals over its control surface (CS, n_j is the x_j-component of the unit vector normal to CS and pointing outward).

In the above equation, the term $-\oiint_{CS} \tilde{u}_j n_j dS$ represents the effects of convective transport across vents; an inflow of mass ($\tilde{u}_j n_j < 0$) tends to increase the compartment pressure, whereas an outflow ($\tilde{u}_j n_j > 0$) decreases it. The second term in the numerator of Eq.(4.1) denotes the effects of convective/radiative heat transfer across CS (predominantly wall losses) as well as those of combustion: wall losses tend to decrease the compartment pressure whereas combustion tends to increase it.

Because it is numerically stiff, Eq.(4.1) does not provide a suitable expression to calculate pressure in the case of vented compartments as will be discussed below. However, this dilemma can be bypassed by adopting a classical zone model strategy. Assuming steady state and using a Bernoulli expression for the outflow velocities,

$$\tilde{u}_j = (\frac{2\Delta\bar{P}_{eq}}{\bar{\rho}})^{1/2} \tag{4.2}$$

wherever $\tilde{u}_j n_j > 0$, with $\Delta\bar{P}_{eq} = (\bar{P} - P_\infty)$ the compartment over-pressure and P_∞ the external atmospheric pressure, one obtains:

$$\Delta\bar{P}_{eq} = \frac{-\oiint_{CS,\tilde{u}_j n_j<0} \tilde{u}_j n_j dS + \iiint_{CV} \frac{\gamma-1}{\gamma\bar{P}} (\frac{\partial}{\partial x_i}(\bar{\rho}\frac{\nu_t}{Sc_t}c_p\frac{\partial\tilde{T}}{\partial x_i}) - \frac{\partial\overline{\dot{q}''_{R,j}}}{\partial x_i} + \overline{\dot{q}_c'''})dV}{\oiint_{CS,\tilde{u}_j n_j>0}(\frac{2}{\bar{\rho}})^{1/2}dS} \tag{4.3}$$

where the surface integrals over the vent openings of CS are conditioned on inflow or outflow state. In scenarios where the compartment is first sealed, then a vent bursts open due to overpressure at time $t = t_0$, the following scheme is proposed:

(1) When $0 \leq t \leq t_0$, the bulk pressure $\bar{P}(t)$ is calculated according to Eq. (4.1);

(2) Store the value $\bar{P}(t = t_0)$ at the time of vent opening;

(3) For $t > t_0$, a ramp function is used to calculate the bulk pressure:

$$(\bar{P} - P_\infty) = (\bar{P}(t = t_0) - P_\infty) \times exp(-(t - t_0)/\tau) + \Delta\bar{P}_{eq} \times (1 - exp(-(t - t_0)/\tau)) \quad (4.4)$$

where τ is a relaxation time scale assumed to be fast (here we adopt $\tau = \Delta t$, the initial computational time step in FDS). It will be seen in the following section that this scheme provides a smooth transition from the ordinary differential equation model in Eq. (4.1) to the quasi-steady algebraic expression in Eq. (4.3) without numerical instabilities.

4.2 Evaluation of the modified pressure model

A verification test is done here to evaluate the performance of the proposed pressure model from the above section, along with the comparison with the performance of the original pressure model in FDS. The configuration is a 0.4 × 0.4 × 0.4m^3 cubic box, with a vent size 0.4 m × 0.1 m located at the base of one vertical wall, which can be closed or open, as shown in Fig 4.1. A square vent is located in the middle of the floor to blow air in at the rate of 2 g/s. The numerical grid is $40 \times 40 \times 40$, and the grid size is $\Delta = 1$ cm. The quantities of interest here include the vent flow rates and the bulk pressure.

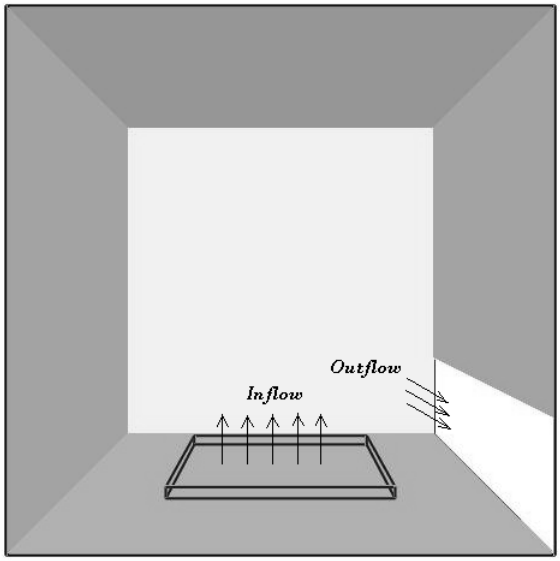

Figure 4.1: Compartment configuration for bulk pressure tests

In the following, 3 cases are considered: the first case has the outflow vent open from the beginning of the simulation; the second case has the outflow vent sealed during the entire simulation; the third case has the outflow vent open a few seconds after the start of the simulation; individually they are labeled as the open-vent case, the sealed-vent case and the shift-vent case. In the open-vent case, Fig 4.2 shows the calculated mass flow rates using the FDS pressure algorithm while Fig 4.3 shows the mass flow rates using the modified pressure algorithm; the inflow rate is the prescribed mass injected from the floor, the outflow rate is the mass going through the vertical vent (if the compartment is sealed, the outflow will be zero). In both figures, the rates of mass inflow and outflow balanced out. A slight delay with larger fluctuations before reaching steady state is observed in the mass outflow curve in Fig 4.2.

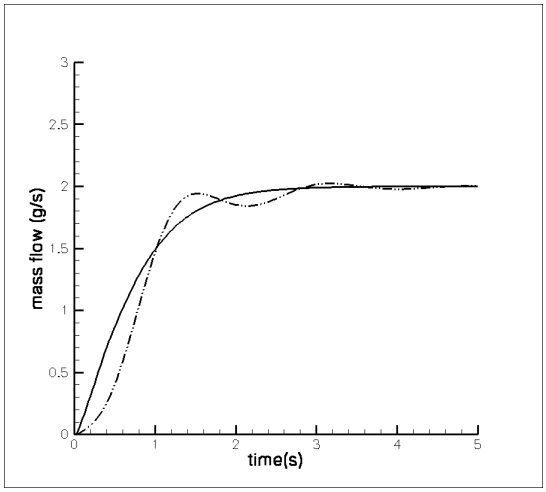

Figure 4.2: Mass inflow and outflow rates in the open-vent case using the FDS pressure algorithm: Inflow (solid), outflow (dashdot)

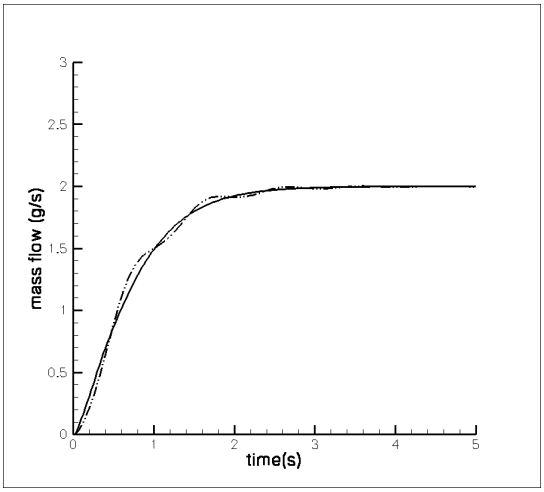

Figure 4.3: Mass inflow and outflow rates in the open-vent case using the modified pressure algorithm: Inflow (solid), outflow (dashdot)

Figs (4.4-4.5) show the corresponding time evolution of the bulk compartment pressure ($\bar{P} - P_\infty$) versus time. While the original FDS pressure algorithm gives a steady state over-pressure of 600 Pa, the modified algorithm calculates a much smaller steady state over-pressure. Considering that the vent is open from the very beginning of the simulation that the vent size is large and inflow rate is moderate, it is expected that the compartment over-pressure will be a fraction of 1 Pa. The results in Fig 4.4 are clearly incorrect.

The second case correspond to a case in which the outflow vent is closed, so in Fig 4.6 there is not outflow curve. The pressure evolution given by the FDS algorithm is in that case working correctly and predicts a linear increase of pressure

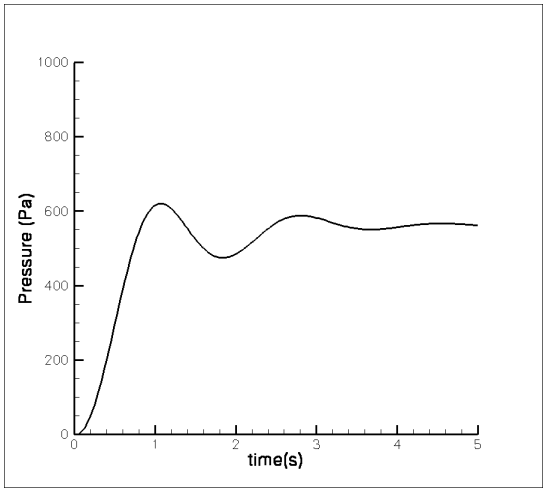

Figure 4.4: Time evolution of the bulk pressure in the open-vent case using the FDS pressure algorithm

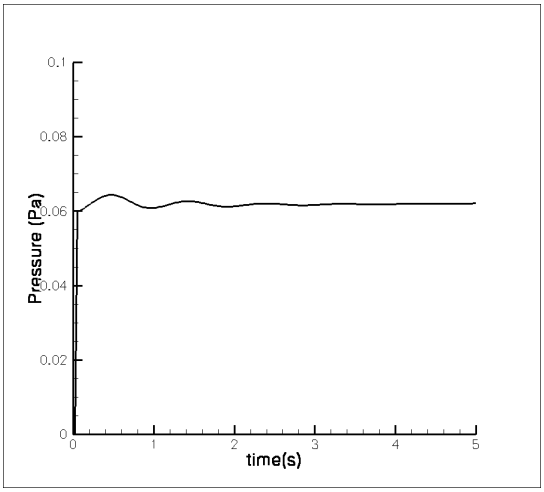

Figure 4.5: Time evolution of the bulk pressure in the open-vent case using the modified pressure algorithm

with time (see Fig 4.7). In this case, there is no modification from the original FDS pressure model.

In the third case the outflow vent is initially closed and becomes open after a time delay arbitrarily set at t = 1 s. This case features mass and pressure build up in the initial phase, followed by a transition to a constant mass and slight over-pressure regime.

In Fig 4.8 and 4.9, both algorithms predict a sharp increase of the mass outflow rate when the vent is open, followed by a relaxation to a mass balanced regime. The modified algorithm has a higher peak for the mass outflow rate. At transition, the original FDS pressure algorithm takes about 4 seconds for the pressure to drop from

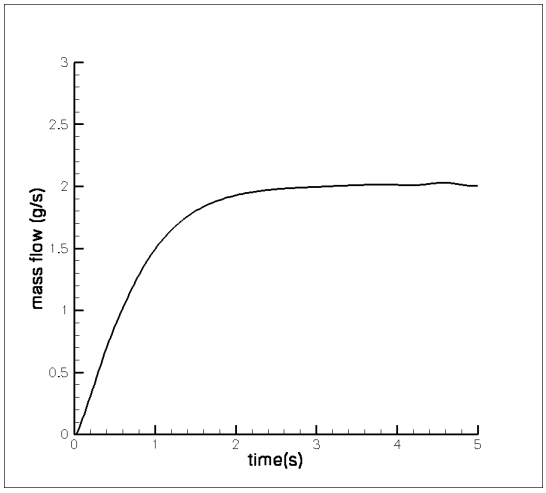

Figure 4.6: Mass inflow rate in the sealed-vent case using the FDS pressure algorithm: Inflow (solid)

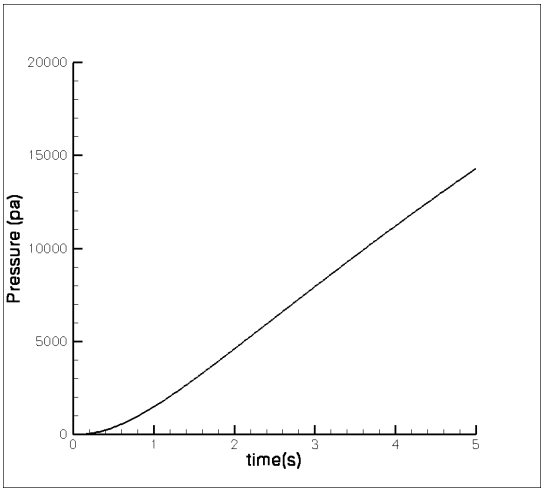

Figure 4.7: Time evolution of the bulk pressure in the sealed-vent case using the FDS pressure algorithm

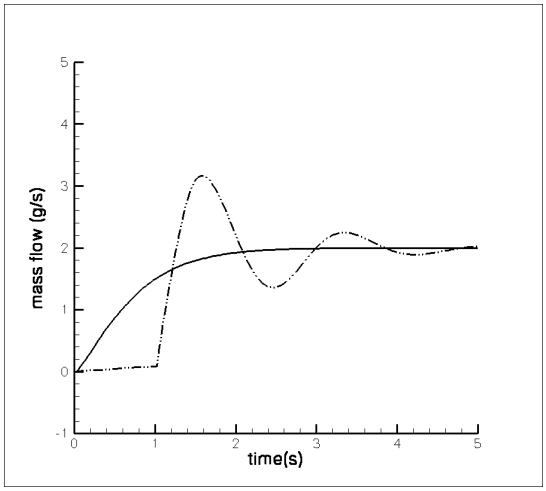

Figure 4.8: Mass inflow and outflow rates in the shift-vent case using the FDS pressure algorithm: Inflow (solid), outflow (dashdot)

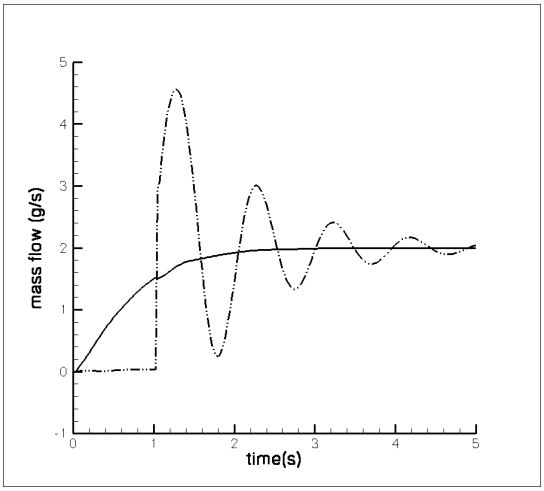

Figure 4.9: Mass inflow and outflow rates in the shift-vent case using the modified pressure algorithm: Inflow (solid), outflow (dashdot)

its peak value to steady state (Fig 4.10), which is still at a high value of 1000 Pa. In contrast, the modified pressure algorithm predicts a faster transition to steady state (about 0.5 s) and the overpressure level is very low.

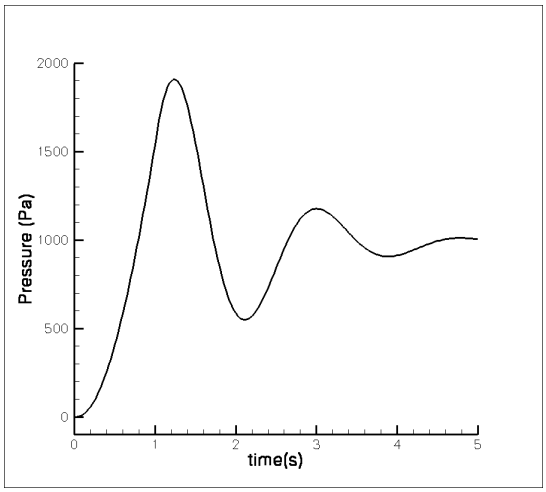

Figure 4.10: Time evolution of the bulk pressure in the shift-vent case using the FDS pressure algorithm

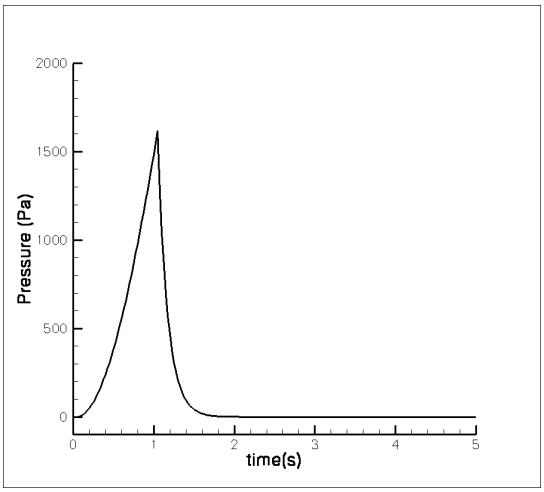

Figure 4.11: Time evolution of the bulk pressure in the shift-vent case using the modified pressure algorithm

In general, the modified pressure algorithm provides correct value of the pressure in open-vent cases; while when the vent is burst open, the modified pressure algorithm also allows a faster transition to steady state, as well as predict a stronger mass flow upon vent opening compared to the original FDS pressure algorithm. This suggested algorithm will then be adopted to simulate large-scale vented explosions in the next chapter.

Chapter 5

Simulation of Low-Pressure Explosive Combustion in Compartment Fires

The in-house version of FDS version 5, enhanced by both a partially-premixed combustion model and a modified bulk pressure algorithm, is now evaluated via detailed comparisons with an experimental database previously developed by FM Global Research. The configuration corresponds to controlled ignition followed by explosive combustion in an enclosure filled with vertically-stratified mixtures of propane in air, both with and without venting, and with and without obstacles [81, 82]. The database was originally developed for vent sizing studies in explosion hazards scenarios associated with flammable liquid spills or releases of heavy flammable vapors in enclosures, and here it is well-suited to test the PPC model since it includes cases in which combustion is predominantly premixed and cases in which it is primarily non-premixed.

5.1 Configuration

The FM Global explosion chamber (FMRC 2250-ft^3 Chamber) is a rectangular-shaped 63.7 m^3 enclosure with a 4.57 $\times$ 4.57 m^2 (15 $\times$ 15 ft^2) square base and a 3.05 m (10 ft) height, as shown in Fig 5.1. It has an entry door for the operator, but it is closed and treated as sealed during the experiments. Ten rectangular open-

ings (0.51 × 1.12 m^2 or 20 × 44 in^2) are available on the roof of the chamber for explosion venting, covered with a sheet of polyethylene, and in some tests, one or two ceiling vents will burst open due to over-pressure. In the present study, 4 cases are considered: two are sealed and two others are vented. Other than the vents, the enclosure is made as tight as possible by covering all the joints with a coat of silicone sealant.

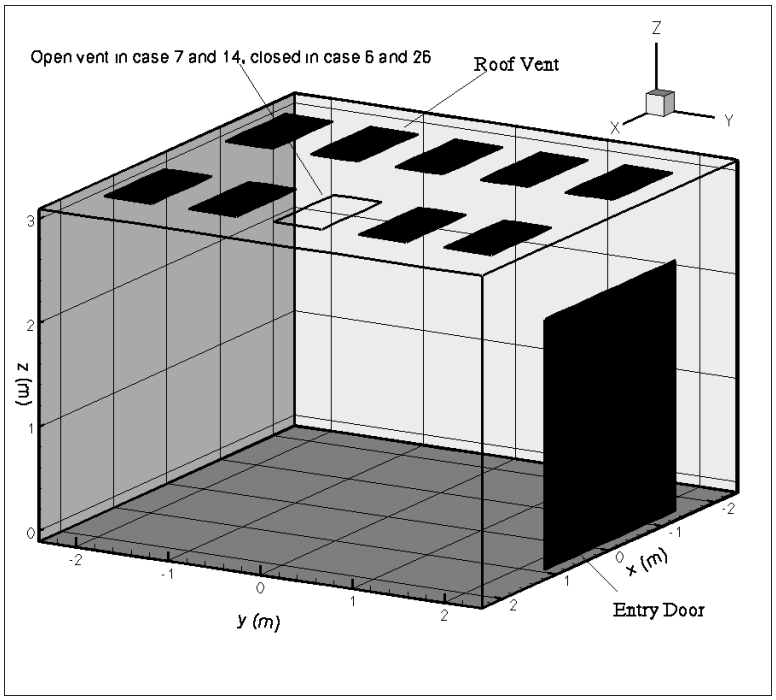

Figure 5.1: Configuration of the FM Global test chamber

The walls of the enclosure are made of 38 mm (1.5 in) plywood panels that are steel-faced (0.41 mm, or 0.016 in), while the floor is made of concrete material. Particular care is done to make the floor surface flat and smooth, and a coat of sealant is also applied as a finish. In addition, a significant number of tests are

conducted with obstacles that are introduced to study the effects of blockage; the obstacles array corresponds to 0.76 $\times$ 0.76 m^2 (2.5 $\times$ 2.5 ft^2) steel plates installed horizontally in a checked pattern 0.46 m (1.5 ft) above the floor, as can be seen in Fig 5.2, the array provides a 50% blockage to vertical flow/flame expansion (but less resistance to horizontal motions).

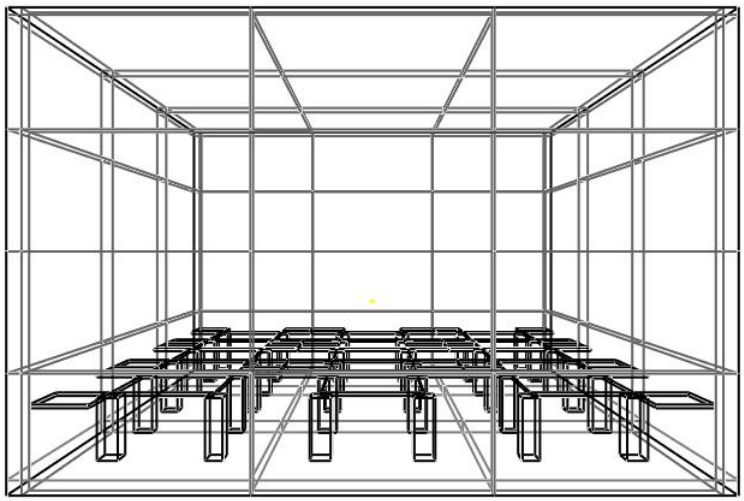

Figure 5.2: FM test chamber with obstacles in checked pattern

Four experimental cases are studied in more detail in the present work: case 6 that is unvented and without obstacle; case 26 that is unvented and with obstacles; case 7 that is vented (1 roof vent) and without obstacle; case 14 that is vented (1 roof vent) and with obstacles. Propane is injected prior to ignition into the chamber through a regulated-pressure, floor-level, low-velocity source that mimics the vapor diffusion process, to provide a quasi-one-dimensional, vertically-stratified layer of flammable gas. The mixture composition is monitored in time by a gas analysis

system. Ignition is triggered in the center of the chamber using an arrangement known as a "Jacob's ladder" [81].

The list of experimental diagnostics include visual observations and video recording of the flames and measurements of the time history of the chamber pressure. Because of the presence of uncontrolled leaks, the pressure measurements are corrected to provide an estimate of the pressure that would have been obtained in the absence of leaks and wall heat losses. The corrected pressure versus time will be the main diagnostic used for comparison with FDS results in unvented cases.

In the numerical calculation, the computational domain corresponds to the test chamber and the simulation starts at ignition and uses the case-dependent experimentally measured initial mixture composition. Fig 5.3 shows the prescribed initial mixture fraction distributions in the FDS simulations and the measured distributions in the experiments. The computational grid corresponds to a uniform rectangular mesh; the mesh size differs from case to case, according to the grid study in the next section. Simulations are performed on a multi-processor Linux cluster available at the University of Maryland, using the parallel MPI-based version of FDS.

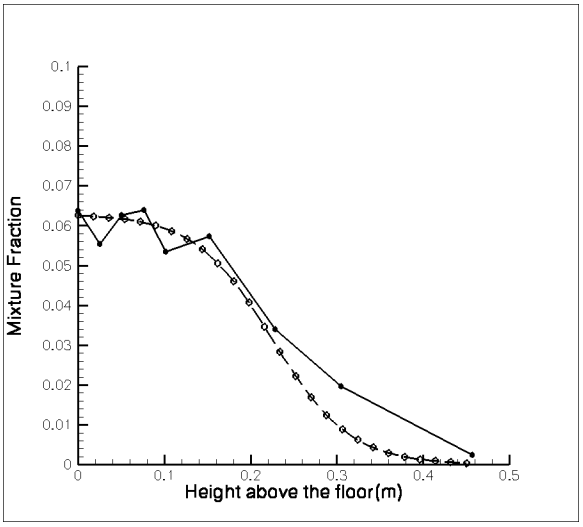

(a)

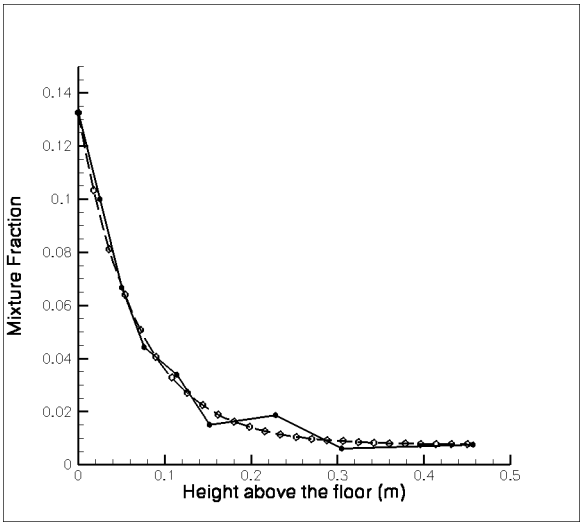

(b)

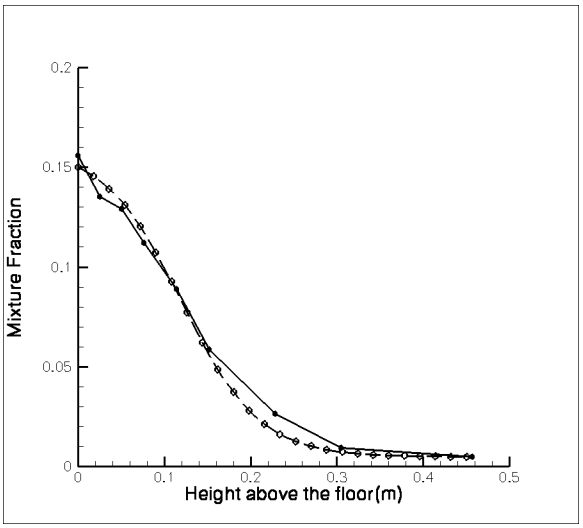

(c)

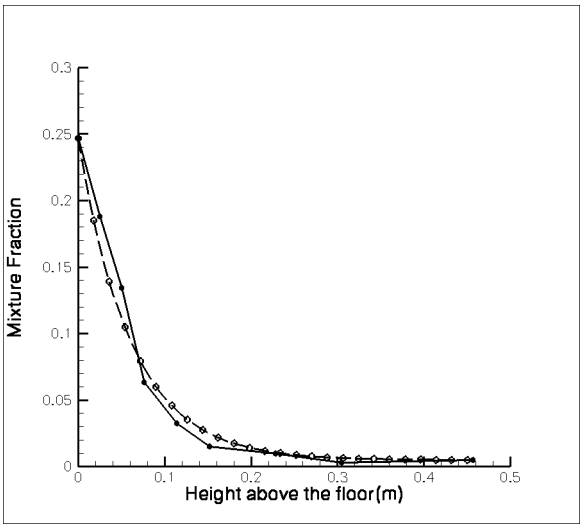

(d)

Figure 5.3: Initial mixture fraction distribution before ignition, experimental measurement (solid line with solid symbols) and numerical approximations (dash line with circles). (a) case 6; (b) case 26; (c) case 7; (d) case 14.

5.2 Characterization of flame structure and combustion mode

For case 6, flame is seen to expand from the ignition point location in both horizontal and (upward) vertical directions. The horizontal spread is associated with a premixed flame (*i.e.* the deflagration or flash fire), as seen in Fig 5.4; while the vertical spread is associated with the buoyancy-driven diffusion flame (*i.e.* the fireball) (Fig 5.5). Since the premixed flame propagates into a fuel-rich mixture, products of premixed combustion are carbon dioxide and water vapor, mixed with nitrogen and (unburned) excess fuel. The excess fuel found in post-premixed-flame gases subsequently mixes with upper-layer air and burns in a diffusion flame mode. Thus the intensity of the diffusion flame is initially much smaller than that of the deflagration, but its relative weight may change as the fire develops. Generally the relative intensity of both flames depends strongly on the state of the propane-air mixing field found at ignition time. [81, 82]

A quantitative effort to characterize the mixture composition for the 4 cases is to calculate the filled fractions for the premixed and rich layers, which can be done by dividing the initial distribution of mixture fraction in Fig 5.3 into two parts, the fuel with a mass fraction between the lower flammability limit of propane ($Y_f = 0.03$) and 80% above stoichiometry ($Y_f = 0.108$) is predicted to burn in a premixed combustion mode, while the fuel with a mass fraction richer than 0.108 is predicted to burn in a diffusion flame mode. The definition of the premixed layer does not go all the way up to the upper flammability limit of propane ($Y_f = 0.15$),

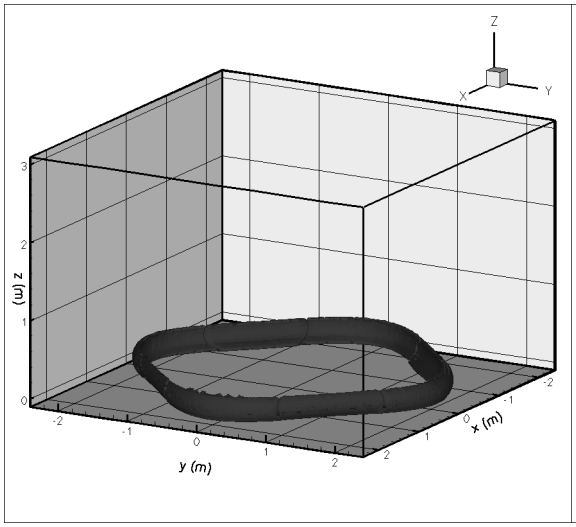

Figure 5.4: Horizontal propagation of the premixed flame 0.5 seconds after ignition in case 6 (Contour of mixture fraction at stoichiometric surface)

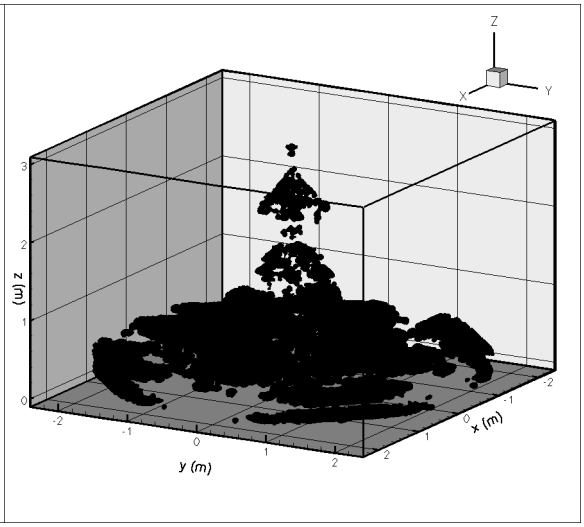

Figure 5.5: Vertical propagation of the diffusion flame 0.7 seconds after ignition in case 6 (Contour of mixture fraction at stoichiometric surface)

in recognition of the fact that, under very fuel-rich conditions, the flame speed is very low and the mixtures would be unlikely to burn in a premixed mode. Although this cut-off of 80% is somewhat arbitrary, the approach provides a simple estimate of the relative weight of premixed versus non-premixed combustion for arbitrary initial compositions of fuel vapor clouds.

The initial estimates of the relative weight of premixed and diffusion burning is shown in Table 5.1. In case 6, the propane cloud is flammable fuel-lean and combustion is predominantly premixed, while in cases 7, 14 and 26, the bulk of the propane cloud is flammable fuel-rich/fuel-lean and combustion is partially-premixed.

Table 5.1: Relative weight of premixed and diffusion combustion modes

Case [82]	Premixed	Diffusion
6	1	0
7	0.6986	0.3014
14	0.3249	0.6751
26	0.2279	0.7721

5.3 Grid sensitivity study

Following the discussion of the grid size requirement of premixed combustion in vertically-stratified layers in Chapter 3.4, a limited study is performed here for the larger scale FM test. Case 6 is chosen for this study, with 5 different values of L_z/Δ_c ranging from 2 to 6. Again the height of gas layer in the flammable range is fixed, and the 5 tests are made possible by varying the numerical grid size. The simulation with $L_z/\Delta_c = 2$ corresponds to a mesh of 5 million cells, and the trial with $L_z/\Delta_c = 6$ corresponds to a mesh of 130 million cells, so the calculation cost is a factor that has to be considered.

Fig 5.6 and 5.7 present the simulated premixed and diffusion combustion heat release rate, they sum up to be the total heat release rate in Fig 5.8, while the bulk pressure curve is presented in Fig 5.9 including comparisons with the experimental data. It can be seen that the $L_z/\Delta_c = 2$ case has a 20% under-estimation of premixed combustion and about 20% over-estimation of the diffusion combustion

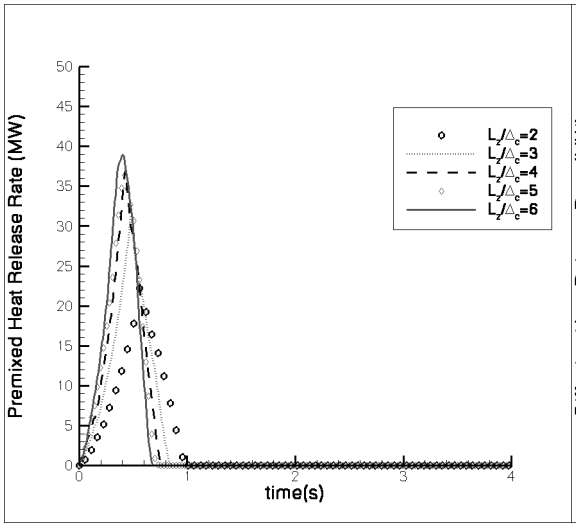

Figure 5.6: Comparison of the time evolution of the premixed combustion heat release rate in case 6 for 5 different grid sizes

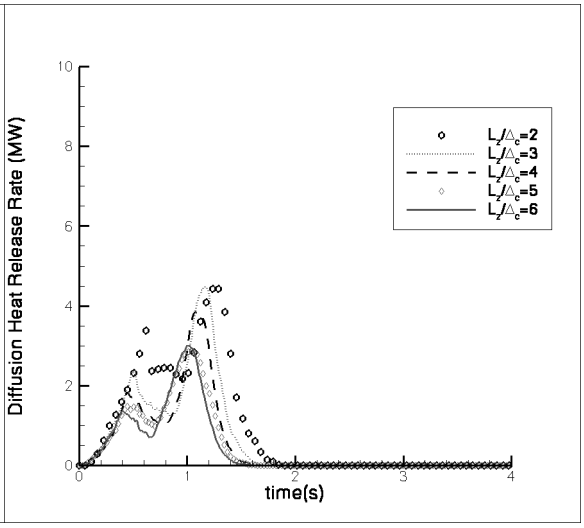

Figure 5.7: Comparison of the time evolution of the diffusion combustion heat release rate in case 6 for 5 different grid sizes

compared to $L_z/\Delta_c = 6$. All cases under-estimate the bulk pressure when compared to the experimental results, and the most refined simulation ($L_z/\Delta_c = 6$) still underestimates the pressure by more than 10%. If comparing the calculated total heat release rate from Fig. 5.6-5.7, $L_z/\Delta_c = 2$ and $L_z/\Delta_c = 3$ case calculate a 10 MW gap of difference in the peak HRR, while $L_z/\Delta_c = 3$ and $L_z/\Delta_c = 6$ case calculate another 10 MW gap of difference in the peak HRR. Considering the calculation cost, it would be suggested that $L_z/\Delta_c = 3$ be used. However, in the following, we select the grid size so that $L_z/\Delta_c = 2$ because of relative difference of grid requirement between each case, and $L_z/\Delta_c = 2$ is affordable for cases while $L_z/\Delta_c = 3$ is too expensive in terms of the calculation cost for some cases.

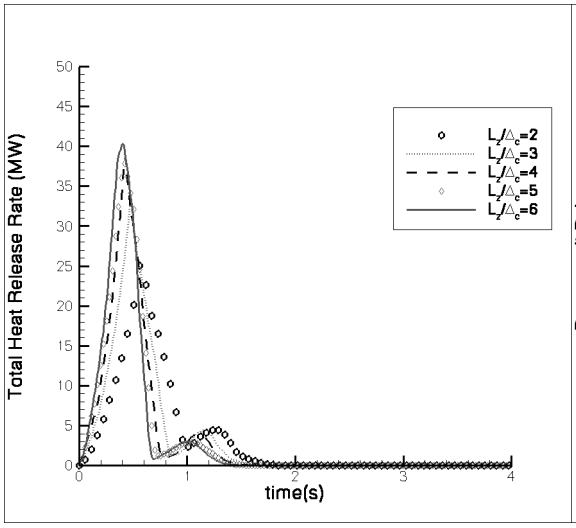

Figure 5.8: Comparison of total heat release rate in case 6 for 5 different grid sizes

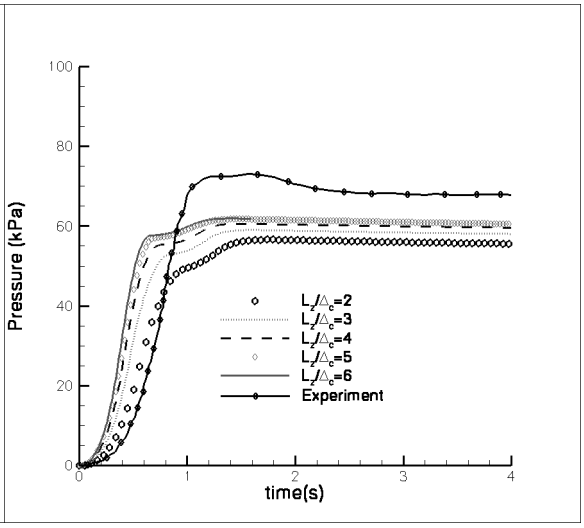

Figure 5.9: Evolution of bulk pressure in case 6 for 5 different grid sizes and comparison to (corrected) experimental pressure data

5.4 Numerical results

Based on the grid sensitivity study above and the consideration of affordable calculation cost, the grid spacing is determined so that $L_z/\Delta_c = 2$ for all four case simulated cases. This corresponds to $\Delta = 2.5$ cm in case 6 and 14, $\Delta = 1.25$ cm in case 7 and $\Delta = 0.8$ cm in case 26. The flame speed model parameters are: $Z_{LFL} = 0.032$, $Z_{UFL} = 0.153$, $Z_{st} = 0.06$ and $s_{L,st} = 0.44$ m/s [91]. The filter-to-grid length scale ratio is equal to 5, $(\Delta_c/\Delta) = 5$. Based on the initial trial, the flame wrinkling factor is fixed at a relatively high value, $\Xi = 4$,however, the premixed combustion are found to be too fast in some cases, and a lower value of $\Xi = 2$ is tested for some cases in Appendix C to illustrate the effect of the wrinkling factor

on the premixed combustion speed in the PPC model. Appendix C reveals that a correct simulation of explosion combustion must involve a more elaborate treatment of the wrinkling factor, which is beyond the scope of the discussion in this study.

We analyse in the following the time evolution of the heat release rate and bulk pressure. The simulated pressure will be compared to the experimental data, adiabatic pressure in sealed cases and actual pressure in vented case, for reasons that are explained in section 5.1. The heat release rate is maximum shortly after ignition (at $t = 0.5$ s in case 6, at $t = 1.2$ s in case 26) and reaches a peak value that ranges from 15 MW (case 7 and 26) to more than 25 MW (case 6 and 14) (Fig 5.10). In all cases, the combustion phase is short and lasts between 1.5 and 2 s; combustion ceases because of fuel depletion. By integrating the total premixed heat release rate and diffusion heat release rate, the relative contribution of premixed and non-premixed burning can be quantified, as shown in table 5.2, which can be compared to the categorization of all cases in terms of the initial fuel mass distribution in table 5.1. This comparison is illustrated in Fig 5.10, that the x-axis represents the relative weights of premixed and diffusion combustion predicted from the fuel filled fraction, and the y-axis is the one concluded by numerical calculation as in table 5.2. It can be seen that the numerical calculation provides the correct dominant combustion mode.

Case 6 is calculated to be premixed-combustion dominated (Fig 5.11(a)), a result that is consistent with prediction in Table 5.1. In contrast, the propane cloud in Case 26 features a large ultra-rich layer, and the combustion is dominated

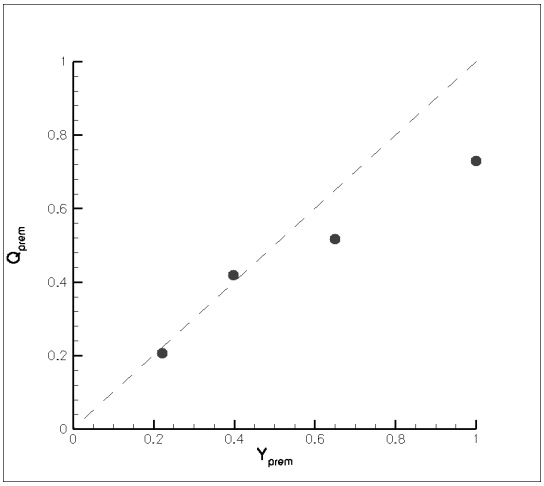

Figure 5.10: Relative weights of premixed and diffusion combustion: From initial fuel fill fraction (upper subplot); From calculated heat release rate (lower subplot)

by diffusion combustion (Fig 5.11(d)). Finally, in cases 7 and 14, the bulk of the propane cloud is flammable fuel-rich/fuel-lean and combustion is partially-premixed (Fig 5.11(c)-(d)). In all cases, premixed burning peaks when the deflagration impinges on the vertical side walls of the chamber, while diffusion burning peaks when fuel depletion effects become dominant.

Table 5.2: Relative weights of premixed and diffusion combustion modes

Case	Q_{premix}	$Q_{diffusion}$
6	0.7290	0.2710
7	0.5177	0.4823
14	0.4181	0.5819
26	0.2066	0.7934

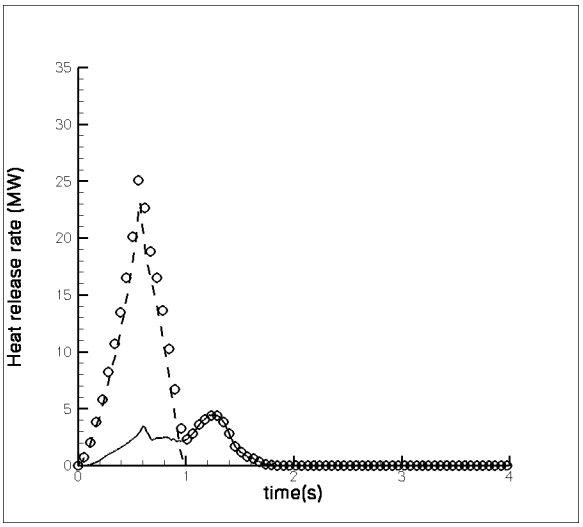

(a)

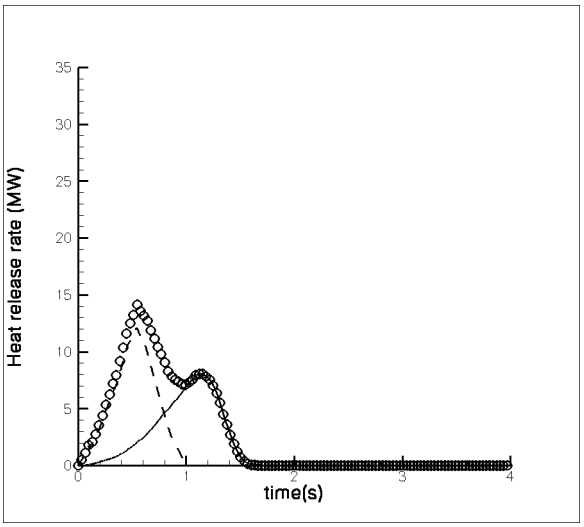

(b)

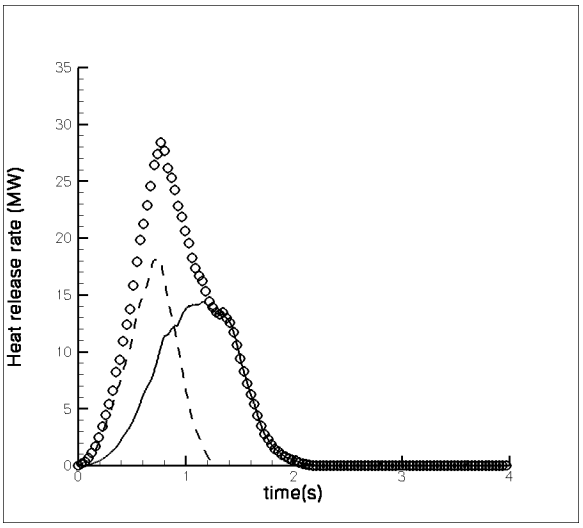

(c)

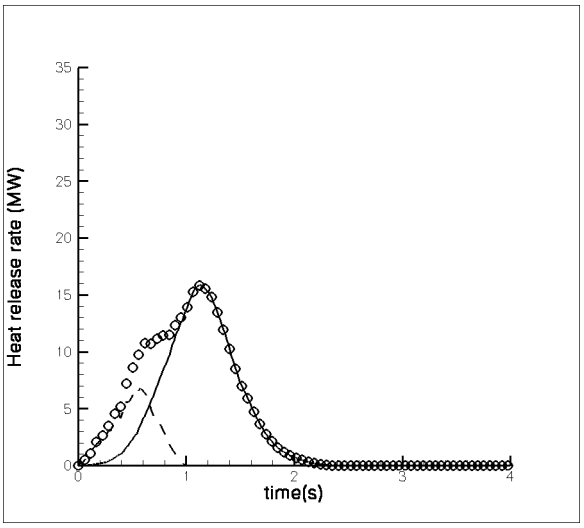

(d)

Figure 5.11: Time variations of the global heat release rate (HRR): total HRR (circles) as well as its premixed flame (dashed line) and diffusion flame (solid line) components. (a) case 6; (b) case 7; (c) case 14; (d) case 26.

Figure 5.12 compares the experimental and simulated time histories of bulk pressure. As mentioned earlier, the experimental data are corrected for the presence of leaks and wall heat losses. In cases 6 and 26 (sealed), the pressure increases to more than 60 Kpa and remains at a high level once the combustion is completed (Fig. 5.12(a),(d)). The good agreement between experimental data and numerical results, suggesting that the rate of combustion is reasonably well predicted in Ref. [81, 82], the turbulent flame speed that characterizes the burning intensity of the deflagration wave is estimated to be 1.75 ± 0.25 m/s). The fair agreement when comparing the post-combustion pressure level suggests that the total amount of fuel mass consumed is predicted less accurately (within 20% - 30%).

In case 7 and 14 (vented), the pressure variations feature two peaks (Fig 5.12(b-c)): the first peak is associated with the sudden opening of the roof when the bulk pressure reach the failure pressure of the polyethylene sheet at the ceiling vent(at $\bar{p} \approx 3$ Kpa); the second peak corresponds to the timing of maximum heat release rate (Fig 5.11 (b-c)). The magnitude of the second peak is under-predicted in both cases, which can be explained by the grid resolution here that tends to under-predict the combustion intensity, recognizing that $L_z/\Delta_c = 2$ is adopted here in all cases, which predicts a heat release rate of 20% lower than $L_z/\Delta_c = 6$ trials, from the grid study of case 6 presented in the previous section.

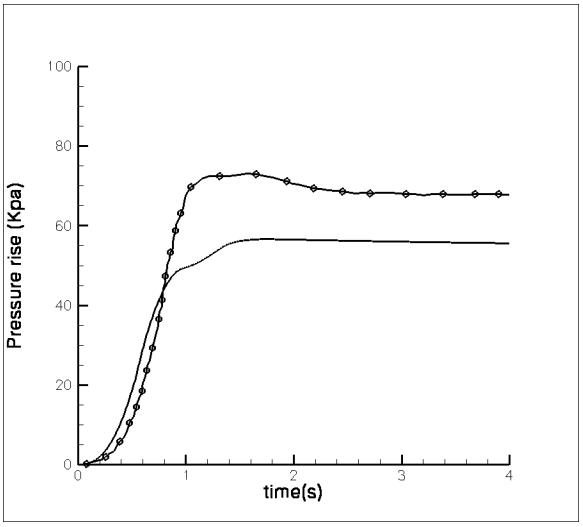

(a)

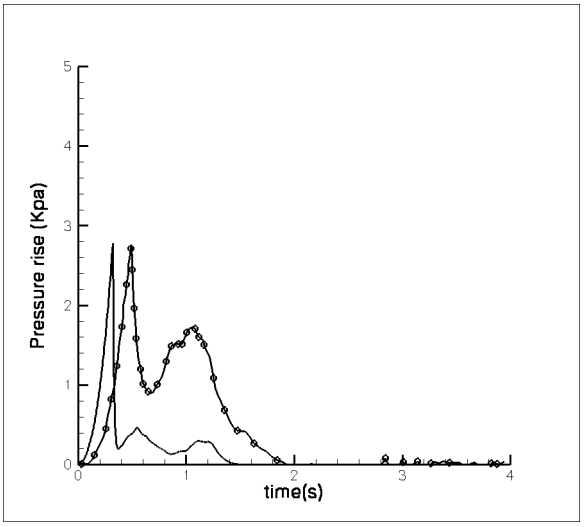

(b)

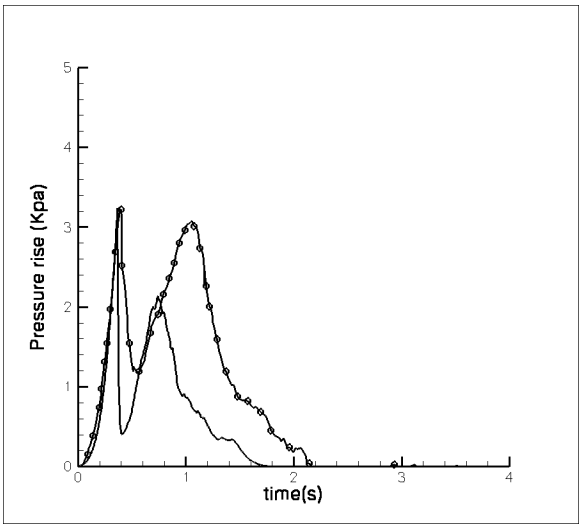

(c)

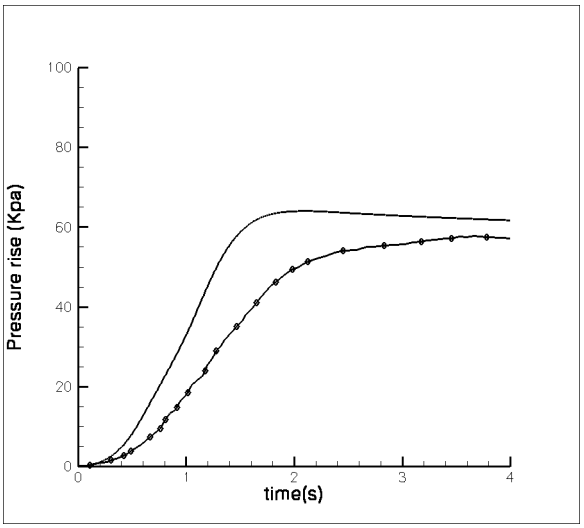

(d)

Figure 5.12: Time variations of the bulk compartment pressure: experimental data (circles) and computational results (solid line). (a) case 6; (b) case 7; (c) case 14; (d) case 26.

Chapter 6

Velocity-Pressure Coupling (VPC) Scheme

In this chapter an alternative method to simulate the pressure development in FMG experiments is investigated, by correcting the velocity boundary condition at the open vent in FDS. It has been pointed out that the coupling between the momentum and mass conservation equations for incompressible flows is often the major cause of the slow convergence of iterative solution techniques [74], which makes it crucial to treat correctly the velocity-pressure coupling that exists between the mass and momentum conservation equations. For clarity, the treatment of pressure boundary condition in FDS will be first reviewed. Then a new model for the velocity boundary condition at open vent is introduced, which constitutes a velocity-pressure coupling (VPC) scheme. This scheme will be evaluated and tailored through a series of verificaiton tests and finally be used for simulating vented gas explosions in the FMG experiments in Chapter 7.

6.1 Pressure boundary conditions at open vents

Consider the simple scenario of compartment with a vent as in Fig 6.1-6.2, the pressure treatment on the vent boundary is usually differed in inflow and outflow condition. For outflow (Fig 6.1), the flow moves from the left side with high pressure $\bar{P}$ to the right side with low pressure P_∞, while the vent section can be considered

as an elongated tube, the inlet of the tube connects to the compartment, while the outlet of the tube connects to the outside atmosphere [41].

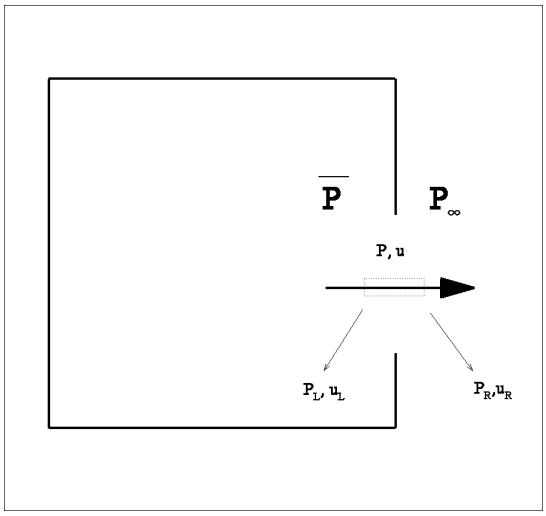

Figure 6.1: Pressure boundary condition for outflow at the vent

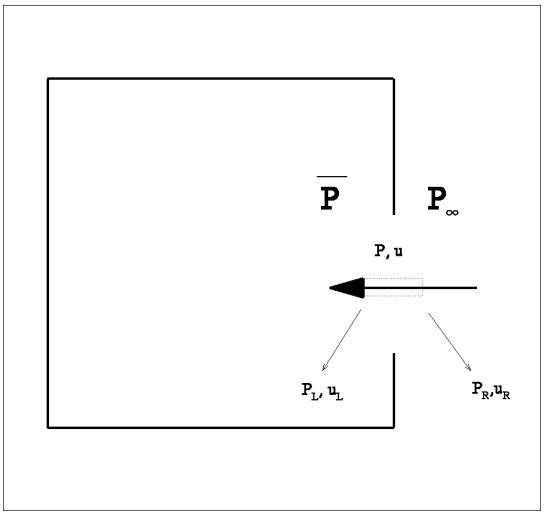

Figure 6.2: Pressure boundary condtion for inflow at the vent

The flow in the vent section can be considered as a free jet through a tube, which dissipates its kinetic energy due to viscous action. The static pressure over the outlet of the tube P_R is then close to the outside atmospheric pressure P_∞, and the flow accelerates from the inside compartment pressure $\bar{P}$ to a low static pressure P_L at the inlet of the tube. The decrease of pressure at the inlet of tube from $\bar{P}$ is depending on the flow velocity, and the Bernoulli equation can be applied to relate the static pressure and the velocity at the inlet of the tube to the compartment pressure $\bar{P}$. Therefore the relations of the pressure at the both ends of the tube can be expressed as:

$$\bar{P} = P_L + \rho_\infty \frac{u_L^2}{2}$$

$$P_\infty = P_R \tag{6.1}$$

Similarly, for inflow (Fig 6.2), the pressure at both ends of the tube can be written:

$$\begin{aligned} P_\infty &= P_R + \rho_\infty \frac{u_R^2}{2} \\ \bar{P} &= P_L \end{aligned} \tag{6.2}$$

u_L and u_R can be treated to be the velocity at vent u in both cases for convenience.

In FDS, the pressure at the boundary of the vent P is treated as the pressure at the outlet of the imaginary tube, which can be summarized as:

$$\begin{aligned} P + \rho_\infty \frac{u^2}{2} &= P_\infty \qquad \text{(constant stagnation pressure for inflow)} \\ P &= P_\infty \qquad \text{(constant static pressure for outflow)} \end{aligned} \tag{6.3}$$

where u is the velocity at the vent.

An experiment on explosion development in linked vessels by Razus [77] measured the pressure development in two vessels connected by a cylindrical tube, which shows a difference of pressure level in the two vessels, with a synchronization in time. The results for the difference of the pressure level in the vessels on both sides of the

tube support the treatment of pressure boundary condtions at open boundaries described above.

6.2 Velocity boundary conditions at open vents

Inspired by the experimental study of vented explosion in Refs. [17, 52, 53], it is clear that an improved description of the velocity boundary condtion at open vents is desired in FDS. The formulation of velocity boundary conditions at open boundaries must be sensitive to the difference between the bulk pressure inside the compartment and the external ambient pressure. One way of adding this pressure effect is by adding a term in the momentum equation of FDS at open vent location. To illustrate this, we use the configuration in Chapter 4 where the vent is in the positive x-direction of the compartment, as in Fig 6.3.

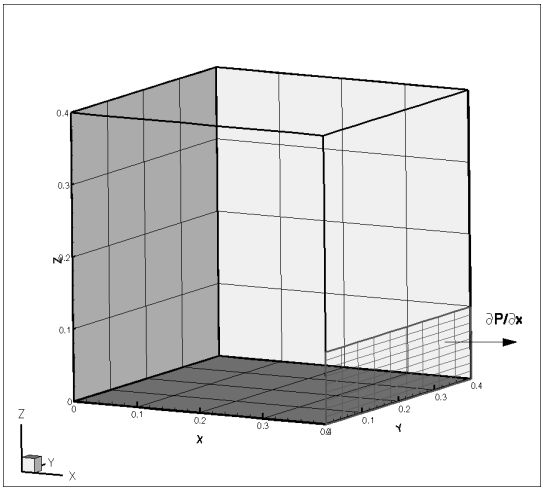

Figure 6.3: Schematic of the vented compartment showing coordinate system

For the selected coordinate system using u,v,w as the velocity in the x,y,z direction, the mass and momentum equations can be written as:

Conservation of Mass:

$$\frac{\partial \rho}{\partial t} + \mathbf{u} \cdot \nabla \rho = -\rho \nabla \cdot \mathbf{u} \tag{6.4}$$

Conservation of Momentum:

$$\frac{\partial \mathbf{u}}{\partial t} + \mathbf{u} \times \omega + \nabla \mathcal{H} = \frac{1}{\rho}((\rho - \rho_0)\mathbf{g} + \mathbf{f}_b + \nabla \cdot \tau_{ij}) + \frac{\Delta \bar{P}}{\rho L} \tag{6.5}$$

in which $\Delta \bar{P} = \bar{P} - P_\infty + \epsilon \frac{\rho u^2}{2}$ ρ is the gas density in the field, $\dot{m}_b'''$ is the mass injected in, μ the viscosity, g_x, g_y, g_z the gravity force, f_x, f_y, f_z the external forces such as the drag exerted by liquid droplets, the total pressure $P = \bar{P} + \tilde{p}$ where $\bar{P}$ is the bulk pressure, which is of interest in this section, $\tilde{p}$ is the pressure perturbation solved by the poisson equation in FDS [57]. Notice that in the x-momentum equation the term $\partial \bar{P}/\partial x$ cannot be neglected at the open vent, since this term scales like $\bar{P} - P_\infty$ and may take very large values in explosion scenarios. Currently this term is not included in the momentum equation at the open vent boundary in FDS. To formulate a model expression for this term, we first consider a zero-dimensional problem corresponding to a pressurized tank open at initial time to the ambient atmosphere. This problem is studied with MATLAB. The bulk pressure equation is a simplified version of Eq. (4.1) assuming no combustion:

$$\frac{d\bar{P}}{dt} = \frac{(\gamma - 1)}{V}(-\epsilon \dot{m}_v c_p T_v) \tag{6.6}$$

where V is the compartment volume, c_p is the heat capacity at constant pressure, $\dot{m}_v$ is the mass flow rate through the vent ($\dot{m}_v \geq 0$), T_v is gas temperature at the

vent, $\epsilon = +1$ for outflow, $\epsilon = -1$ for inflow. Assuming ideal gas behavior, T_v and $\dot{m}_v$ can be written as:

$$\begin{aligned} T_v &= T_0(\bar{P}/P_0)^{(\gamma-1)/\gamma} && \text{for } \epsilon = +1(outflow) \\ &= T_0 && \text{for } \epsilon = -1(inflow) \\ \dot{m}_v &= C_d A_v \rho_v |u_v| \\ \rho_v &= \rho_0(\bar{P}/P_0)^{1/\gamma} && \text{for } \epsilon = +1(outflow) \\ &= \rho_0 && \text{for } \epsilon = -1(inflow) \end{aligned} \tag{6.7}$$

where ρ_0, T_0 are the ambient gas density and temperature, ρ_v is the gas density at the vent. A_v is the vent area, C_d is an empirical flow (or discharge) coefficient.

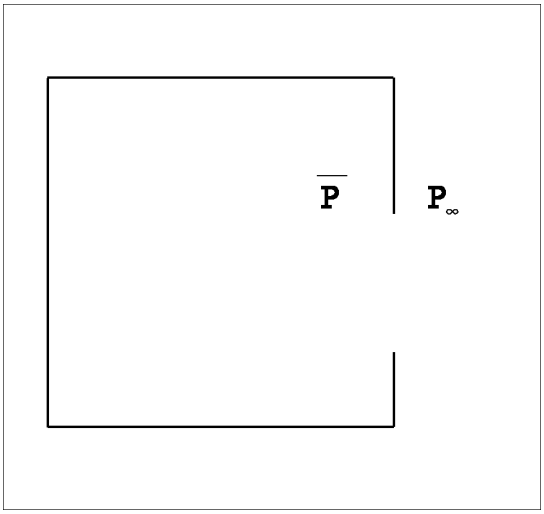

Figure 6.4: Vented compartment configuration of velocity-pressure coupling

The vent flow velocity equation may be formulated as follows:

$$\frac{du_v}{dt} = \frac{(\bar{P} - P_\infty)}{\rho L} \tag{6.8}$$

where L is the effective length of the vent neck proposed by Kinsler [42] and is also used by Bauwens et al [2] in their most recent study of numerical simulation of methane-air deflagrations in vented enclosures, empirically $L = 0.8\sqrt{A_v} + l$ [2, 42], with l the actual length of the vent.

Combining Eq. (6.6) and (6.8), a velocity-pressure coupling (VPC) scheme can be formulated, designated as Scheme 1 (S1):

$$\begin{aligned} \frac{d\bar{P}}{dt} &= \frac{(\gamma - 1)}{V}(-\epsilon \dot{m}_v c_p T_v) \\ \frac{du_v}{dt} &= \frac{(\bar{P} - P_\infty)}{\rho L} \end{aligned} \tag{6.9}$$

This scheme is unstable and corresponds to a Helmholtz resonance system, with a characteristic frequency

$$f_H = \frac{1}{2\pi}\sqrt{\frac{\gamma P_0}{\rho_0}}\sqrt{\frac{C_d A_v}{VL}} \tag{6.10}$$

Additional details on the Helmholtz system can be found in Refs. [16, 33]. Fig 6.5 and 6.6 present results obtained from a MATLAB solution of Eq.(6.9) for a case corresponds to a pressurized tank, pressure at 1000 Pa, and open at $t = 0$ to

ambient atmosphere.

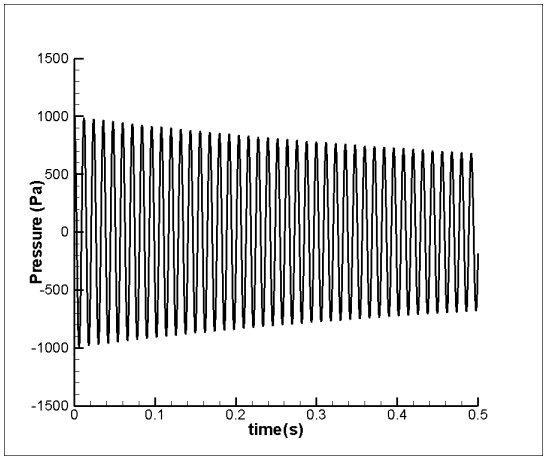

Figure 6.5: Pressure evolution with VPC scheme S1 (At $t = 0$,$\bar{P} = 1000Pa$)

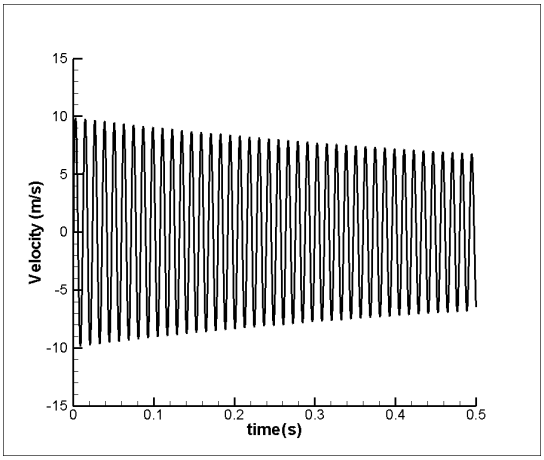

Figure 6.6: Vent velocity evolution with VPC scheme S1

Slow convergence is observed in this case, and the initial velocity when gas bursts out of the vent is predicted to be about 10 m/s. The period of the oscillation is about 0.01s, which agrees with the calculation from the frequency formula in Eq.(6.10): given $\gamma = 1.4$, $P_0 = 101325\ Pa$, $\rho_0 = 1.2\ kg/m^3$, $C_d = 0.6$, $A_v = 0.04\ m^2$, $V = 0.4 \times 0.4 \times 0.4 = 0.064\ m^3$, $L = 0.8\sqrt{A_v} = 0.16\ m$ neglecting the actual vent length, $f_H = \frac{1}{2\pi}\sqrt{\frac{\gamma P_0}{\rho_0}}\sqrt{\frac{C_d A_v}{VL}} = 83$, which corresponds to a period of about 0.01s. Note that Helmholtz oscillations have been observed in pressurized vented sstem, the oscillations are typically damped within a few cycles and the results in Figs 6.5-6.6 are incorrect.

The second model is suggested by reexamining the velocity boundary condition as in Fig 6.1 and 6.2. Instead of using $\bar{P}$ and P_∞ to calculate the pressure difference at the vent, P_L and P_R are adopted instead as the pressure at both ends of the vent. Thus for inflow:

$$\frac{du_v}{dt} = \frac{P_L - P_R}{\rho L} = \frac{\bar{P} - P_\infty}{\rho L} + \frac{\rho u_v^2/2}{\rho L} \tag{6.11}$$

For outflow:

$$\frac{du_v}{dt} = \frac{P_L - P_R}{\rho L} = \frac{\bar{P} - P_\infty}{\rho L} - \frac{\rho u_v^2/2}{\rho L} \tag{6.12}$$

Eqs. (6.11) and (6.12) together with the pressure Eq. (6.6), form the second VPC scheme S2, which can be summarized here:

$$\begin{aligned} \frac{d\bar{P}}{dt} &= \frac{(\gamma - 1)}{V}(-\epsilon \dot{m}_v c_p T_v) \\ \frac{du_v}{dt} &= \frac{P_L - P_R}{\rho L} = \frac{\bar{P} - P_\infty}{\rho L} - \frac{\epsilon \rho u_v^2/2}{\rho L} \end{aligned} \tag{6.13}$$

with $\epsilon = +1$ for outflow ($u_v > 0$), $\epsilon = -1$ for inflow ($u_v < 0$). The pressure and vent velocity evolution calculated using this scheme is shown in Figs 6.7 and 6.8.

The pressure and velocity oscillations are much more damped with this modification, with the frequency still the same as when using S1. After 0.5 seconds, the amplitude of the oscillation is about 200 Pa, a value that seems unrealistically high. In a third scheme, an artificial term $2f_H u_v$ is added to the velocity equation to accelerate the damping, where f_H is the characteristic Helmholtz frequency calculated

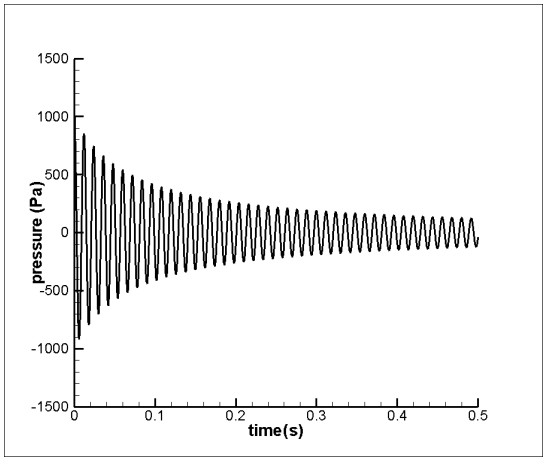

Figure 6.7: Pressure evolution with VPC scheme S2

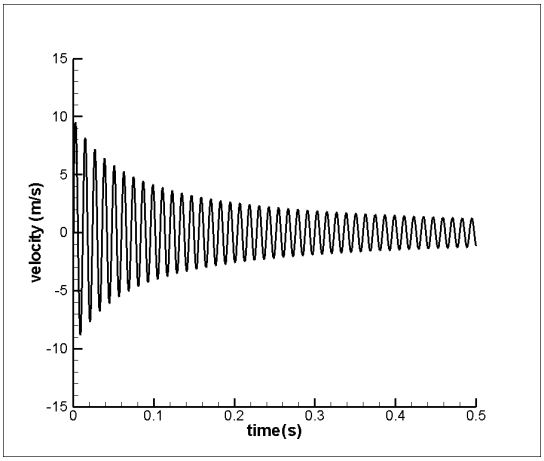

Figure 6.8: Vent velocity evolution with VPC scheme S2

from Eq. (6.10). The VPC scheme S3 in as follows:

$$\begin{aligned} \frac{d\bar{P}}{dt} &= \frac{(\gamma-1)}{V}(-\epsilon\dot{m}_v c_p T_v) - 2f_H(\Delta\bar{P}_{eq}) \\ \frac{du_v}{dt} &= \frac{P_L - P_R}{\rho L} = \frac{\bar{P} - P_\infty}{\rho L} - \frac{\epsilon\rho u_v^2/2}{\rho L} \end{aligned} \tag{6.14}$$

The MATLAB results are presented in Figs 6.9 and 6.10. The pressure is damped to the ambient level in less than 0.05 seconds, while the initial velocity peaks after the vent opening, at around 8 m/s, which meets the modeling objective that high peak velocities are described, while the compartment bulk pressure drops to the ambient level quickly after a few periods of Helmholtz oscillation.

6.3 Verification of VPC scheme in a small compartment

We now implement the VPC scheme S3 in FDS and simulate one of the test cases considered in Chapter 4. In this case, air is pumped into a $0.4m \times 0.4m \times 0.4m$

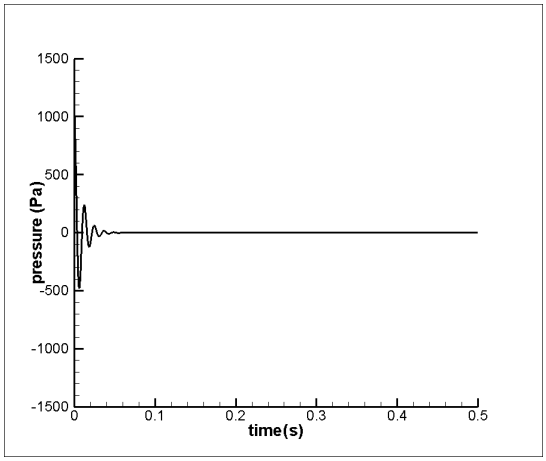

Figure 6.9: Pressure evolution with the VPC scheme S3

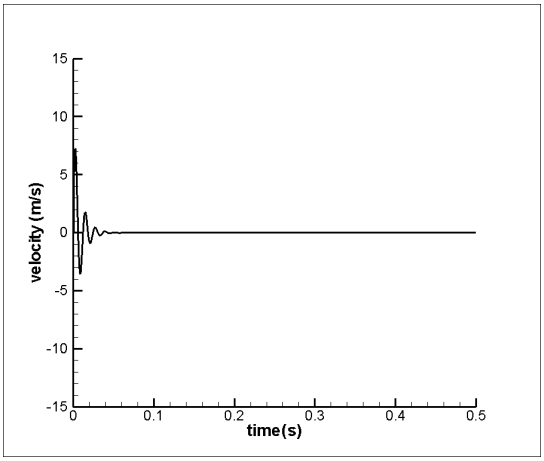

Figure 6.10: Vent velocity evolution with the VPC scheme S3

cubic compartment at $2g/s$, the compartment is initially sealed, followed by a vent opening (vent sizes $0.4m \times 0.1m$) at $t = 1s$. The evolutions of the pressure, mass flow and gas velocity through the vent are shown in Figs 6.11-6.13.

Compared to Fig 4.10-4.11, bulk pressure in the room drops much faster to an ambient level, also with a Helmholtz oscillation that was not observed before. The mass flow and velocity results in Fig 6.12-6.13 illustrate a much stronger burst of vent outflow. In Chapter 4, a mass outflow through the vent upon its opening is calculated to be 6 g/s with the improved pressure model, which corresponds to a vent outflow velocity of 0.1 m/s, and that is much lower than the maximum velocity described in Fig 6.10 (MATLAB) and Fig 6.13 (FDS), which is about 6 m/s.

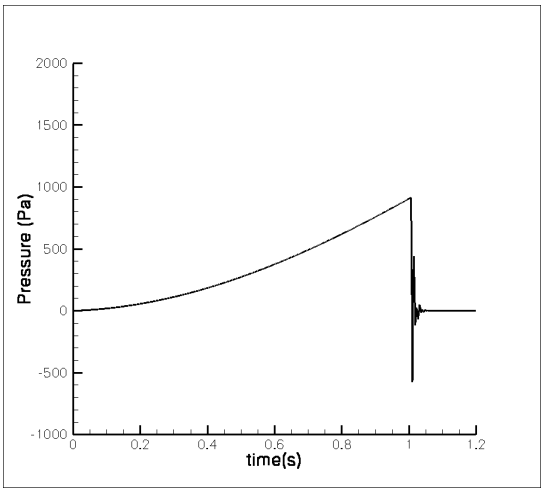

Figure 6.11: Bulk pressure evolution in the compartment with VPC scheme S3 implemented in FDS

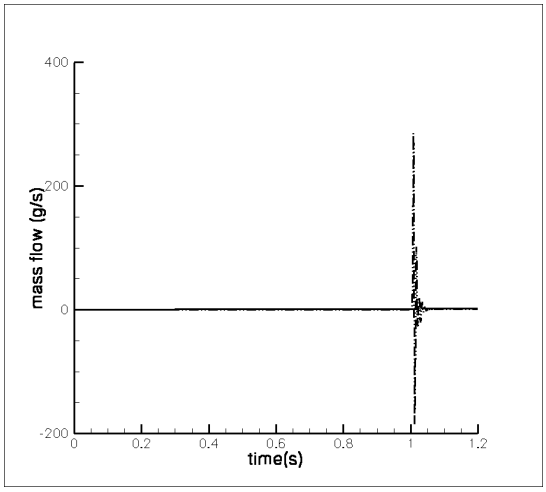

Figure 6.12: Mass flow through vent with VPC scheme S3 in FDS

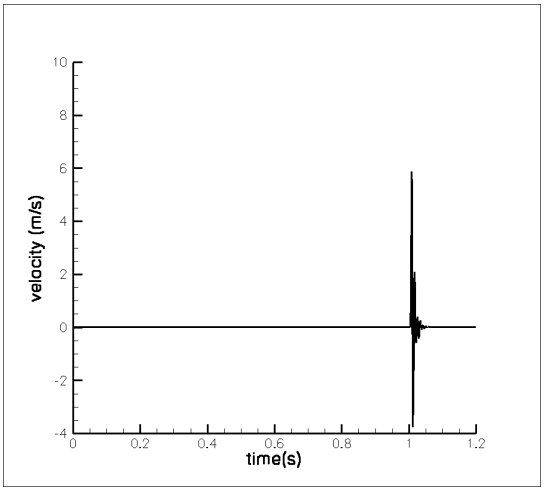

Figure 6.13: Vent velocity at vent with VPC scheme S3 in FDS

Chapter 7

Simulation of Vented Gas Explosions Using the VPC Scheme

It is reported by DeHaan et al.[17] that in a vented explosion experiment in a $3.6m \times 2.4m \times 2.4m$ chamber, a negative pressure of 2 Kpa is observed following the opening of the relief vent at a failure pressure of 6 Kpa, and that Helmholtz oscillations of the pressure are also observed after the vent opening. Because the VPC scheme S3 allows for high transient vent flow velocities and Helmholtz oscillations, new FDS simulations of the FMG test configuration using the VPC scheme S3 are performed. In contrast to tests performed in Chapter 6, the simulations discussed in the following correspond to violent combustion events and feature strong outflow velocities.

Cases 7 and 14 are re-simulated here, with the same configuration as in Fig 5.1, i.e., $4.57 \times 4.57 \times 3.05$ m^3. The initial fuel gas (vaporized propane) distribution is the same as in Fig 5.3(c,d). Grid size is chosen so that $L_z/\Delta_c = 2$.

Fig 7.1 and 7.2 show the calculated heat release rate in case 7 and 14, which is almost identical to Fig 5.11 (b,c). The total HRR, premixed HRR and diffusion HRR are plotted; the total HRR features two peaks corresponding to maximum premixed combustion and maximum diffusion combustion. In case 7, the premixed

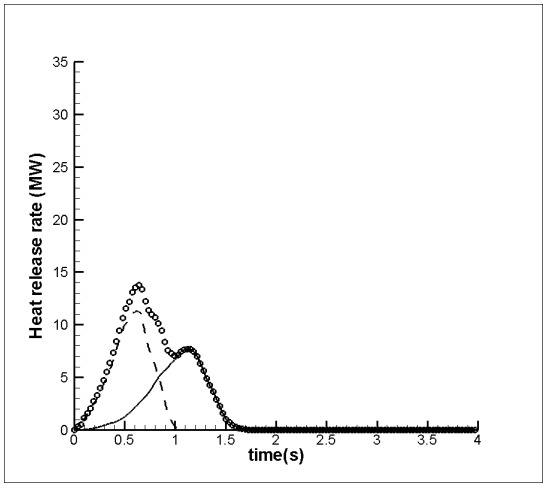

Figure 7.1: Time variations of heat release rate (HRR) in FMG case 7 simulated with the VPC scheme S3: total HRR (circles) as well as its premixed flame (dashed line) and diffusion flame (solid line) components.

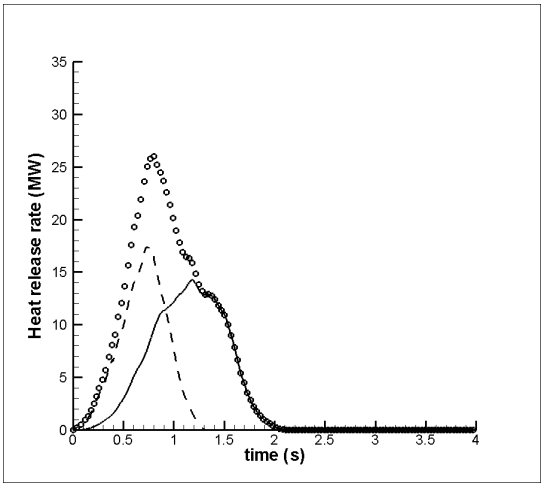

Figure 7.2: Time variations of heat release rate (HRR) in FMG case 14 simulated with the VPC scheme S3: total HRR (circles) as well as its premixed flame (dashed line) and diffusion flame (solid line) components.

combustion fraction is 0.52, while in case 14, it is 0.42, so both cases still feature partial-premixed combustion. The difference between the simulations presented here and those of chapter 5 is the treatment of bulk pressure as well as the gas velocity at the vent.

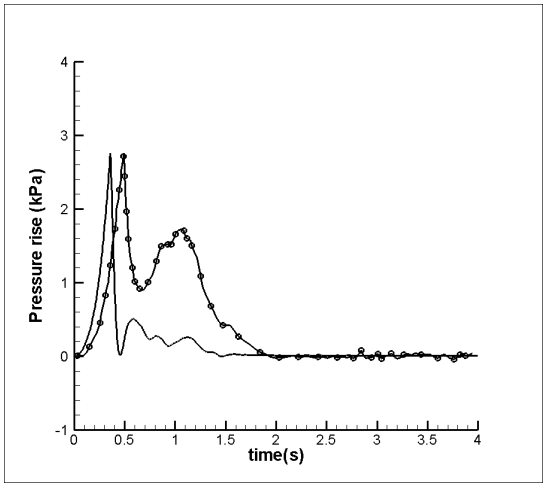

Figure 7.3: Time variations of bulk pressure in FMG case 7 simulated with the VPC scheme S3: experiment (dotted line), simulation (solid line)

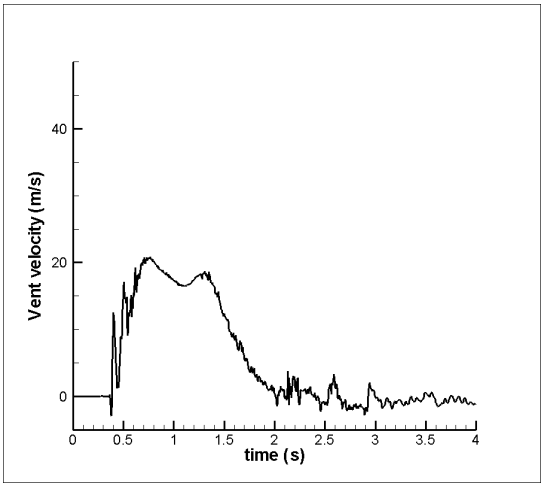

Figure 7.4: Gas velocity at vent in FMG case 7 simulated with the VPC scheme S3

Fig 7.3 presents the calculated bulk pressure in case 7. The vent is forced to open when the pressure reaches a critical level of about 3 Kpa (0.4 psi), as measured from the experiment. The pressure drops to 0 in less than 0.1 s. It is then followed by a few oscillations, which takes about 1 s before stabilizing. The oscillations feature a second pressure peak of 400 Pa. This second peak is much lower than that observed in the experiment (which is due to peak diffusion burning), mostly because

the VPC scheme has a strong effect of damping the pressure variations. No negative pressure is observed here, although it is reported by DeHaan [17] in vented explosion experiment.

Fig 7.4 shows the gas velocity at vent in case 7. When the vent breaks open, the gas bursts out to a maximum velocity of 20 m/s, which lasts for about 1 s, corresponding to the stage when the bulk pressure oscillates before relaxing to ambient pressure. The oscillation behavior of the velocity is more pronounced than in the pressure signal in Fig 7.3. Slight negative velocity is observed, indicating a shifting behavior of flow movement at vent after the pressure relaxes to ambient.

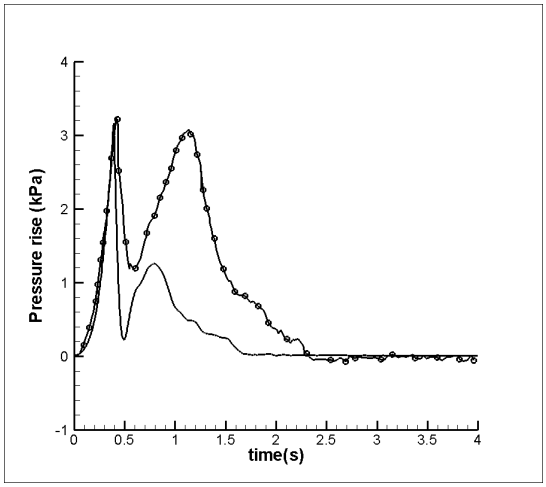

Figure 7.5: Time variations of bulk pressure in FMG case 14 simulated with the VPC scheme S3: experiment (dotted line), simulation (solid line)

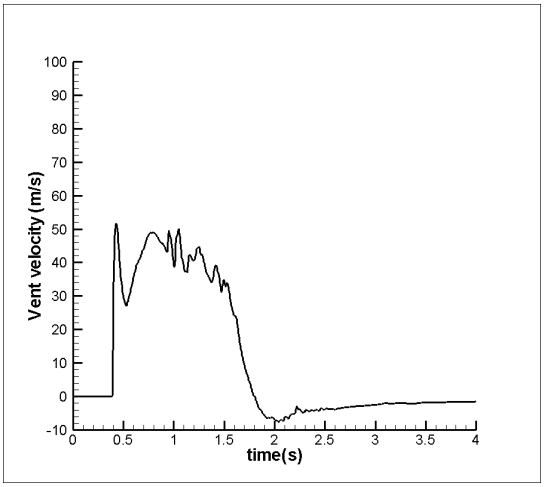

Figure 7.6: Gas velocity at vent in FMG case 14 simulated with the VPC scheme S3

Fig 7.5-7.6 present the calculated bulk pressure and the gas velocity at vent in case 14. The vent is forced to open at a critical pressure level of about 3 Kpa (0.4 psi), as measured from the experiment. Due to a stronger combustion compared to case 7, the pressure signal features a higher second peak that is closer to the second peak measured in the experiment. Gas velocity at the vent reaches a maximum level of 50 m/s upon vent opening. After the pressure is stabilized, the velocity falls to a negative level as low as -8 m/s, similar to the behavior observed in experiments when the bulk pressure is below atmospheric pressure.

In conclusion, the VPC S3 scheme is proposed to simulate vented explosions and is successful at predicting strong outflow velocities and a large pressure drop upon vent opening, as well as Helmholtz oscillations of the pressure and vent velocity. Flow reversal at the vent is observed when pressure relaxes to ambient conditions, which mimics the phenomena in experiments when the internal pressure is below ambient pressure, although here the internal bulk pressure is not calculated to be below outside ambient pressure. The results are encouraging, since it shows that with the VPC scheme in FDS, no artificial treatment of the bulk pressure needs to be done as was initially proposed in chapter 5. While predictions remain qualitative rather than quantitative, important features of the dynamics are correctly predicted (the presence of two pressure peaks, high vent flow velocities, possible Helmholtz oscillations, flow reversal when combustion stops).

Chapter 8

Conclusion

The present study is aimed at adapting current large eddy simulation capabilities to a description of low-pressure explosions in fuel vapor clouds, with an emphasis on scenarios featuring delayed ignition followed by coupled deflagration and diffusion burning. The proposed model formulation is based on a filtered reaction progress variable approach to treat premixed combustion, mixture-fraction-based model (FDS version 4) or an Eddy Dissipation Concept model (FDS version 5) for non-premixed combustion, and the flame index concept to provide a coupling interface. The partially-premixed combustion (PPC) model is implemented in the Fire Dynamics Simulator (Version 5) developed by the National Institute of Standards and Technology.

Its performance is first evaluated in a 2-D tunnel configuration for flame speed verification tests, with different boundary conditions. It is concluded that the model gives satisfactory results when the flame is propagating towards the wall or an opposed flow, but is inaccurate when the flame is propagating away from the wall. This suggests that future work need to be done to clarify this issue. A grid sensitivity study is also performed in a similar configuration, where a premixed flame propagates horizontally through a vertically-stratified flammable mixture layer. The

study suggests that $L_z/\Delta_c \geq 2$ is required for quasi grid-independent predictions of the premixed combustion rate, where L_z is the thickness of the flammable layer, and Δ_c is the LES filter size.

The bulk pressure algorithm in FDS is then tested in a small HVAC-like compartment configuration. It is found that the current pressure algorithm is not capable of predicting the pressure in the presence of an open vent. This problem is addressed by using an algebraic quasi-steady pressure model. While this model provides a qualitatively correct behavior of pressure, it does not address the problem of the vent flow velocities which are independent of over/under-pressurization in FDS and are consequently severely under-estimated.

The experimental database used for validation is a database previously developed by FM Global Research; the database corresponds to explosive combustion tests in an enclosure filled with vertically-stratified mixtures of propane in air, both with and without venting, and with and without obstacles.

The experimental database is well-suited to test the PPC model since it includes some cases in which combustion is predominantly premixed and other cases in which it is essentially non-premixed. The unvented compartment cases develop bulk over-pressures up to approximately 60 Kpa (9 psi); the vented cases develop over-pressures up to 3 Kpa (0.4 psi). Using the modified pressure algorithm, the comparison between numerical results and experimental data ranges from fair to

good and confirms the feasibility of a numerical treatment of explosive combustion.

Another approach to model vented explosions is also explored in the current study. This approach considers the effect of pressure on vent flow velocities. The model is developed by considering the velocity-pressure coupling that occurs in pressurized vented compartments using a zero-dimensional approach and MATLAB as the solution framework. The model features pressure-driven vent flow velocities and Helmholtz oscillations. The presence of Helmholtz oscillations in vented explosions is reported by several studies (experimental and numerical).

The proposed velocity-pressure coupling scheme is used to simulate the vented explosion cases from FMG experimental database. The simulated pressure features two peaks corresponding to maximum premixed combustion and maximum diffusion combustion; while the magnitude of the second peak is under predicted compared to experimental data, the main global features of the bulk pressure variations seem to be correctly captured. The results are encouraging and confirm the potential of the proposed modeling capability for simulations of low pressure fuel vapor cloud explosions.

Chapter A

Derivation of Pressure Algorithm in the Original FDS Version

Start from the energy equation:

$$\frac{\partial}{\partial t}(\rho h) + \nabla \cdot \rho h \mathbf{u} = \frac{Dp}{Dt} + \dot{q}''' - \nabla \cdot \mathbf{q} \tag{A.1}$$

in which h is the enthalpy, ρ is the density, u is the velocity, p is the pressure, $\dot{q}'''$ is the density, $\nabla \cdot \mathbf{q}$ is the heat loss (conduction, convection, radiation). Focus on the LHS of Eq.(A.1), the first term on LHS can be written as:

$$\frac{\partial}{\partial t}(\rho h) = \rho \frac{\partial h}{\partial t} + h \frac{\partial \rho}{\partial t} = \rho c_p \frac{\partial T}{\partial t} + h \frac{\partial \rho}{\partial t}$$

The second term on LHS of Eq.(A.1) can be written as:

$$\nabla \cdot \rho h \mathbf{u} = \nabla h \cdot \rho \mathbf{u} + h(\nabla \cdot \rho \mathbf{u})$$

Combine the above two expressions, Eq.(A.1) becomes:

$$\rho c_p \frac{\partial T}{\partial t} + h(\frac{\partial \rho}{\partial t} + \nabla \cdot \rho \mathbf{u}) + \nabla h \cdot \rho \mathbf{u} = \frac{Dp}{Dt} + \dot{q}''' - \nabla \cdot \mathbf{q} \tag{A.2}$$

Since $\frac{\partial \rho}{\partial t} + \nabla \cdot \rho \mathbf{u} = 0$ (Conservation of Mass), Eq.(A.2) simplifies to

$$\rho c_p \frac{\partial T}{\partial t} + \nabla h \cdot \rho \mathbf{u} = \frac{Dp}{Dt} + \dot{q}''' - \nabla \cdot \mathbf{q} \tag{A.3}$$

Expand $\nabla h \cdot \rho \mathbf{u}$:

$$\nabla h \cdot \rho \mathbf{u} = c_p \nabla T \cdot \rho \mathbf{u} = \rho c_p (\mathbf{u} \cdot \nabla T)$$

So the LHS of Eq.(A.3) becomes:

$$\rho c_p \frac{\partial T}{\partial t} + \rho c_p(\mathbf{u} \cdot \nabla T) = \rho c_p(\frac{DT}{Dt})$$

Now we have the form of Eq.(A.3) to be changed to:

$$\rho c_p(\frac{DT}{Dt}) = \frac{Dp}{Dt} + \dot{q}''' - \nabla \cdot \mathbf{q} \tag{A.4}$$

From the ideal gas law:

$$T = \frac{pM}{\rho R} \Rightarrow lnT = lnp + lnM - ln\rho - lnR$$

Take the material derivative of both sides, considering that R is gas constant:

$$\frac{d(lnT)}{dt} = \frac{d(lnp)}{dt} + \frac{d(lnM)}{dt} - \frac{d(ln\rho)}{dt} - \frac{d(lnR)}{dt}$$

$$\frac{1}{T}\frac{DT}{Dt} = \frac{1}{p}\frac{Dp}{Dt} + \frac{1}{M}\frac{DM}{Dt} - \frac{1}{\rho}\frac{D\rho}{Dt}$$

Multiply by $\rho c_p T$ on both sides:

$$\rho c_p T(\frac{1}{T}\frac{DT}{Dt}) = \frac{\rho c_p T}{p}\frac{Dp}{Dt} + \frac{\rho c_p T}{M}\frac{DM}{Dt} - c_p T\frac{D\rho}{Dt} \tag{A.5}$$

while

$$c_p = \frac{R}{M}\frac{\gamma}{\gamma - 1} \Rightarrow \frac{\rho c_p T}{p} = \frac{\rho T R}{pM}\frac{\gamma}{\gamma - 1} = \frac{\gamma}{\gamma - 1} \tag{A.6}$$

From the conservation of mass:

$$\frac{\partial \rho}{\partial t} + \nabla \cdot \rho\mathbf{u} = 0 = \frac{\partial \rho}{\partial t} + \nabla\rho \cdot \mathbf{u} + \rho(\nabla \cdot \mathbf{u}) = \frac{D\rho}{Dt} + \rho(\nabla \cdot \mathbf{u})$$

$$\Rightarrow \frac{D\rho}{Dt} = -\rho(\nabla \cdot \mathbf{u})$$

Substitute the above expressions into Eq.(A.5), assuming $\frac{DM}{Dt}$ is small, we have:

$$\rho c_p(\frac{DT}{Dt}) = \frac{\gamma}{\gamma - 1}\frac{Dp}{Dt} + \rho c_p T(\nabla \cdot \mathbf{u}) \tag{A.7}$$

Combine Eq.(A.7) and Eq.(A.4):

$$\begin{aligned} \frac{1}{\gamma-1}\frac{Dp}{Dt} &= -\rho c_p T(\nabla\cdot\mathbf{u}) + \dot{q}''' - \nabla\cdot\mathbf{q} \\ \frac{Dp}{Dt} &= -\gamma p(\nabla\cdot\mathbf{u}) + (\gamma-1)(\dot{q}''' - \nabla\cdot\mathbf{q}) \end{aligned} \tag{A.8}$$

The heat loss term here can be split into the conduction, convection and radiation loss, and write using Einstein notation:

$$\nabla\cdot\mathbf{q} = \frac{\partial}{\partial x_j}(\lambda\frac{\partial T}{\partial x_j} - q_{R,j} - q_{c,j})$$

Expand the whole Eq.(A.8) using Einstein notation:

$$\frac{Dp}{Dt} = \frac{\partial p}{\partial t} + u_j\frac{\partial p}{\partial x_j} = -\gamma p\frac{\partial u_j}{\partial x_j} + (\gamma-1)[\frac{\partial}{\partial x_j}(\lambda\frac{\partial T}{\partial x_j} - q_{R,j} - q_{c,j}) + \dot{q}_j'''] \tag{A.9}$$

With low Mach number assumption: $\frac{\partial p}{\partial x_j}$ is small, we have:

$$\frac{\partial p}{\partial t} = -\gamma p\frac{\partial u_j}{\partial x_j} + (\gamma-1)[\frac{\partial}{\partial x_j}(\lambda\frac{\partial T}{\partial x_j} - q_{R,j} - q_{c,j}) + \dot{q}_j''']$$

or:

$$\frac{1}{\gamma-1}\frac{\partial p}{\partial t} = -\frac{\gamma p}{\gamma-1}\frac{\partial u_j}{\partial x_j} + \frac{\partial}{\partial x_j}(\lambda\frac{\partial T}{\partial x_j} - q_{R,j} - q_{c,j}) + \dot{q}_j''' \tag{A.10}$$

Spatially integrate this equation to get the global pressure:

$$\iiint_{CV}\frac{1}{\gamma-1}\frac{\partial p}{\partial t}dV = \iiint_{CV} -\frac{\gamma p}{\gamma-1}\frac{\partial u_j}{\partial x_j}dV + \iiint_{CV}\frac{\partial}{\partial x_j}(\lambda\frac{\partial T}{\partial x_j} - q_{R,j} - q_{c,j})dV + \iiint_{CV}\dot{q}_j dV$$

Using divergence theorem:

$$\iiint_{CV}\frac{1}{\gamma-1}\frac{\partial p}{\partial t}dV = \frac{d\bar{p}}{dt}\iiint_{CV}\frac{dV}{\gamma-1} = -\bar{p}\iiint_{CV} -\frac{\gamma}{\gamma-1}\frac{\partial u_j}{\partial x_j}dV + \oint_{CS}(\lambda\frac{\partial T}{\partial x_j} - q_{R,j} - q_{c,j})n_j dS + \dot{Q}$$

We get:

$$\frac{dp_0}{dt} = \frac{-p_0\iiint_{CV}\frac{\gamma}{\gamma-1}\frac{\partial u_j}{\partial x_j}dV + \oint_{CS}(\lambda\frac{\partial T}{\partial x_j} - q_{R,j} - q_{c,j})n_j dS + \dot{Q}}{\iiint_{CV}\frac{dV}{\gamma-1}} \tag{A.11}$$

Considering Eq.(A.6), the Eq.(A.11) is equivalent to

$$\frac{dp_0}{dt} = \frac{\iiint_{CV} \frac{1}{\rho c_p T}(\dot{q}''' - \nabla \cdot \mathbf{q})dV - \oint_{CS}(\mathbf{u} \cdot \mathbf{n})dS}{\iiint_{CV}(\frac{1}{p_0} - \frac{1}{\rho c_p T})dV} \tag{A.12}$$

which is the one used in the formulation of bulk pressure in FDS.

Chapter B

Verification of the Modified s_L Algorithm as Function of Pressure and Temperature

The modification of the s_L with regard to pressure p and temperature T is verified here by redo the flame propagation in tunnel configuration (case1). The modification of s_L algorithm is in Chapter 2, for convenience, it is shown here again:

$$\begin{aligned} s_L &= s_{L,ref}(\frac{T_u}{T_{u,ref}})^{\gamma}(\frac{\bar{p}}{\bar{p}_{ref}})^{\beta} \\ \rho_u s_L &= \rho_a s_{L,ref}(\frac{T_u}{T_{u,ref}})^{\gamma-1}(\frac{\bar{p}}{\bar{p}_{ref}})^{\beta+1} \\ \gamma &= 2.18 - 0.8(\phi - 1) \\ \beta &= -0.16 + 0.22(\phi - 1) \\ \phi &= \frac{1 - Z_{st}}{Z_{st}} \times \frac{\tilde{Z}}{1 - \tilde{Z}} \end{aligned} \tag{B.1}$$

In the tunnel of case 1, the pressure would remain constant since there is open-end, so the goal here is to see the effect of temperature in the unburnt gas. Since the pressure and temperature are in similar position in the above formulation, we believe that if we see effect from the temperature modification, we would see effect from pressure modification as well (if the pressure is varied).

The difference in prescription of Fig B.1 and B.2 is that for Fig B.1, the ambient temperature in the unburnt fuel-air mixtures is 20°C, while in Fig B.2, the

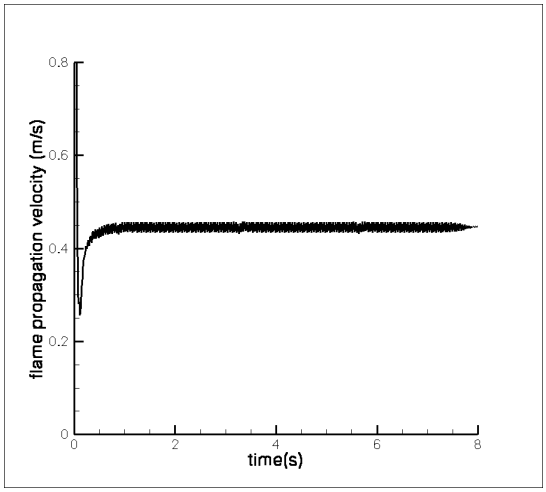

Figure B.1: Time variations of the apparent flame propagation velocity fpv in case 1

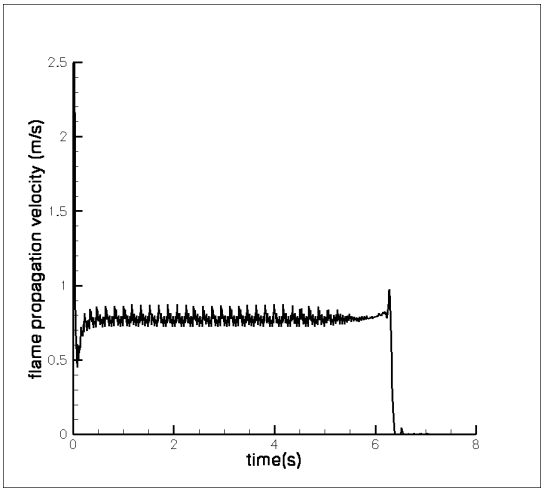

Figure B.2: Time variations of the apparent flame propagation velocity fpv in case 1 with modified s_L algorithm

ambient temperature is 200°C. Since the mixture here is stoichiometric, $Z = Z_{st}$, so according to Eq. (B.1), we would expect to see the flame propagation velocity to be

$$\rho_u s_L = 0.4 \times (\frac{273 + 200}{273 + 20})^{2.18-1} = 0.7038 \tag{B.2}$$

which agrees with the numerical results in Fig B.2.

Chapter C

Effect of Wrinkling Factor in PPC Model

In previous work by [12, 13] elaborate closure model for the subgrid-scale flame wrinkling factor Ξ is proposed, however in Chapter 5 when the FMG cases are simulated Ξ is set to be a constant value $\Xi = 4$. In Fig 5.11, case 6 and 14 calculates resembling pressure building up speed, indicating that the combustion which is backing the pressure build up is at the same speed as in the experiment, but case 7 and 26 calculate faster combustion. Here in this section a lower subgrid-scale wrinkling factor $\Xi = 2$ is chosen for case 7 and 14, so that the effect of Ξ on the flame speed can be illustrated.

In Fig C.1-C.2, the time evolution of heat release rate and bulk pressure in case 7 is shown, when adopting $\Xi = 2$. Compared to Fig 5.10(b), the combustion occurs slower now, with a lower peak of heat release rate of about 10 MW. The pressure reach the first peak a little later than the experimental measure pressure, instead of much more ahead in Fig 5.11(b). This indicates that choosing a wrinkling factor lower than $\Xi = 4$ in Chapter 5 will give a better simulation of case 7.

However, for case 14, the story is different. In Fig 5.11(c), the first peak of pressure coincides with the one in the experimental curve, which indicates an agree-

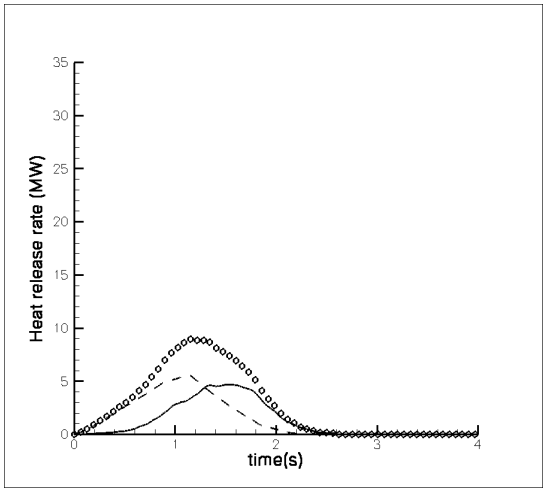

Figure C.1: Time variations of heat release rate(HRR) in FMG case 7 using wrinkling factor at 2.0: total HRR (circles); premixed HRR(dashed line); diffusion HRR(solid line)

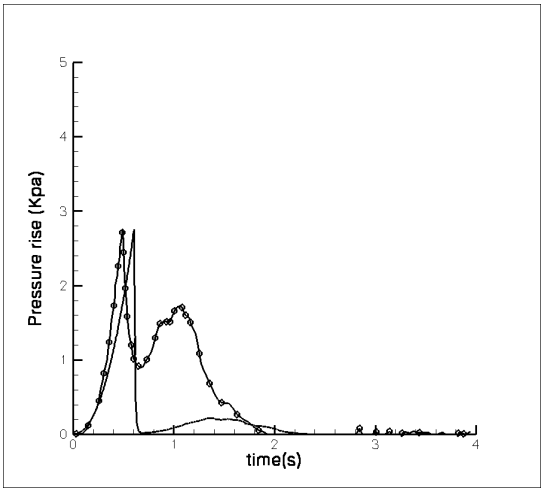

Figure C.2: Time variations of bulk pressure in FMG case 7 using wrinkling factor at 2.0: experimental pressure (circles); simulated pressure(solid line)

ing combustion speed modeling. Here in Fig C.3-C.4, the combustion occurs slower, resulting in a lower heat release peak, and a slower pressure build up, due to the effect of lower wrinkling factor.

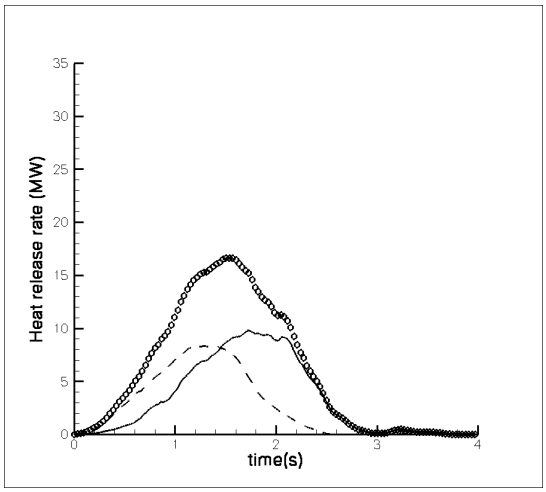

Figure C.3: Time variations of heat release rate(HRR) in FMG case 14 using wrinkling factor at 2.0: total HRR (circles); premixed HRR(dashed line); diffusion HRR(solid line)

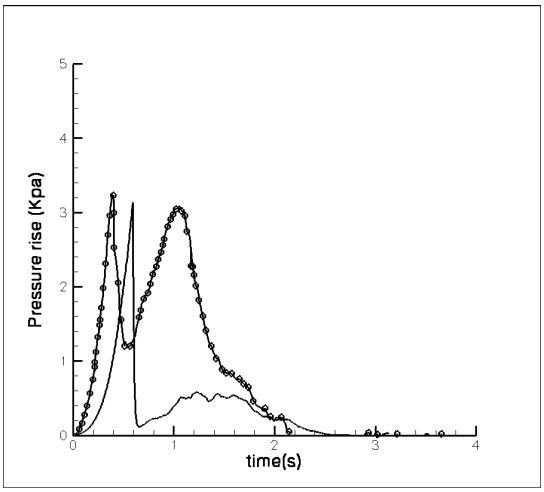

Figure C.4: Time variations of bulk pressure in FMG case 14 using wrinkling factor at 2.0: experimental pressure (circles); simulated pressure(solid line)

Summarized by above, different wrinkling factors should be adopted for a correct modeling of combustion, depending on different cases, suggesting that an elaborate model for wrinkling factor is still needed in PPC model for successful simulation of partially-premixed combustion. Here in current study uniform subgrid-scale wrinkling factor is assumed for preliminary study,

Bibliography

[1] W.Baker, M.Tang, *Gas, Dust and Hybrid Explosions*, Elsevier (1991)

[2] C.Bauwens, J.Chaffee, S.Dorofeev, "Experimental and Numerical Study of Methane-air Deflagrations in a Vented Enclosure",*Fire Safety Science, Proceedings of the Ninth International Symposium* (2008)

[3] C.Beyler, "Flammability Limits of Premixed and Diffusion Flames", *SFPE Handbook of Fire Protection Engineering, NFPA(3rd Ed.)*, **2**, 172-187 (2002)

[4] M.Boger, D.Veynante, H.Boughanem, A.Trouve, "Direct Numerical Simulation Analysis of Flame Surface Density Concept for Large Eddy Simulation of Turbulent Premixed Combustion", *Proceedings of the Combustion Institute*, **27**, 917-925 (1998)

[5] M.Boger, D.Veynante, "Large Eddy Simulation of a Turbulent Premixed V-Shaped Flame", *Advances in Turbulence*, Dopazo C. (ed.), Cimne, Barcelona, 449-452 (2000)

[6] M.Boger, "Modelisation de Sous-Maille pour la Simulation aux Grandes Echelles de la Combustion Turbulente Premelangee", *Ph.D. Thesis, Ecole Centrale Paris*, France (2000)

[7] D.Bradley, T.Cresswell, J.Puttock, "Flame Acceleration due to Flame-Induced Instabilities in Large-Scale Explosions", *Combustion and Flame*, **124**, 551-559 (2001)

[8] D.Bradley, A.Mitcheson, "The Venting of Gaseous Explosions in Spherical Vessels. I-Theory", *Combustion and Flame*, **32**, 221-236 (1978)

[9] D.Bradley, A.Mitcheson, "The Venting of Gaseous Explosions in Spherical Vessels. II-Theory and Experiment", *Combustion and Flame*, **32**, 237-255 (1978)

[10] R.Cant, W.Dawes, A.Savill, "Advanced CFD and Modeling of Accidental Explosions", *Annual Review Fluid Mechanics*, **36**, 97-119 (2004)

[11] F.Charlette, A.Trouve, M.Boger, D.Veynante, "A Flame Surface Density Model for Large Eddy Simulations of Turbulent Premixed Flames", *Joint Meeting of the British, German and French Sections of the Combustion Institute*,Combustion Institute, Nancy, France (1999)

[12] F.Charlette, C.Meneveau, D.Veynante, "A Power-Law Flame Wrinkling Model for LES of Premixed Turbulent Combustion Part I: Non-Dynamic Formulation and Initial Tests", *Combustion and Flame*, **131**, 159-180 (2002)

[13] F.Charlette, C.Meneveau, D.Veynante, "A Power-Law Flame Wrinkling Model for LES of Premixed Turbulent Combustion Part II: Dynamic Formulation", *Combustion and Flame*, **131**, 181-197 (2002)

[14] C.Conrado, V.Vesovic, "The Influence of Chemical Composition on Vaporization of LNG and LPG on Unconfined Water Surfaces", *Chemical Engineering Science*, **55**, 4549-4562 (2000)

[15] M.Cooper, M.Fairweather, J.Tite, "On the Mechanisms of Pressure Generation in Vented Explosion", *Combustion and Flame*, **65**, 1-14 (1986)

[16] J.Coudert, V.Rat, D.Rigot, "Influence of Helmholtz Oscillations on Arc Voltage Fluctuations in a Dc Plasma Spraying Torch", *Journal of Physics D: Applied Physics*, **40**, 7357-7366 (2007)

[17] J.DeHaan, D.Crowhurst, D.Hoare, M.Bensilum, M.Shipp, "Deflagrations involving Stratified Heavier-than-air Vapor/Air Mixtures", *Fire Safety Journal*, **36**, 693-710 (2001)

[18] P.Domingo, L.Vervisch and K.Bray, "Partially Premixed Flamelets in LES of Nonpremixed Turbulent Combustion", *Combustion Theory and Modeling*, **6**, 529-551 (2002)

[19] D.Ermack, "User's Manual for SLAB: An Atmospheric Dispersion Model for Denser-Than-Air Releases", *A.a.G.S.D Physics Department, Lawrence Livermore National Laboratory* (1990)

[20] M.Fairweather, "A Mathematical Model for the Prediction of Overpressures Generated in Totally Confined and Vented Explosions", *Proceedings of the Combustion Institute*, **19**, 645-653 (1982)

[21] J.Fay, "Model of Spills and Fires from LNG and Oil Tankers", *Journal of Hazardous Materials*, **96**, 171-188 (2003)

[22] G.Ferrara, A.Benedetto, E.Salzano, G.Russo, "CFD Analysis of Gas Explosions Vented through Relief Pipes", *Journal of Hazardous Materials*, **137**, 654-665 (2006)

[23] S.Ferraris, J.Wen, S.Dembele, "Large Eddy Simulation of the Backdraft Phenomena", *Fire Safety Journal*, **43**, 205-225 (2008)

[24] C.Fleischmann, P.Pagni, R.Williamson, "Salt Water Modeling of Fire Compartment Gravity Currents",*Fire Safety Science, Proceedings of the Fourth International Symposim*, 253-264 (1994)

[25] C.Fleischmann, *"Backdraft Phenomena"*, Ph.D. Thesis, University of California, Berkeley (1993)

[26] C.Fleischmann, P.Pagni, R.Williamson, "Quantitative Backdraft Experiments", *Fire Safety Science, Proceedings of the Fourth International Symposium*, 337-348 (1994)

[27] G.Forney, W.Moss, "Analyzing and Exploiting Numerical Characteristics of Zone Fire Models", *Fire Science and Technology*, **14**, 49-60 (1994)

[28] D.Gottuk, M.Peatross, J.Farley, F.Williams, "The Development and Mitigation of Backdraft: A Real-Scale Shipboard Study", *Fire Safety Journal*, **33**, 261-282 (1999)

[29] D.Gottuk, F.Williams, J.Farley, "The Development and Mitigation of Backdrafts: a Full-scale Experimental Study", *Fire Safety Science, Proceedings of the Fifth International Symposium*, 935-946 (1997)

[30] J.Havens, "A Dispersion Model for Elevated Dense Gas Jet Chemical Release: Volume 2, User's Guide", *Environmental Protection Agency: Research Triangle Park, North Carolina* (1988)

[31] E.Hawkes, R.Cant, "A Flame Surface Density Approach to Large-Eddy Simulation of Premixed Turbulent Combustion",*Proceedings of the Combustion Institute*, **28**, 51-58 (2000)

[32] E.Hawkes, R.Cant, "Implications of a Flame Surface Density Approach to Large Eddy Simulation of a Premixed Turbulent Combustion", *Combustion and Flame*, **126**, 1617-1629 (2001)

[33] A.Hersh, B.Walker, J.Celano, "Helmholtz Resonator Impedance Model", *AIAA Journal*, **51**, 795-820 (2003)

[34] A.Horvat, Y.Sinai, "Numerical Simulation of Backdraft Phenomena", *Fire Safety Journal*, **42**, 200-209 (2007)

[35] Z.Hu, Y.Utiskul, J.G.Quintiere, A.Trouve, "A Comparison Between Observed and Simulated Flame Structures in Poorly Ventilated Compartment Fires", *Fire Safety Science, Proceedings of the Eighth International Symposium* (2005)

[36] Z.Hu, Y.Utiskul, J.G.Quintiere, A.Trouve, "Towards Large Eddy Simulations of Flame Extinction and Carbon Monoxide Emission in Compartment Fires", *Proceedings of the Combustion Institute*, **31**, 2537-2545 (2007)

[37] Z.Hu, G.Panafieu, J.Stauder, A.Trouve, "A Presumed PDF Approach to Model Turbulent Non-premixed Combustion in FDS", *Intl. Tech. Congress on Computational Simulation Models in Fire Engr. and Res.*, Ed. J.A. Capote Abreu, Gidai, Univ. Cantabria, Santander, Spain, 281-295 (2004)

[38] Z.Hu, A.Trouve, "Numerical Simulation of Explosive Combustion Following Ignition of a Fuel Vapor Cloud", *Fire Safety Science, Proceedings of the Ninth International Symposium* (2008)

[39] Z.Hu, *Flame Extinction and Air Vitiation Effects in FDS in Poorly Ventilated Compartment Fires*, Master Thesis, University of Maryland, College Park (2005)

[40] T.Iijima, "Effects of Temperature and Pressure on Burning Velocity", *Combustion and Flame*, **65**, 35-43 (1986)

[41] K.Kelkar, D.Choudhury, "Numerical Method for the Prediction of Incompressible Flow and Heat Transfer in Domains with Specified Pressure Boundary Conditions", *Numerical Heat Transfer*, **38**, 15-36 (2000)

[42] L.Kinsler, A.Frey, "Fundamentals of Acoustics", John Wiley.

[43] M.Kirkpatrick, S.Armfield, A.Masri, S.Ibrahim, "Large Eddy Simulation of a Propagating Turbulent Premixed Flame", *Flow, Turbulence and Combustion*, **70**, 1-19 (2003)

[44] R.Knikker, D.Veynante, C.Meneveau, "A Priori Testing of a Similarity Model for Large Eddy Simulations of Turbulent Premixed Combustion", *Proceedings of the Combustion Institute*, **29**, 2105-2111 (2002)

[45] B.Magnussen, B.Hjertager, "On Mathematical Modeling of Turbulent Combustion With Special Emphasis on Soot Formation and Combustion", *Proceedings of the Combustion Institute*, **16**, 719-729 (1976)

[46] D.Makarov, V.Molkov, Y.Gostintsev, "Comparison Between RNG and Fractal Combustion Models for LES of Unconfined Explosions", *Combustion Science and Technology*, **179**, 401-416 (2007)

[47] G.Makhviladze, J.Roberts, S.Yakush, "Modeling the Fireballs from Methane Releases", *Proceedings of the Fifth International Symposium*, 213-224 (1997)

[48] G.Makhviladze, J.Roberts, S.Yakush, "Numerical Modeling of Fireballs from Vertical Releases of Fuel Gases", *Combustion Science and Technology*, **132**, 199-223 (1998)

[49] G.Makhviladze, J.Roberts, S.Yakush, "Combustion of Two-Phase Hydrocarbon Fuel Clouds Released into the Atmosphere", *Combustion and Flame*, **118**, 583-605 (1999)

[50] G.Makhviladze, J.Roberts, S.Yakush, "Modeling and Scaling of Fireballs from Single-and Two-Phase Hydrocarbon Release", *Proceedings of the Sixth International Symposium*, 1125-1136 (2000)

[51] G.Makhviladze, S.Yakush, "Modeling of Fires Following Bursts of Pressurized Fuel Tanks", *Fire Safety Science – Proceedings of the Seventh International Symposium*, International Association for Fire Safety Science, 643-654 (2003)

[52] D.McCann, G.Thomas, D.Edwards,"Gasdynamics of Vented Explosions. Part I:Experimental Studies", *Combustion and Flame*, **59**, 233-250 (1985)

[53] D.McCann, G.Thomas, D.Edwards,"Gasdynamics of Vented Explosions. Part II:One-Dimensional Wave Interaction Model", *Combustion and Flame*, **60**, 63-70 (1985)

[54] J.McGill, *Simulation of Vaporization and Combustion of a Large-Scale Cryogenic Liquid Methane Pool*, M.S. Thesis, University of Maryland, College Park (2006)

[55] C.Fleischmann, K.McGrattan,"Numerical and Experimental Gravity Currents Related to Backdraft", *Fire Safety Journal*, **33**, 21-34 (1999)

[56] K.McGrattan, R.Rehm, H.Baum, "Fire-Driven Flows in Enclosures", *Journal of Computational Physics*, **110**, 285-291 (1994)

[57] K.McGrattan, H.Baum, R.Rehm, A.Hamins, G.Forney, J.Floyd, S.Hostikka, "Fire Dynamics Simulator (Version 5) - Technical Reference Guide", *National Institute of Standards and Technology Report NIST Special Publication 1018-5*, Gaithersburg, MD, USA (2007)

[58] K.McGrattan, J.Floyd, G.Forney, H.Baum, S.Hostikka, "Improved Radiation and Combustion Routines for a Large Eddy Simulation Fire Model", *Fire Safety Science – Proceedings of the Seventh International Symposium*, International Association for Fire Safety Science, 827-838 (2003)

[59] V.Molkov, D.Makarov, A.Ryzhov, A.Duval, "Modeling and Simulations of Large-Scale Accidental Combustion", *Proceedings of the Technical Congress on "Computational Simulation Models in Fire Engineering and Research"*,University of Cantabria, Santander, Spain, 315-341 (2004)

[60] V.Molkov, D.Makarov, A.Grigorash, "Cellular Structure of Explosion Flames: Modeling and Large-Eddy Simulation",*Combustion Science and Technology*, **176**, 851-865 (2004)

[61] V.Molkov, D.Makarov, F.Verbecke, Z.Mansurov, M.Zhumabaev, "LES Model of Vented Explosion:Hydrogen-Air Mixtures", *5th International Seminar on Fire and Explosion Hazards* (2007)

[62] V.Molkov, "Hydrogen Safety Research: State-of-the-art", *5th International Seminar on Fire and Explosion Hazards* (2007)

[63] V.Molkov, R.Dobashi, M.Suzuki, T.Hirano, "Venting of Deflagrations: Hydrocarbon-Air and Hydrogen-Air Systems", *Journal of Loss Prevention in the Process Industries*, **13**, 397-409 (2000)

[64] V.Molkov, R.Dobashi, M.Suzuki, T.Hirano, "Modeling of Vented Hydrogen-Air Deflagrations and Correlations for Vent Sizing", *Journal of Loss Prevention in the Process Industries*, **12**, 147-156 (1999)

[65] V.Molkov, A.Grigorash, R.Eber, "Vented Gaseous Deflagrations: Modeling of Spring-Loaded Inertial Vent Covers", *Fire Safety Journal*, **40**, 307-319 (2005)

[66] V.Molkov, D.Makarov, H.Schneider, "LES Modeling of an Unconfined Large-scale Hydrogen-air Deflagration", *Journal of Physics D: Applied Physics*, **39**, 4366-4376 (2006)

[67] J.Morehart, E.Zukoski, "Chemical Species Produced in Fires Near the Limit of Flammability", *Fire Safety Journal*, **19**, 177-188 (1992)

[68] G.Mulholland, "The Effect of Oxygen Concentration on CO and Smoke Produced by Flames", *Fire Safety Science, Proceedings of the Third International Symposium*, 585-594 (1991)

[69] C.Muller, H.Breitbach, N.Peters, "Partially Premixed Turbulent Flame Propagation in Jet Flames", *Proceedings of the Combustion Institute*, **25**, 1099-1106 (1994)

[70] D.Park, Y.Lee, A.Green, "Prediction for Vented Explosions in Chambers with Multiple Obstacles", *Journal of Hazardous Materials* (2007)

[71] C.Pierce, P.Moin, "A Dynamic Model for Subgrid-Scale Variance and Dissipation Rate of a Conserved Scalar", *Physics of Fluids*, **10**, 3041-3044 (1998)

[72] T.Poinsot, D.Veynante, *Theoretical and Numerical Combustion, Edwards* (2001)

[73] B.Porterie, J.Loraud, *The Prediction of Some Compartment Fires. Part 1: Mathematical Model and Numerical Method*, **39**, 139-153 (2001)

[74] G.Raithby, G.Schneider, " Numerical Solution of Problems in Incompressible Fluid Flow: Treatment of the Velocity-Pressure Coupling",*Numerical Heat Transfer*, **2**, 417-440 (1979)

[75] J.Quintiere, "Fundamentals of Enclosure Fire Zone Models", *Journal of Fire Protection Engineering*, **1**, 99-119 (1984)

[76] D.Razus, U.Krause, "Comparison of Empirical and Semi-Empirical Calculation Methods for Venting of Gas Explosions", *Fire Safety Journal*, **36**, 1-23 (2001)

[77] D.Razus, D.Oancea, F.Chirila, N.Ionescu, "Transmission of an Explosion Between Linked Vessels", *Fire Safety Journal*, **38**, 147-163 (2003)

[78] R.Rehm, G.Forney, "The Pressure Equations in Zone-Fire Modeling", *Fire Science and Technology*, **14**, 61-73 (1994)

[79] A.Snegirev, G.Makhviladze, V.Talalov, A.Shamshin, "Turbulent Diffusion Combustion Under Conditions of Limited Ventilation: Flame Projection Through an Opening", *Combustion, Explosion, and Shock Waves*, **39**, 1-10 (2003)

[80] R.Strehlow, "Unconfined Vapor Cloud Explosions - an Overview", *Proceedings of the Combustion Institute*, **14**, 1189-1200 (1973)

[81] F.Tamanini, J.Chaffee, "Mixture Reactivity in Explosions of Stratified Fuel/Air Layers", *Process Safety Progress*, **19**, 219-227 (2000)

[82] F.Tamanini, "Partial-Volume Deflagrations – Characteristics of Explosion in Layered Fuel/Air Mixtures", *Proceedings of 3rd Intl. Seminar on Fire and Explosion Hazards*, Edinburgh, U.K., p.103 (2001)

[83] S.Tullis, R.Cant, "Scalar Transport Modeling in Large Eddy Simulation of Turbulent Premixed Flames", *Proceedings of the Combustion Institute*, **29**, 2097-2104 (2002)

[84] S.Turns, "A Introduction to Combustion – Concepts and Applications (2nd ed)", McGraw-Hill (2000)

[85] L.Vervisch, R.Hauguel, P.Domingo, and M.Rullaud, "Three Facets of Turbulent Combustion Modeling: DNS of Premixed V-Flame, LES of Lifted Nonpremixed Flame and RANS of Jet-Flame", *Journal of Turbulence*, **5**, 004 (2004)

[86] D.Veynante, L.Vervisch, "Turbulent Combustion Modeling", *Progress in Energy and Combustion Science*, **28**, 193-266 (2002)

[87] J.Wiley, A.Trouve, "Large Eddy Simulations of Flash Fires Following Ignition of A Fuel Vapor Cloud", *5th US Combustion Meeting, University of California, San Diego* (2007)

[88] J.Wiley, A.Trouve, "Large Eddy Simulation of Ignition and Transient Combustion in Fuel Vapor Clouds", *5th International Seminar on Fire and Explosion Hazards* (2007)

[89] J.Wiley, *Numerical Simulation of Ignition and Transient Combustion in Fuel Vapor Clouds*, Master Thesis, University of Maryland, College Park (2007)

[90] D.William, "The detonation of explosive", *Scientific American*, **256**, 106-112 (1987)

[91] F.Williams, *Combustion Theory, Benjamin/Cummings(2nd Ed.)* (1985)

[92] J.Williamson, J.McGill, A.Trouve, "A Filtered Progress Variable Approach to Model Turbulent Premixed Combustion in FDS", *Intl. Tech. Congress on Computational Simulation Models in Fire Engr. and Res.*, Ed.J.A.Capote Abreu, GIDAI,Univ.Cantabria, Santander, Spain, 7-16 (2004)

[93] J.Williamson, J.McGill, A.Trouve, "Large Eddy Simulation Modeling of Turbulent Deflagrations", *Fire Safety Science, Proceedings of the Eighth International Symposium* (2005)

[94] K.Yu, A.Trouve, J.Daily, "Low-Frequency Pressure Oscillations in a Model Ramjet Combustor", *The Journal of Fluid Mechanics*, **232**, 47-72 (1991)

[95] R.Zalosh, "Explosion Protection", *The SFPE Handbook of Fire Protection Engineering (3rd ed)*, National Fire Protection Association

[96] D.Zhu, F.Egolfopoulos, C.Law, "Experimental and Numerical Determination of Laminar Flame Speeds of Methane-Air Mixtures as Function of Stoichiometry,

Pressure, and Flame Temperature", *Proceedings of the Combustion Institute"*, **22**, 1537-1545 (1988)